UNCLASSIFIED

AD NUMBER

AD110259

NEW LIMITATION CHANGE

TO

Approved for public release, distribution unlimited

FROM

Distribution authorized to U.S. Gov't. agencies and their contractors; Administrative/Operational Use; OCT 1956. Other requests shall be referred to Geophysics Research Directorate, Air Force Cambridge Research Center, Bedford, MA.

AUTHORITY

AFCRL ltr dtd 3 Nov 1971

THIS PAGE IS UNCLASSIFIED

QC 801
U54
no.51

210
MENT NO. AD-110259

GEOPHYSICAL RESEARCH PAPERS
NO. 51

CLOUD REFRACTIVE INDEX STUDIES

AD-110259

ROBERT M. CUNNINGHAM
VERNON G. PLANK
CHARLES F. CAMPEN, JR.

OCTOBER 1956

GEOPHYSICS RESEARCH DIRECTORATE
AIR FORCE CAMBRIDGE RESEARCH CENTER
AIR RESEARCH AND DEVELOPMENT COMMAND

Requests for additional copies by Agencies of the Department of Defense, their contractors, and other government agencies should be directed to the:

ARMED SERVICES TECHNICAL INFORMATION AGENCY,
DOCUMENT SERVICE CENTER,
DAYTON 2, OHIO

Department of Defense contractors must be established for ASTIA services, or have their 'need-to-know' certified by the cognizant military agency of their project or contract.

All other persons and organizations should apply to the:

U. S. DEPARTMENT OF COMMERCE
OFFICE OF TECHNICAL SERVICES,
WASHINGTON 25, D. C.

ERRATA SHEET

Author's Name reads:

CHARLES M. CAMPEN

This should read:

CHARLES F. CAMPEN, Jr.

Last page of book, item No. 49, reads:

No. 49. Theory of Motion of a Thin Metallic Cylinder Carrying a High Current, C.W. Dubs, Geophysics Research Directorate, October 1955.

This should read:

No. 49. Theory of Motion of a Thin Metallic Cylinder Carrying a High Current, C.W. Dubs, Geophyiscs Research Directorate, October 1956.

AFCRC-TR-56-210
ASTIA DOCUMENT NO. AD-110259

U. S. WEATHER BUREAU
NWRC LIBRARY

GEOPHYSICAL RESEARCH PAPERS
NO. 51

CLOUD REFRACTIVE INDEX STUDIES

ROBERT M. CUNNINGHAM
VERNON G. PLANK
CHARLES F. CAMPEN, JR.

OCTOBER 1956

GEOPHYSICS RESEARCH DIRECTORATE
AIR FORCE CAMBRIDGE RESEARCH CENTER
BEDFORD MASSACHUSETTS

CONTENTS

LIST OF ILLUSTRATIONS

LIST OF ILLUSTRATIONS (CONTINUED)

LIST OF ILLUSTRATIONS (CONTINUED)

LIST OF ILLUSTRATIONS (CONTINUED)

LIST OF ILLUSTRATIONS (CONTINUED)

LIST OF TABLES

TABLE OF SYMBOLS

Symbol	Definition	Units
B_s	Altitude of cloud base	feet, P.A.
C	Cloud thickness along flight path as determined visually, knowing aircraft velocity	feet
C_D	Cloud thickness along flight path as indicated by refractometer; i.e., thickness of region where N_c prevails. (Excludes transition zones)	feet
e	Pressure of aqueous vapor	millibars
e_s	Saturated pressure of aqueous vapor	millibars
H	True compass heading of aircraft	degrees
i	Subscript indicating data taken on entry into cloud	
N	Modified refractive index = $(n-1) \times 10^6$	N units
N_A	Measured ambient refractive index	N units
N_a	Ambient refractive index computed from radiosonde data	N units
N_b	Probable refractive index in interior of invisible, nonsaturated, rising bubble. (Bubbles are presumed to be the agents which, up to a certain stage of cloud development, feed air having the properties of some lower level into the cloud through its base.)	N units
N_c	Measured refractive index in saturated portion of cloud	N units
N_s	Saturated refractive index computed from radiosonde data, under assumption that $T_d = T$	N units

TABLE OF SYMBOLS (CONTINUED)

Symbol	Definition	Units
N_1	Refractive index at outer edge of transition zone	N units
N_2	Average refractive index a short distance away from cloud	N units
o	Subscript indicating data taken on exit from cloud	
q	Specific humidity (for practical purposes the same as mixing ratio)	gm./kg.
q_b	Specific humidity presumed to exist in an invisible, nonsaturated, rising bubble	gm./kg.
R	Horizontal range to cloud center	feet
T	Temperature	°C
T_d	Temperature of the dew point	°C
T_p	Altitude of cloud top	feet, P.A.
T_v	Temperature which dry air must have at given pressure, in order to have the same density as air containing water vapor which is at the same pressure and given temperature. (Where indicated, T_v takes into account the contribution to moist air density due to condensed liquid water.)	°C
U	Direction from which wind is blowing and the wind velocity	Degrees and knots
W	Gross width of cloud or cloud tower probed (not necessarily the width at flight altitude).	feet
X_{min}	Minimum distance in transition zone over which 75 per cent of the refractive index change occurs	feet

TABLE OF SYMBOLS (CONTINUED)

Symbol	Definition	Units
X_T	Thickness of transition zone at edge of cloud as indicated by refractive index trace	feet
ΔN	Difference between N values (specifically identified where used)	feet
P.A.	Pressure altitude of aircraft (flight altitude)	feet
LWC	Condensed liquid water content	gm/m^3
Osc.	Number of oscillations of refractive index in transition zone	

ABSTRACT

Special problems inherent in the measurement of refractive index in cloudy regions are considered and reasons for refractive index change in and near clouds are discussed Various theories of cumulus convection are reviewed for later reference.

Measurement methods, data gathering procedures, and analysis aims and techniques are described. Data analyzed to date are presented and the tentative conclusion is drawn that with judicious use of radiosonde data a good estimate can be made of the refractive index changes in and around clouds. The complex character of these refractive index changes is tentatively explained.

CLOUD REFRACTIVE INDEX STUDIES

1. Introduction

Certain radio and radar systems are affected by the inhomogeneities in atmospheric refractive index that occur in and around clouds (primarily cumuliform). For purposes of better system design and predictability of system operation, it is important to know the refractive characteristics of clouds and to understand how these characteristics change with the meteorological factors that govern cloud birth, growth and decay. This report describes work directed toward this end.

During the summer of 1955, members of the Aircraft Weather Unit, Geophysics Research Directorate (GRD) utilized a B-29 aircraft to make measurements of refractive index and cloud physics parameters in cloudy regions over various geographical locations in the United States. Flight was made through cumuliform clouds at a number of altitudes under various weather conditions. A University of Texas-model refractometer was used to measure refractive index; cloud physics parameters were measured with the instruments shown in Fig. 1.

A portion of the data for the summer flights has been analyzed. Gross features of tropospheric refractive index have been determined from radiosonde data for each of the flight days; and the theoretical refractive differences between clouds and surrounding clear air and between subcloud and surroundings have been computed. Records of flight measurements through clouds have been analyzed; and cross sections showing traces of refractive index, temperature, virtual temperature, vapor pressure, saturation vapor pressure and liquid water content have been constructed. Microrefractive characteristics of clouds have been studied and the theoretical and observed properties of cloudy regions compared.

2. Background

2.1 Refractive Index of Clear and Cloudy Regions

The refractive index of clear air at microwave frequencies can be measured directly by means of a refractometer or can be computed using the empirical equation,

$$N_A = (n-1) \times 10^6 = \frac{74.4}{T} (P - e/7 + \frac{4973e}{T}), \qquad (1)$$

where: n = refractive index
N_A = modified refractive index for air without liquid water
P = total pressure in millibars

e = pressure of aqueous vapor
T = temperature in degrees Kelvin.

The refractive index of the conglomerate comprised of air containing cloud and or precipitation particles cannot be measured directly with present equipment. There are two major reasons for this; one is that air cannot flow freely through the sensing head of the refractometer (a microwave resonant cavity) and thus a true cloud or particle sample cannot be obtained. The second is that the refractometer is calibrated under the assumption that an isotropic, homogeneous medium exists within the cavity. The presence of water particles and or condensed liquid water on the walls cannot be taken into account.

According to Enenstein,[8] the contribution to refractive index due to water droplets can be computed under the assumption that water mass has infinite electrical conductivity and contributes to the total refractive index as would metal. His equation for air containing droplets is,

$$N_{WD} = \frac{79}{T} \left(P - \frac{e}{7} + \frac{4800e}{T} + 1.5 \times \frac{4}{3} \pi \alpha^3 \rho S\right)^* \qquad (2)$$

$$= 79/T \left[P - e/7 + \frac{4800e}{T} + 1.5\ (LWC)\right]$$

where: N_{WD} = modified refractive index of air with water drops
α = average radii of drops in meters
ρ = density of water in gm/m^3
S = number of drops per m^3
LWC = liquid water content in gm/m^3

From this equation it can be shown that the refractive contribution for all normally observed clouds and rain is small (about 0.6N units maximum for cloud (2 gm/m^3 LWC) and 0.5N units maximum for rain (100 mm/hr)).

To date, Enenstein's equation remains unverified. Considerable controversy exists regarding the reality of his assumptions. This controversy will probably not be resolved until measurements of propagation velocity through cloud and rain are made in conjunction with measurements of cloud physics parameters.

No method exists to allow computation of the refractive contribution of suspended ice particles. These particles undoubtedly contribute less per unit mass than do water droplets, since the dielectric constant of ice is less than that of water. Knowledge of their exact contribution

---

* The constants used here by Enenstein differ from those used by us.

also awaits experiment.

Fortunately for the purposes of the present study, the contribution of solid and liquid water mass to the total refractive index seems negligible. Errors introduced appear to be of the same order or less than other errors of measurement or calculation.

The very considerable measurement error that could occur, if water mass were permitted to enter the sensing cavity of the refractometer instrument, was avoided in this study. As installed in the B-29 aircraft, the cavity was mounted in a reverse flow duct. The air intake for the duct was a tube which extended some eighteen inches into the airstream and curved backward (see Fig. 1). The tube end was flanged; the opening faced downstream. Air drawn through the tube contained no liquid or solid particles, since the free stream momentum of the particles effectively prohibited their entry.

2.2 Refractive Index Changes

With proper recording equipment it is a simple matter to measure microscale fluctuations in refractive index. For our purposes, neither the resonant cavity nor the electronic circuitry of the refractometer imposes restrictive response times. Measurement lags are due solely to recorder design and the rate at which the sensing cavity is flushed. It is fortunate that the refractometer instrument exists; for it would be unsatisfactory at present to attempt to determine rapid refractive index changes from separate measurements of the independent atmospheric parameters, the chief difficulty being that humidity cannot be measured rapidly and accurately. The refractometer also obviates the computational inconvenience of working through the refractive index equation.

The University of Texas refractometer used by us is primarily a relative indicator. It measures refractive differences with an accuracy of about ± 1 N unit. With some difficulty, it can be calibrated to give absolute index values to about ± 5 N units. This error can be reduced by taking into account temperature and pressure effects on the cavities

By making simultaneous measurements of refractive index, temperature and pressure; humidity can be computed. In this way all independent atmospheric parameters contributing to refractive index can be isolated. The humidity computation is greatly simplified for measurements made at a constant pressure, as most of ours were.

Differences in refractive index measured from an aircraft result principally from spatial variations in one or more of the independent atmospheric parameters. By differentiating the refractive index equation (Eq. 1) and writing a corresponding difference equation, we can see how such differences arise.

$$dN_A = \frac{3.70 \times 10^5}{T^2}\ de - \left(\frac{74.4P}{T^2} + \frac{7.40 \times 10^5 e}{T^3}\right) dT + \frac{74.4}{T}\ dP \qquad (3)$$

and

$$\Delta N_A = \frac{3.70 \times 10^5}{\bar{T}^2}\ \Delta e - \left(\frac{74.4\bar{P}}{\bar{T}^2} + \frac{7.40 \times 10^5\ \bar{e}}{\bar{T}^3}\right) \Delta T + \frac{74.4}{T}\ \Delta P, \quad (4)$$

where the bar signifies an average value. (The second order term, $-\frac{74.4e}{T^2}$ in Eq. (1) was ignored.)

In a typical aircraft pass through clouds, values of the quantities in Eq. (4) might be: $\bar{T}$ = 278°K, ΔT = +2°, $\bar{e}$ = 6.5 mb, Δe = +4.4 mb (a relative humidity change of 50 per cent), $\bar{P}$ = 700 mb, ΔP = +3 mb (an altitude change of 100 feet). Thus the terms contributing to ΔN_A in Eq. (4) would have the values,

$$\Delta N_A = 21.2 - 1.8 + 0.8 = 20.2.$$

It can be seen that the first term on the right hand side of Eq. (4) is by far the largest. Under all but extremely cold conditions this humidity term will always predominate. (The fact that Δe and $\bar{e}$ in Eq. (4) are of the same order doesn't influence this statement, since the term containing $\bar{e}$ is small.)

Since variability in the water vapor content of the air is the primary cause of refractive inhomogeneities, those regions in the atmosphere in and around clouds are quite naturally suspected as being regions of considerable refractive index change. Early refractometer flights by Crain and Deam,[7] of the University of Texas, indicated this to be true; more recent flights by Rogers and Chapman, Electronics Research Directorate, Air Force Cambridge Research Center, add further substantiation.

2.3 Mechanisms of Cumulus Convection

It is important to understand the dynamics of cumulus clouds to be able to interpret measured refractive index changes. An understanding of the reasons for these changes will allow a logical prediction from the more common, nonaircraft data.

Problems relating to cumulus cloud dynamics have been treated in various ways since the dawn of meteorological science. For many years the cumulus cloud was considered the saturated (and thus visible) upper portion of a vertical air current having its base at the ground. The temperature lapse rate below the cloud was assumed to be dry adiabatic, that in the

cloud moist adiabatic. The temperatures in the cloud for some distance above the base were, therefore, believed to be considerably higher than the surrounding temperatures, thus giving the cloud great buoyancy. These ideas, in essence the "parcel method," have been used for a long time to explain and help predict (with some success) the development of cumulus clouds and thunderstorms. A later development, the slice method, Bjerknes[4] and Petterssen,[20] included the effect of the descending environment on the temperature contrast between cloud and dry air. This development did not improve the prediction of cumulus cloud formation. It appears (Ludlam and Scorer[11]) that the compensating downflow of air does not necessarily occur in the immediate vicinity of the cloud.

Observation and theoretical calculations concerning trade wind cumulus made by personnel of the Woods Hole Oceanographic Institution, first by Stommel[25] and then later by Malkus,[16] emphasize the strong effects of mixing with the environment. Austin[1] and Austin and Fleisher[2] worked out a theoretical circulation model for the cumulus cloud, assuming a steady upward flow (jet) and mixing (entrainment) of dry air from the sides. Houghton and Cramer,[9] at Massachusetts Institute of Technology, and Bunker,[5] of Woods Hole, later worked out the theoretical details of entrainment in the jet model.

Careful study of time lapse pictures of cumulus clouds led Scorer and Ludlam[23] to the development of a bubble theory of convection which emphasized the intermittent nature of convection, mixing only occurring in the wake of the bubbles. Further field, laboratory, and theoretical work done jointly by Malkus and Scorer[17] and Scorer[24] indicates that a combination of the bubble and mixing theories best describes the cumulus cloud dynamics and distribution of physical properties. There probably is no single theory of cumulus convection. Several processes and types of circulation predominate for various sizes of cumuli. The smallest-sized cumulus is close to being the visible upper portion of a random turbulent eddy or small rising bubble. The medium-sized cumuli may be the visible evidence of a series of bubbles and wake air which rise into undisturbed air, mix, gain momentum and lean down-shear (usually the same direction as downwind) and evaporate. A more vigorous family of bubbles may result in a larger overall cloud mass with individual bubbles rising well into the upper undisturbed air and disappearing down-shear, while the main mass develops a more steady inflow into the base (as reported by glider pilots). At this stage the intermittent bubbles may have their source in the middle of the cloud, as envisioned by Malkus and Scorer.[17] In the final or thunderstorm stage, a quasi-steady circulation has developed which is associated with the entire thundercloud mass. This circulation varies with the age of the thunderstorm, as described by Byers and Braham.[6]

The medium-sized cumulus cloud is of greatest interest in this present study. This cloud penetrates the upper, usually drier, air mass; yet is small compared to the volume of upper dry air so that it does not appreciably moisten it or affect the general air motion. The largest and

sharpest refractive index changes are to be expected in this case. As mentioned, the type of circulation applying to the medium-sized cloud is best described by a modification of the bubble theory. A composite bubble scheme is portrayed in Fig. 2 and is discussed below. The scheme seems applicable to our summer's data. Some extra touches have also been added to Fig. 2, as suggested by this data.

Briefly, the bubble theory says that disorganized small-warm-volumes will coagulate into larger bubbles between ground and bubble forming level. Bubbles rise and grow by collecting smaller bubbles, but they also lose some of their substance along their upper skin and along the wake, a region of mixing with the surrounding air. One of the larger bubbles is shown in Fig. 2. The wake (indicated by the "springs") is rising relative to the ground below the convective condensation level, but it rises more slowly than the bubble head. Above the condensation level the wake and the skin of the cloud may fall relative to the ground and to the bubble head, because of the cooling effect of the evaporating cloud. The cloud base first appears at (3), the convective condensation level (a level whose altitude is governed primarily by the ground moisture content); later at (5) and (6) the base rises because it becomes part of the wake region (a region containing a mixture of air from the surface and intervening altitudes). When there is an inversion with wind shear our observations indicate a blocking effect of the cumulus bubble, so that some of the dry air above the inversion is dynamically forced downward around the edge of the clouds. This forced current is presumably assisted by downward-moving, evaporating, cloud air at the cloud edge, particularly in the older stage of the cloud. However, when the cloud or bubble first penetrates the inversion, all parts may be moving upward relative to the inversion and the ground.

Figure 2 is illustrative of a "one" bubble cloud. As stated, a family or series of bubbles is usually involved. If the cumulus builds to medium size, a modification of the bubble scheme is necessary. The cloud then appears to attract a steady stream of bubbles with the result that a quasi-steady current rises into the base area. However, bubbles still appear to be the principal elements of the circulation, breaking the upper portion of the cloud (space and timewise) into a series of puffs. Mixing with the environment occurs above the base along the skin of the individual bubble or puff (perhaps indicated in some cases by what we later call the transition zone (x_t) of our cloud passes) and also between bubbles where large volumes of outside air are trapped inside the cloud to eventually mix with it (indicated in our data by marked dry spots in the cloud interior). The clouds of interest in this study have diameters several times those of the individual bubbles; the center of the cloud is, therefore, protected to a large degree from the desiccating and cooling effect of mixing with the environment. The simplest type of medium-sized cumulus, where the wind shear is small, thus theoretically exhibits a cool turbulent exterior and a relatively warm interior.

3. Instrumentation

The cloud refractive index work of this Unit has been directed toward measuring the refractive changes in cloudy regions and assessing the reasons for such changes. Refractive index, temperature, pressure, humidity, and cloud liquid water content measurements, and visual and photographic observations were obtained. A B-29 aircraft, which had previously been instrumented for cloud physics research, was utilized. To outfit it for refractive index studies, a refractometer, a rapid response vortex thermometer, and a four-channel Sanborn recorder were added. An Australian type liquid water content (LWC) meter was also converted to record on the Sanborn. With this new instrumentation, refractive index could be measured to a relative accuracy of 1 N unit, temperature to a relative accuracy of .2°C, and liquid water content to within 25 per cent of actual. Response times were about .01 sec (approximately 3 feet in space at B-29 speeds) for the refractometer and vortex thermometer and .5 sec for the LWC meter. (Shortly after the end of the data period of this report the response time of the latter instrument was improved to .1 sec.)

3.1 Instruments

As mentioned, the sensing cavity of the refractometer was located in a reverse flow duct. Outside air was sucked through the duct, preventing particles from entering.

Refractive index values measured in such a duct do differ somewhat from free stream values. This is the result of aerodynamic effects about the duct intake tube and within the duct and cavity. A correction can be made, providing that temperature and pressure are known both within the cavity and in the free air. In our B-29 installation, provision was made to measure and record all these quantities. Actually, a correction is required only if absolute index values are desired. In the initial phase of this study we have been primarily concerned with relative changes under conditions where pressure was constant. An alternate technique of obtaining absolute index values under these conditions will be discussed presently.

An improved, rapid-response, vortex thermometer was designed for this study. The temperature sensing element was a 1 mil diameter wire two inches long which was wound, in an open helix, around two small insulated rods supported at one of their ends. Element resistance was nominally 14 ohms at 10°C; the characteristic time of the entire measuring circuit, which consisted of element, amplifier and recorder, was approximately .01 second.

The temperature element was positioned in the center of the vortex tube, about halfway between the entrance and exhaust ports. Its support was located downstream, effectively eliminating any air flow distortion, heat convection, or water "stream-back" errors. Heat conduction

between element and support was negligible.

The principle of operation of the vortex thermometer is well known and will not be discussed here. (See Vonnegut.[26]) Suffice it to say that our particular instrument was a tangential flow type designed according to our previous experience and that of Cornell University (Packer[19]). Its unique feature was the method of mounting the element facing into the airstream.

Two separate instruments were used to measure the liquid water content in clouds. For temperatures above freezing, measurements were made with an Australian LWC meter; under supercooled cloud conditions, a rotating-disk icing-rate-meter was substituted.

In the Australian instrument a ribbon of paper from a roll passes across a slit exposed to the airstream. Droplets impinge on this ribbon and the amount of wetting is determined from the electrical resistance of the paper. Knowing the paper calibration, paper speed, slit width and the true aircraft speed, the LWC can be computed.

The rotating-disk icing-rate-meter consists of a thin metal disk exposed edgewise into the airstream. The disk, which is about two inches in diameter, rotates slowly and supercooled water droplets strike and freeze on its leading edge. A layer of ice builds up and is rotated under a spring loaded feeler arm. The ice lifts the arm above its normal position, the amount of motion being translated electrically into a measure of the ice thickness. After measurement, the ice is scraped away. A continuous indication of the ice deposited in each single revolution of the disk is obtained. This can be related in a semiquantitative fashion to LWC.

Since the icing-rate-meter was not recorded on the rapid response Sanborn recorder, LWC resolution was appreciably lessened in supercooled clouds.

Various other parameters were also measured. However, since these measurements primarily provided auxiliary or "check type" information, they will not be discussed here. Those instruments which were available and which were usually operated during flight are listed in Fig. 1. Their location on the aircraft is also shown.

3.2 Aircraft Positions

There were four cloud physics positions in the aircraft, as shown in Fig. 1: the nose observer, position 2; the forward instrument operator, position 11; the refractometer controller, position 24; and the waist instrument operator, position 44.

The nose observer planned and controlled the flight. He made visual and photographic observations of the weather situation and operated

switches which marked on an Esterline-Angus, 20 pen recorder the time of entry (exit) into cloud, rain, snow, etc. and the time of a photograph or other event. He recorded his observations verbally (by means of a tape recorder) or in written form.

The forward instrument operator controlled and monitored most of the cloud physics instruments. He also made detailed observations (written and tape recorded) to note the presence and types of all ice crystals and hydrometeors. (These observations were made by watching the particles impinge on the flat, black-colored face of a "stick" which extended out into the airstream. White scales engraved on the black face facilitated size and number determinations.)

The refractometer controller operated and monitored the performance of the refractometer, the vortex thermometer, and the thermometer mounted in the refractometer duct. Normally, this person would also operate the Capillary Collector LWC meter; however, during these flights the instrument was inoperative.

The waist instrument operator tended most of the recorders, monitored the power from the inverters, and operated the tape recorder. Early during each flight, he also set up and activated the master timing equipment which provided synchronism for all flight records.

4. Flight Program

The program objective is to obtain an adequate, three dimensional sampling of the refractive index-meteorological structure of regions with cumuliform clouds so that the general limits of refractive index variability over the United States can be specified, and the physical reasons for variability determined. Once the reasons are established, synoptic forecasts of future refractive conditions become feasible and a variety of charts showing the geographical, seasonal, monthly, occurrence frequency, etc. features of refractive conditions can be constructed from climatological data.

To date, this objective has not been attained. Although the several flights have yielded a considerable amount of excellent data, a semicomplete analysis has been made for only a few select situations. The resulting information, while permitting general statements concerning the structure of cloudy regions, prohibits precise specification of mechanisms. Certain correlations between observation and meteorological theory are apparent, but their integrated implications are as yet unclear

The program has been hampered by the usual lack of trained personnel, by the fact that the B-29 type aircraft is semiobsolete, and because of the practical and legal limitations regarding mode of flight. All possible steps have been taken to alleviate the first two difficulties; the latter one is basic. It has limited our data gathering and has been the major

influencing factor in our selection of locales for study.

To obtain a complete three dimensional picture of the refractive index conditions over an area, restrictions to manner of flying are intolerable. Clouds and surroundings must be probed at various altitudes and in several directions. It may also be desirable to penetrate individual clouds several times. In practice, the only safe way in which these freedoms can be obtained is to fly in an off-airway area under ground radar control. Flight under VFR rules is unsatisfactory; the rules prohibit entry into cloud. IFR rules are equally bad in that deviations from flight altitude or course must be CAA approved. (Securing such approval is time consuming and frequently an approvable change differs appreciably from that requested.) Nonground-controlled flight in off airways regions is risky in that other aircraft, obscured by clouds, may be flying a collision course. Flight in off-airways areas under radar control is the only really acceptable method. Unfortunately, establishing such a setup is difficult. During the period reported herein, we utilized a ready-made setup in Tucson, Arizona, but could not get one in the New England area (subsequently an arrangement has been worked out). For the most part, in the interest of job accomplishment, we accepted the calculated risk of noncontrolled flight in off-airways areas.

Refractive index data were gathered on nine flights during the period 1 June to 1 August 1955. Five flights have been analyzed to the extent reported herein. Of these, four were flown solely for project purposes; the other was a flight wherein useful data were obtained while the aircraft was in transit. The time and location of each flight are given below. The ones analyzed are marked with an asterisk.

*22 June,	0743-1047 MST	Near Pikes Peak, Colorado
23 June,	1447-1645 MST	Vicinity of Denver
*24 June,	1130-1853 EDT	Cross-country, Denver-Boston
*30 June,	1347-1705 EDT	NW of Boston
1 July,	1356-1746 EDT	NW of Boston
17 July,	1125-1417 MST	Cross-country, Boston-Tucson, Arizona
*19 July,	1201-1541 MST	NE of Tucson
*31 July,	1105-1928 MST	NE of Tucson, cross-country Tucson-Los Angeles and off coast near Los Angeles
1 August,	1035-2205 MST	Cross-country, San Bernardino, California-Boston

Tucson was selected as a base of operations because the Institute of Atmospheric Physics at the University of Arizona was making extensive studies of cumulus clouds and the University of Chicago, under Air Force (GRD) contract, had a radar ground control system worked out for a cloud physics aircraft. An additional attraction was the fact that cumulus clouds are very prevalent over Arizona during July.

5. Analysis Methods

The analysis was designed to extract a maximum of potentially usable

information from the flight data. Specific analysis objectives were:

a. To obtain the measured gross scale refractive index characteristics of cloudy regions for comparisons with these same characteristics as determined from radiosonde data.

b. To ascertain the degree of refractive inhomogeneity in these regions by determining the intensity and extent of refractive gradients in clouds, in the clear surrounding clouds, and at cloud-air boundaries.

c. To establish the detailed microrefractive structure of individual clouds under various synoptic meteorological situations and to relate this to the visual and meteorological cloud structure and to the mechanisms of cloud formation, growth, and decay.

d. To provide three dimensional information regarding the cloud coverage conditions of the lower atmosphere for each flight. (From this the gross refractive index distribution can be assessed.)

5.1 Calculated Refractive Index Cloud to Air Differences ($N_s - N_a$) Compared with Measured Values

A calculated refractive index profile representing the air outside the cloud was computed for each of the regions probed. Data were taken from the nearest radiosonde stations and compared with the measured aircraft data. The principal assumptions made in utilizing radiosonde data for this purpose were:

a. Air through which the radiosonde ascended was characteristic, space and timewise, of the air probed by the aircraft.

b. The radiosonde did not intersect a cloud.

c. The lag of the humidity element (a serious difficulty in computing ducting effects) was not serious enough in this case to affect the overall result. Lag was, in fact, beneficial since it served as an averaging tool.

A second refractive index profile was computed to represent the air inside the cloud and in the bubbles or thermals below the cloud. In order to do this, certain additional assumptions were made:

d. The air inside the cloud was at the same temperature as the air outside (observations showed this to be very nearly true).

e. The air was saturated (i.e. at 100 per cent RH) inside the cloud.

f. The air below the cloud in the bubbles (thermals) contained the same amount of water vapor as the air at cloud base.

A few comments on some of these assumptions are pertinent. The density of radiosonde stations in the American network is not sufficient, spacewise or timewise, to show the frequent, rapid changes in moisture distribution which actually occur. Most of the differences between computed N_s-N_a and measured N_c-N_A shown in our data are probably due to this fact.

The amount of cloud coverage is usually small when large N_c-N_A values exist. The probability that the radiosonde remains in clear air in its ascent is, therefore, good for the conditions of greatest interest here.

The classic representation of cumulus cloud air temperature would require the cloud temperature to be considerably higher than the surrounding air. Measurements from aircraft over the past ten years by others, as well as ourselves, have shown that temperatures inside cumulus clouds are close to the external temperature. Considerable controversy has existed on this subject; methods for measuring cloud temperature were severely criticized (and correctly so); however, recently improved instruments, such as the vortex thermometer, plus theoretical work on mixing (entrainment) have indicated the reality of these measurements. Figures 23 and 49 from our recent data indicate that if an average cloud temperature is required, the outside air temperature is a good estimate. It is surprising to note that this is true even for the case of a cloud penetrating an inversion. The mixing process between cloud and outside air apparently proceeds more rapidly than previously imagined.

It can be shown that the humidity in clouds must be nearly 100 per cent when the cloud is composed of the normal small drops. The evaporation rate of such drops is so great that they do not exist long in an unsaturated atmosphere. In general, our observations have borne out these statements. Small portions of the cloud have been found to have humidities down to 90 per cent -- the cloud in this case was probably composed predominantly of large-sized cloud drops (approaching drizzle size) which were evaporating.

The frequent good check between cloud base and the convective condensation level (as computed from that value of water vapor content which characterizes the layer near the ground) implies that the bubbles or the more continuous type thermals (in larger clouds) rise from lower levels without mixing appreciably with the air around them, at least in that region below the cloud.

Two calculated refractive index profiles (one for N_a, one for N_s) were plotted for each region for a time corresponding to that of the flight data. Differences between these two profiles provided altitude plots of N_s-N_a and N_b-N_a to be compared with similar parameters derived from measurements of the aircraft instruments.

On the cross-country flights, comparisons of N_s-N_a computed and measured are made at only one altitude, the flight altitude. On the days

where many cloud passes were made at numerous altitudes, a scatter diagram of the measured N_C-N_A values is shown, upon which the computed difference profile is drawn for comparison.

5.2 The Degree of Refractive Inhomogeneity In and Around Cumulus Clouds

A number of parameters were developed to describe, in numerical terms, those various characteristics of the fluctuations in refractive index recorded in and around cumulus clouds. Selection was based on present or possible future pertinence to the problems of radio-radar propagation. Their development permitted construction of the scatter diagrams shown in Figs. 12-20, 38-46, and the summary diagrams of Figs. 21, 22, 24, 47, 48, and 50. Although the parameters must be subjectively evaluated, the degree of subjectivity involved in analyzing to assign numbers is not sufficiently serious to negate the validity of the diagrams nor the conclusions.

The parameters chosen are most readily explained by reference to Fig. 3 and the Table of Symbols. Reproductions of certain original records of refractive index fluctuations through clouds are shown in Figs. 7, 9, 11, 31, 33-37, 55, 59 and 63.

5.3 Structure of Single Clouds

Continuous traces of refractive index, temperature and liquid water content were obtained on the Sanborn recorder during each pass through a cumulus. Pressure, airspeed, and compass heading were recorded by an aerograph. Pictures were taken to record cloud appearance, several being taken at spaced intervals to enable triangulation for cloud dimensions.

We wished to obtain a comprehensive picture of the microrefractive and micrometeorological structure of single clouds and to relate this to the cloud appearance and to various mesoscale synoptic meteorological features (such as wind shear, instability, vertical structure of surroundings, etc.). To do this we could not utilize the records in their original form. For one thing, the Sanborn record was taken at a high chart speed and the amplitude fluctuation of the traces was only a small fraction of the length of chart which pertained to a single cloud pass. For another, we wished to derive other useful meteorological parameters from the measured quantities and plot their traces along with the other traces. We wanted all traces for an individual cloud to be on a single diagram so that we could gain intelligence by observing interrelationships between variables. In presentation, we would show this diagram in conjunction with a dimensioned cloud photograph.

It was apparent that the fluctuations in the traces on the Sanborn record had to be magnified. Likewise, it was obvious that the task of replotting high resolution traces was enormous, and that the problem of computing derived quantities and plotting their traces was equally great.

Machine methods were indicated. Fortunately, the data were such that a relatively simple machine could be designed to accomplish our aim.

In essence, the machine worked as follows: The pertinent portion of the Sanborn chart was placed around a drum. The drum rotated slowly, moving the chart. A stylus was affixed to a frame in front of the drum in such a manner that the tip of the stylus rested on the moving chart. An operator could move the stylus to follow one of the traces on the chart (refractive index, temperature or liquid water content). Stylus motion rotated a variable voltage dividing resistor. By suitable circuitry, resistance changes were converted into voltage changes and fed into a recording potentiometer (a rapid response, two pen, Brown Instrument Co. type). The trace on the Sanborn chart was reproduced on the Brown instrument; total trace length remained the same (drum speed and Brown chart speed were the same, but the trace fluctuations were amplified. With the desired absolute scale, amplification could be adjusted so that the reproduced trace was an accurate plot of the measured quantity.

In actuality, there were two styli. Two operators were used; two traces could be reproduced at one time. Traces showing the horizontal variation through clouds of the three measured quantities were obtained in this manner. Vertical variations were excluded, since passes were flown at constant pressure altitude.

To obtain a trace of absolute refractive index an assumption was necessary. Our refractometer measured relative changes and the recorded trace had a relative scale. In order to assign an absolute scale, absolute refractive index values must be known at one or more points on the recorded trace. We obtained one such value for each cloud pass by assuming that the air was saturated in the mid-portion of the largest region of homogeneous cloud.

Three parameters were derived from the measured quantities. They were: 1) saturated vapor pressure, 2) vapor pressure, and 3) virtual temperature. It was possible to obtain traces of each, using the machine.

A trace of saturation vapor pressure was obtained from the trace of temperature. The relationship between change in saturation vapor pressure and change in temperature is given by the Clausius-Clapeyron equation,

$$\frac{d\, e_s}{dT} = \frac{L}{T\,(v_g - v_f)} \qquad (5)$$

where: e_s = saturation vapor pressure
T = absolute temperature
L = latent heat of vaporization

v_g = specific volume of water vapor

v_f = specific volume of liquid water

Writing a corresponding difference equation, we can neglect v_f since $V_g \gg v_f$. Thus:

$$\frac{\Delta e_s}{\Delta T} = \frac{L}{T v_g} \tag{6}$$

In our application, ΔT is the horizontal change of temperature; Δe_s is the horizontal change of saturation vapor pressure. Since both L and v_g vary appreciably with the atmospheric variables, $\Delta e_s/\Delta T$ is not simply related to T. However, the numerical value of $\Delta e_s/\Delta T$ does not change appreciably with small changes in these variables, and therefore we can evaluate Eq. (6) for the average conditions which prevailed during the aircraft pass. We may then compute values of Δe_s from ΔT. The circuitry of the machine was such that variations in temperature (i.e., the stylus movements that occurred when the temperature trace was tracked) were multiplied by the factor $\Delta e_s/\Delta T$. A trace of e_s was drawn on the Brown recorder and scaled in absolute units.

A trace of vapor pressure was obtained from the traces of refractive index and temperature. The relationship between vapor pressure (e), temperature (T), and refractive index (N) is best shown by solving the refractive index equation [Eq. (1)] for e. (The term $\frac{74.4e}{T^2}$ in Eq. (1) was ignored.) Thus,

$$e = 2.703 \times 10^{-6} T^2 N_A - 2.01 \times 10^{-4} TP \tag{7}$$

Now the total differential of e is,

$$de = \frac{\partial e}{\partial N_A} d N_A + \frac{\partial e}{\partial T} dT + \frac{\partial e}{\partial P} dP, \tag{8}$$

and since e is not a function of P and since in our passes $dP \cong 0$, this equation reduces to,

$$de = \frac{\partial e}{\partial N_A} d N_A + \frac{\partial e}{\partial T} dT. \tag{9}$$

The corresponding difference equation is,

$$\Delta e = \left(\frac{\Delta e}{\Delta N_A}\right)_T \Delta N_A + \left(\frac{\Delta e}{\Delta T}\right)_{N_A} \Delta T \qquad (10)$$

From Eq. (7) we can write,

$$\left(\frac{\Delta e}{\Delta N_A}\right)_T \cong \frac{\partial e}{\partial N_A} = 2.7 \times 10^{-6} T^2 \qquad (11)$$

$$\left(\frac{\Delta e}{\Delta T}\right)_{N_A} \cong \frac{\partial e}{\partial T} = (5.4\ T\ N_A - 201\ P) \times 10^{-6} \qquad (12)$$

Over the range of N_A and T observed during aircraft passes, the above approximations hold adequately well. (Errors are an order of magnitude less than machine reproduction errors.) Pressure is, of course, a constant in the latter equation.

With the machine, it was possible to "track" simultaneously the recorded traces of N_A and T. The changes in N_A (stylus movements) were multiplied electronically by $(\Delta e/\Delta N_A)_T$ and added to the changes in T multiplied by $\left(\frac{\Delta e}{\Delta T}\right)_{N_A}$. Pen motions of Δe [a solution of Eq. (10)] resulted on the Brown recorder and a trace of e was obtained when an absolute scale was specified.

A trace of virtual temperature (T_v) was also obtained from the traces of refractive index and temperature. In a manner analogous to the way we handled vapor pressure and knowing that

$$T_v \cong T\ (1 + .379\ e/P), \qquad (13)$$

we can utilize Eq. (1) to write,

$$T_v \cong T + \frac{1.024 \times 10^{-6}\ T^3\ N_A}{P} - 7.62 \times 10^{-5}\ T^2 \qquad (14)$$

The total differential is,

$$d T_V = \frac{\partial T_V}{\partial N_A} d N_A + \frac{\partial T_V}{\partial T} d T + \frac{\partial T_V}{\partial P} d P. \quad (15)$$

During our aircraft passes through clouds, $d P \cong 0$, thus Eq (15) reduces to,

$$d T_V = \frac{\partial T_V}{\partial N_A} d N_A + \frac{\partial T_V}{\partial T} d T, \quad (16)$$

and the corresponding difference equation is,

$$\Delta T_V = \left(\frac{\Delta T_V}{\Delta N_A}\right)_T \Delta N_A + \left(\frac{\Delta T_V}{\Delta T}\right)_{N_A} \Delta T. \quad (17)$$

From Eq. (14) we can write

$$\left(\frac{\Delta T_V}{\Delta N_A}\right)_T \cong \frac{\partial T_V}{\partial N_A} \cong \frac{1\,024 \times 10^{-6}\, T^3}{P} \quad (18)$$

$$\left(\frac{\Delta T_V}{\Delta T}\right)_{N_A} \cong \frac{\partial T_V}{\partial T} \cong 1 + \frac{3.07 \times 10^{-6}\, T^2 N_A}{P} \cong 1.524 \times 10^{-4}\, T \quad (19)$$

In Eqs. (18) and (19), P is a constant and over the range of observed N_A and T values in clouds the approximations hold with no serious loss of accuracy.

By simultaneously "tracking" the recorded traces of N_A and T, multiplying ΔN_A and ΔT changes by $\left(\frac{\Delta T_V}{\Delta N_A}\right)_T$ and $\left(\frac{\Delta T_V}{\Delta T}\right)_{N_A}$ respectively, and adding, we were able to use the machine to solve Eq. (17) for ΔT_V. A trace of T_V was obtained on the Brown recorder.

In all those diagrams presented herein which show aircraft passes through clouds, the parameter traces were obtained in the above manner. Table 1 provides information showing the estimated accuracy of final results. In general, the inaccuracies due to the reproduction technique are smaller than or equal to the errors of measurement for relative changes and relative positions along the trace. Measurement errors are appreciably

Table 1. Table of Inaccuracies

	Refractive Index (N units)		Temperature (°C)		Liquid Water Content (%)		Saturation Vapor Pressure (mb.)		Vapor Pressure (mb.)		Virtual Temperature (°C)	
	Rel	Abs	Rel	Abs	Rel	Abs	Rel	Abs	Rel	Abs	Rel	Abs
1. Estimated instrumental measurement error	±1.0	±1.5	±.2	±1.0	±10	±25						
2. Estimated inaccuracy in deriving parameter from measured quantities							±.2	±1.0	±.2	±.3	±.5	±1.5
3. Inaccuracy of reproduced trace in showing recorded trace when similar points are compared; i.e. maximum points, minimum points, inflection points, etc. (an rms value)												
(a) Regions of large fluctuations	± .2	± .2	±.3	± .3	±10	±10	±.05	± .05	±.1	±.1	±.3	± .3
(b) Regions of small fluctuations	± .2	± .2	±.2	± .2	±10	±10	±.05	± .05	±.1	±.1	±.2	± .2
4. Inaccuracy of reproduced trace in showing recorded trace when considering time displacements; i.e., the operator in reproducing the record has led or lagged the fluctuations (an rms value)												
(a) Regions of large fluctuations	±5.0	±5.0	±.5	± .5	±10	±10	±.1	± .1	±.2	±.2	±.7	± .7
(b) Regions of small fluctuations	±2.0	±2.0	±.3	± .3	±10	±10	±.05	± .05	±.1	±.1	±.3	± .3

Inaccuracies marked with the same symbol have a high degree of positive correlation.
Total inaccuracies of parameter are the rms sum of 1 and 3 or 4 or of 2 and 3 or 4.

greater for absolute values. Reproduction inaccuracies are greater for individual points on the trace, due to slight time (space) displacements of the measured values during reproduction.

5.4 Three Dimensional Distribution of Clouds in the Atmosphere

The analysis of the flights of 30 June and 19 July is sufficiently advanced so that we can present a rather detailed picture of the refractive index conditions in and near clouds. The usefulness of this information for the computation of radio-radar propagation effects is greatly enhanced by specifying the distribution and volume extent of clouds in the atmosphere. For the above days we have prepared diagrams showing our best estimate of cloud coverage in several altitude ranges. We have also drawn a cloud cross section for the vertical plane of maximum cloudiness. The diagrams are left in general form; the user can combine them with our cloud refractive index information in any manner pertinent to his needs.

6. Data

Some of the data gathered during the Summer of 1955 are displayed in the back of this report. Two flights were extensively analyzed. The flight of 19 July, a case of relatively simple atmospheric stratification, is presented first. That of 30 June, where the atmospheric structure is complicated by a sharp inversion, is next. Only a limited number of passes were made through clouds on the other days analyzed. A comparison of the analyzed pass data with the radiosonde derived data will illustrate some of the points of difference and show the inherent difficulty of comparing calculated and measured refractive index changes.

The analyzed data for each day are arranged in a specific order First the general atmospheric structure is indicated by a plot of the data from the nearest radiosonde. Calculated refractive index profiles and differences come next, then individual cloud passes, which show typical features of the measured refractive index changes as well as the variation in the associated meteorological parameters. For the two extensively analyzed days, an additional series of scatter diagrams shows the altitude variation of the detailed refractive index changes in and around clouds. The first of these scatter diagrams presents the principal result of these studies; i.e., the comparison between the calculated refractive index changes and those observed. Nine bar graphs then show the frequency of occurrence of the various values of those parameters which were chosen to describe the character of the refractive index changes

In order to calculate the cloud refractive index from radiosonde data, an assumption was made that the temperature in cloud was equal to the ambient temperature level for level. The assumption was tested by plotting both the adjusted cloud temperatures and the adjusted ambient temperatures versus altitude. (The adjustment allowed for the general atmospheric temperature changes during time of flight.) The temperature profiles were

also of obvious interest in the study of the mechanisms of cumulus convection.

For use in connection with specific problems of radio propagation through cumulus cloud systems, several charts were plotted to show the average conditions prevailing during the extensively analyzed days of 19 July and 30 June.

6.1 Data for 19 July 1955

Considerable data were obtained northeast of Tucson, Arizona on 19 July, during that region's wet monsoon period. The plot of radiosonde data on the pseudoadiabatic diagram, Fig. 4, is according to standard practice; i.e., T_d = dew point temperature, T = temperature, q_b = specific humidity $\cong$ mixing ratio in g/kg at cloud base. The iso-value of q_b at the cloud base is carried downward to indicate the approximate source level of bubbles, assuming no mixing. Cloud base and tops are indicated by the cloud sketch. This diagram indicates that the temperature structure was quite unstable, with a minor inversion at 17,000'. (Aircraft measurements do not show this inversion.) Most of the clouds were topped at 18,000'; however, a few went to great heights, 30-40,000'. The radiosonde data show that the instrument rose through a less cloudy region than that of the aircraft data. The dew points computed from the refractometer records scatter around the radiosonde dew point curve and the scattering is greater at the lower elevations because of the presence of moist remains of previous clouds or downdrafts of dry air caused by return circulations from nearby clouds. Note that the specific humidity at cloud base (q_b) is that which is characteristic of the layer from 3,000' to 10,000' and that this is essentially the surface layer, since the terrain of this region ranges 3,000' to 8,000'.

The N profiles and differences computed from the radiosonde data are shown in Fig. 5. Na is computed from T and T_d (radiosonde values). N_s is computed, assuming the air to be saturated at temperature T. N_b is computed, assuming the air contains the moisture content given by q_b, Fig. 4. The cloud region is indicated by the cross hatching: therefore, N_s has meaning only in the cross hatched region. Note that the peak of the ΔN graph at 18,000' is due to the decrease in dew point temperature which exists in the radiosonde record at this height. This structure is not shown by the dew points computed from the aircraft data.

Figure 6 is a black and white reproduction of a kodachrome photograph which shows a cloud typical of those encountered on this day. The aircraft intercepted this cloud at the base of what is apparently the head portion of a cloud bubble. Note the partially detached (probably evaporating) cloud fragments at flight level. The cloud coverage was not as general as might be suggested by this particular photo.

Figure 7 is a machine plot (obtained using methods described in

Section 5.3) of the refractive index, temperature and liquid water traces, as well as the derived virtual temperature and vapor pressure traces. The solid bars show those periods when the aircraft was inside visual clouds (as noted by the observer). The arrows at the edges of the cloud (upper trace) show the distance selected from the traces as being the transition zone (x_t). The long arrow shows the interior region of cloud (C_D) as deduced from the records. This is the reduced data for the pass through the cloud of Fig. 6 just subsequent to the taking of the photograph. It is a particularly symmetrical record. Note the marked cold edge of the cloud and its warm center. In spite of the high water content, the cloud is buoyant in its center portion, but "heavy" at the edge The edge or outer skin is probably moving downward. Liquid water is present, but must be rapidly evaporating, thereby cooling and moistening the air This pass is quite typical of most on this day.

Figure 8 is a photograph of another cloud which was also probed. This cloud is apparently not as vigorous as the previous one; it may be in a late stage of its life cycle. The area cloud coverage which existed over this particular region can be noted by looking at the right side of the photograph. It is representative of the average coverage for the day. The high cloud sheet present on the left is the product of anvil clouds from the few thunderstorms which developed; and is at a great distance from the plane compared with the other visible clouds.

Figure 9 shows the data gathered on passing through the cloud of Fig. 8. Again a symmetrical pattern appears The dips in the refractive index and vapor pressure curves that appear about one third of the way in from the cloud edges are a frequent characteristic of the cloud passes; they apparently mark the inner boundary of the outer large cells or older bubbles. The temperature and virtual temperatures in this cloud are everywhere lower than the ambient temperature, indicating that the cloud has lost its buoyancy in the place probed and that it is descending or will descend to dissipate. However, in the central portion there still exists a rather uniform region of relatively higher cloud temperature. The refractive index and humidity values next to the cloud are lower than the average ambient values; at this altitude this condition is probably caused by a narrow band of downward flowing dry air (see Fig. 24).

Figure 10 is a photograph of cumulus congestus clouds taken from an altitude near the average top altitude. The aircraft entry point, marked with an X, is quite near the cloud top. The top presents a vigorous appearance, characteristic of a newly rising turret or bubble.

The recorded and computed values shown in Fig. 11 indicate that much of the mid-portion of the top volume of this cloud has come from the cloud interior which would be unmixed and fairly buoyant. The narrow transition zone encountered on entering this cloud is presumably due to the vigorous and actively rising nature of the turret The variable temperature record indicates that violent mixing and evaporational cooling occurred

along the outer edge of the top portion of the cloud as well as on the flanks (also indicated in the previous two cases). In the later portion of the pass three other bubbles or turret tops were encountered, all part of the same general cloud mass. The last two were apparently older turrets, since the internal temperatures were predominantly cooler than ambient.

The characteristics of the refractive index traces for some thirty-two passes made on the 19th of July through clouds similar to the three discussed above are summarized in the following nine scatter diagrams.

Figure 12 compares the computed and observed N differences from inside to outside of cloud. The N value on exit from cloud represents the average ambient value some distance from the cloud. The scatter of the observed differences centers almost perfectly around the computed values, except for that portion between 16 and 18 thousand feet where the radiosonde indicates a dry layer over Tucson. Aircraft data show that this layer did not exist over the more cloudy mountain region. Note the marked increases of scatter in the lower portions of the cloud, an indication that the clouds affect the environment at the lower levels to a greater extent than the upper levels.

Figure 13 is similar to Fig. 12; it shows the altitude variation of refractive index change at the cloud edge. The slightly greater scatter at upper levels here, as compared to Fig. 12, is due to the moistening effect of the cloud on the dry air immediately surrounding it.

The ΔN values plotted on Fig. 13 were converted to equivalent humidity changes and replotted in Fig. 14. For comparison, the radiosonde data are given in terms of 100 per cent minus the recorded humidity. Such presentation, in units more familiar to the meteorologist, again points to the large variability of humidity outside clouds. Minimum variability occurs in the upper cloud regions where the horizontal area of the cloud is smallest and where the volume of affected surrounding air is least. The radiosonde humidity values strike a fair average through the scatter, primarily because of the slow response time of the humidity element. (This is fortunate; it means that N_A values computed from radiosonde data do truly represent the average.)

A rough idea of the interior dimension (C_D) of the clouds penetrated is given in Fig. 15. Values of C_D (also referred to as horizontal cloud distance) are plotted for the abscissa scale. The two points in the upper right hand corner are not representative of the same type of cloud as the other points; they represent passes through an incipient thundershower and associated anvil cloud.

Figure 16 shows the thickness of the transition zone as it varies with altitude. X_T is small ($< 200'$) above 17,000', becoming progressively

larger with decreasing altitude. The single very large value at 18,400' is a long transition zone and is a special case. This observation occurred under a spreading anvil cloud from which snow and soft hail were falling, the same thundercloud mentioned above. Points plotted for this cloud in the subsequent Figs. 17, 18, and 23 are also highly anomalous.

Figure 17 is a scatter diagram showing the thickness of the maximum gradient observed in each transition zone as a function of flight altitude. Greater thicknesses (more gradual gradients) exist at the lower altitudes. This fact reflects the greater frequency of occurrence of less vigorous clouds or portions of clouds in the lower levels; slower circulation allows more time for diffusion and mixing processes to smooth out temperature and humidity contrasts.

The average wavelength of the refractive index oscillations at the edge of clouds is illustrated in Fig. 18. Excluding those cases where there were no oscillations; i.e., $^{\varkappa}T/osc = \infty$; the diagram indicates a typical wavelength of 200' at the cloud base, decreasing to 100' near the top.

Figure 19 shows the maximum change in refractive index within the main cloud mass; it is a measure of the homogeneity of the cloud. The graph shows that at all altitudes there are small breaks within the cloud mass which have N values very close to ambient.

It is of interest to know whether or not the cloud affects the refractive index of the air immediately around it. Figure 20 indicates that on this day of 19 July there was, on the whole, little effect. By contrast, Fig. 46 shows a situation where there was a considerable effect.

A summary of the data for 19 July is presented in Figs. 21 and 22 in the form of frequency bar graphs. The data shown in Fig. 20 have been converted to meteorological units of relative humidity and summarized on the extreme right in Fig. 21. Otherwise, the graphs are self-explanatory

The general technique used to construct Fig. 23 has been explained in Section 6. Here the temperatures from the vortex thermometer have been corrected for scale error (in the individual pass data discussed previously this was not necessary). The dew point curve is derived by drawing a smooth line through the calculated dew points plotted on Fig. 4. The thundercloud symbols at the top of the figure indicate data from a pass through a thunderstorm. [The extremely high temperature recorded in the middle of this cloud indicates that the original source of air for this storm must have been exceptionally warm and moist (resulting in a singularly low cloud base) and no mixing of environment air could have taken place in that volume of air represented by the right hand dot.] The cloud air temperatures shown in Fig. 23 very neatly bracket the ambient air temperatures such that if one temperature must be picked as a representative cloud temperature, the ambient temperature would be a close approximation of the best average. The extension of the maximum and minimum "cloud" temperature below the

average cloud base represents data from a few passes just below the base, plus a few earlier passes through the clouds having lower bases. It is puzzling that the maximum temperature in the base region is about the same as ambient; this fact would indicate that the air had no buoyancy and, therefore, no acceleration into the cloud at this point. This lack of warm temperature at the cloud base may, however, just reflect a bias in the data; i.e., no very young clouds were penetrated at cloud base altitude; the clouds investigated were all well developed and were penetrated farther up. Probably the air feeding into the base at the time of the cloud pass was no longer part of the same bubble or bubbles which initially originated the cloud. This observation supports the thesis mentioned in Section 2.3 that once a cloud is well formed new bubbles originate within the cloud. Because of the increased cloudiness and because a steadier circulation may be set up below the cloud, subcloud bubble activity diminishes. If borne out by further observation, this would mean that the refractive index variations below the cloud base are partially a function of the size, age, and coverage of the clouds above.

An average line was visually drawn on the scatter diagrams in Figs. 12, 13, and 15 through 20. "Average" values were selected from these curves and are shown in Table 2 in conjunction with certain additional data. The values were used as a basis for drawing Fig. 24. Note that the horizontal and vertical scales in this figure are the same. Visual review of a number of cloud photographs and individual cloud pass refractive index measurements helped in the final sketching of this composite picture. Because we haven't yet separated the aircraft cloud passes on a basis of relationship between aircraft heading and wind shear (i.e. our flight direction relative to the lean of the cloud), the cloud shape has been sketched symmetrically about the central vertical axis. Presumably, Fig. 24 represents a cross section perpendicular to the wind shear. Air motions and cloud edge shape were sketched in such a way as to partially explain the "average" refractive index trace. A rounded cloud edge suggests a cloud which is actively growing into dry air, and displacing and mixing with this dry air. The sharp angular edges indicate either dissipating cloud or cloud which is recondensing within air having a former, partially mixed, origin.

The principal points of interest illustrated by the "average" refractive index change traces in Fig. 24 are: the equal gross change at all altitudes; the shift from relatively small gradients of refractive index in the lower levels to sharp gradients higher up; the uniformity of refractive index inside the bubble elements and above the lowest portion of the cloud, and the change with altitude of refractive index fluctuations outside the cloud.

Figure 25 shows our best estimate of the three dimensional distribution of clouds in the flight area. These two sketches were constructed from fifty-eight aircraft cloud photographs plus ground observations. In various instances we also measured the flight distance between clouds. This is an average picture, timewise, through the day. The clouds had

bases near 11,000' in the morning and were fairly uniformly distributed. During the afternoon they thickened over the mountains, spreading out in places (the 16,000' level) into an almost solid deck. The anvil cloud shown at high levels was only present for an hour or so. It is somewhat overemphasized in this average picture.

Cloud coverage patterns are very complex and Fig. 25 points this out. Clouds are not usually randomly distributed; they tend to bunch into families, wind rows, or streets. Clouds also tend to be thicker and more abundant over higher terrain. This is clearly shown.

Table 2. Average values of cloud parameters from scatter diagrams. For 19 July 1955

	Pressure Altitude - Thousands of Feet				
	13	14	15	$16\frac{1}{2}$	$18\frac{1}{2}$
C_D (ft)	5000	3200	4000	7200	1500
X_T (ft)	1100	500	400	300	80
$N_c - N_a$ (N)	12	10	9	10	11
ΔN (N)	11	10	9	11	8
$N_1 - N_2$ (N)	+2	+1	0	-1	0
ΔN_c (N)	6	6	6	7	7
X_{min} (ft)	110	90	70	44	29
Osc (#)	5	2-3	2-3	2-3	1
$M_x \Delta N_a$	4	3 1/2	3	2	1

6.2 Data for 30 June 1955

On 30 June, one of the warmest days of the month, an extensive cloud flight was made some 30-50 miles northwest of Boston. The air on

this day was dry and subsiding in mid-tropospheric levels, and was separated from a moist underlying stratum by a sharp inversion. Above the dry air, moisture was being advected in from the west. This was indicated by increasingly high clouds above the lower cumulus clouds. Some of these features are indicated on the Fort Banks sounding (Fig. 26) which was taken during the flight period (Fort Banks is on the eastern edge of Boston). The cloud cover was scattered, and clouds generally existed in large, widely spaced groups (see Fig. 51). Aircraft temperature and dew points (computed from refractive index data taken in clear air) are shown. The great scattering of dew points indicates the existence of a sharper and more variable inversion than that shown by the radiosonde data.

Figure 27 shows the refractive index profiles and difference profiles as calculated from the data shown in Fig. 26. The symbols used were previously explained in our reference to Fig. 5.

The radiosonde data (Fig. 28) and the refractive index profiles (Fig. 29) pertain to a time some four hours previous to the flight period. The missing section of the dew point curve in Fig. 28 signifies that the air in that region was too dry to give instrumental indication. A comparison with the later data illustrates the rapid changes that can occur in the atmosphere, particularly in respect to the moisture distribution. The dry air layer could have been moistened in the four hours either by convection from below through the inversion or by the advection of more moist air from the west. Other possible examples of the effect of the cumulus cloud convection on the environment will be shown later.

The photograph and pass data in Figs. 30-37 are placed in order of pass altitude. The first cloud pass was made at the level of the top of the inversion. Figure 30 is a photograph of the cloud probed. Unfortunately, it is of poor quality; however, it does show that the top edge of the cloud is sharp and that the lower cloud regions are made up of ragged, broken-up elements. This was a typical cloud structure on this day. The parameter traces for this first pass are shown in Fig. 31; symbols and scales are the same as those described in the Fig. 7 discussion. This cloud pass was typical of those taken near or at the inversion level. The presence of downcurrents just outside the cloud is suggested by the very low relative humidities and the warm sensible and virtual temperatures which occur primarily on the exit side. (The cloud after penetrating the inversion apparently forms a block in the more rapidly moving airstream above the inversion. Air is forced to move around the block and some of it is forced downward. Presumably, in this Fig. 31 case the air forced down is air from above the inversion.) These presumed downcurrents increase the change in refractive index between inside and outside the cloud by almost a factor of 3 over what might otherwise be expected. Note that this cloud is a "cold" cloud; i.e., its temperature is predominantly colder than ambient. This is typical of clouds penetrating a substantial inversion. Its virtual temperature is also colder than ambient, indicating that the cloud air is more dense (heavier) than the environmental air. The liquid

water content of the cloud is shown in the bottom trace. During this particular data period the Australian instrument had a large response time; therefore, detailed fluctuations are not resolved inside this cloud. The water content indicated is about one-tenth of that to be expected from unmixed lifting of a bubble from the condensation level upward (i.e., bubble temperature decreasing with altitude at the moist adiabatic lapse rate). This discrepancy indicates that considerable mixing occurs between bubble air and the ambient air at cloud level whenever the cloud is in a late stage of its history and/or is rapidly falling and evaporating This latter condition is not well verified by the appearance of the cloud in Fig. 30; there the cloud still shows a sharp outline.

The second analyzed cloud pass of 30 June was quite similar to the one just discussed. The photograph, Fig. 32, shows external cloud characteristics much more clearly than Fig. 30. (The difference is probably due to more appropriate camera settings and not to differences in the amount of atmospheric haze. A distinct haze layer was, however, present on this day from the surface to 9,000'.) Note the very ragged base of the cloud in Fig. 32, indicating much mixing of wake air with ambient air.

The aircraft data for the pass through this cloud (Fig. 33) is similar to the pass shown in Fig. 31; however, at this slightly lower altitude the air far removed from the cloud is typical of the air below the inversion. The marked refractive index gradient at 6,100' is the maximum gradient that we have found for clear air conditions. The low water content again points to considerable mixing of the whole cloud mass with the ambient air.

The pass data shown in Fig. 34 was taken at an altitude 200' below that of the previous passes. It again shows the effect of cloud circulation on the environment. This cloud appears to be in a rapidly dissipating stage; very little solid cloud remains. The record also illustrates some of the difficulties in assigning values to the parameters which were chosen to describe the character of the refractive index trace. The double ended arrows should have been shown as a single arrow extending the complete distance between transition zones. It was our policy in defining cloud that if the break in the cloud was smaller than the adjacent cloud elements it was still considered a part of the main cloud mass; i.e., C_D should be continuous through a small break, here in Fig. 34 the arrows are incorrect. It is interesting to note that the humidities in the internal cloud breaks (even some of the small ones) often reach values which are characteristic of the air above the inversion rather than of the ambient air at the particular level, suggesting that the trapping of this air is also accompanied by downward motion.

Figure 35 shows the latter part of a record through a group of clouds. The dry, warm air which has, apparently, descended from above the inversion is evident at the aircraft exit point. The water content reading is about one half theoretical, as might be expected in a larger group of

clouds where mixing with the surrounding air is not as desiccating as in the case of a single bubble or cloud. Several visual cloudlets (traces for which are shown on the left hand side of the figure) were almost completely evaporated. The virtual temperature trace indicates a considerable region of buoyant warm air. This trace is the first of those presented which shows this effect.

Figure 36 presents traces through a small and apparently young cloud. This pass is one of the few analyzed for this day where really buoyant cloud elements were indicated. The dry region next to the cloud on the entrance side is less well marked than in previous cases, and is not indicated at all on the exit side. This pass was made at a level below the inversion where the less buoyant portions of the cloud spread out laterally. The 3000' zone of relatively moist air on the exit side is presumable evi dence of this type of flow.

Figure 37 shows the trace from a moderately large, moist cloud which had a broad, buoyant, center portion. Some of the dry air above the inversion is evident on the exit. The small cloud on the left hand side of the diagram shows an interesting warm-dry spot about three quarters of the way through the cloud (i.e., the cloud as defined by the refractive index record). Note also that at this level and location in the atmosphere the ambient air is very moist.

Nine scatter diagrams are presented in Figs. 38-46. They show the same type of data for our flight of 30 June as was presented in Figs. 12-20 for the flight of 19 July; i.e., they show the altitude distribution of the chosen refractive index parameters.

In Fig. 38 the measured refractive index change (N_C-N_A) from inside the cloud to well outside the cloud is compared with that computed from radiosonde data. Above the inversion the comparison is as good as can be expected. The deviation at higher levels reflects lowering of the more moist upper air to the west and northwest of Boston (above the dry strata). The great scatter of points and the extremely high values at the inversion level are presumably due to both the fluctuating movements of the inversion and to the downdraft around the cloud. The low N_C-N_A values below 8,700' reflect the effect of cloud activity in the flight areas (moistening the air below the inversion) in contrast to the clear Fort Banks area. The two observations indicated at 5,800' (just below the cloud base) were obtained late in the day toward the end of convective activity when all cloud formations were spreading out and disappearing. The spreading action would distribute the moist cloud air over larger portions of the atmosphere below the inversion, thus lowering the refractive index variations in this layer. The mixing downward of air had diminished late in the day, an action which would also lessen the refractive index contrast between air and cloud.

The refractive index change across the transition zone is shown in Fig. 39. This scatter diagram is similar to the N_C-N_A scatter diagram in

Fig. 38. It is presumed that dry downcurrents around the clouds explain the greater scatter of points in Fig. 39.

Figure 40 is a replot of Fig. 39, translated into units of relative humidity which are of more interest to the meteorologist.

The dimensions of the clouds penetrated are indicated in Fig. 41. The distance C_D is plotted here; it is the interior cloud distance between transition zones; it may or may not agree with the visual cloud thickness (C). In spite of the poor sample at altitudes other than 8-10,000', altitude variation of C_D distances agrees fairly well with the generally observed cloud shapes. The effect of the inversion in forcing many of the clouds to spread out between 8-9,000' is obvious.

No significant trend with altitude is seen in the next scatter diagram, Fig. 42, which shows transition zone thickness versus altitude.

In Fig. 43 the existence of several weak refractive index gradients at altitudes just below the inversion probably represents a significant trend. This region is one where some of the clouds are spreading out, evaporating slowly and losing their buoyant kinetic energy.

No significant altitude variation of oscillation wavelength in the transition zone is evident in Fig. 44.

As would be expected, the altitude variation of the maximum refractive index change within clouds ($\Delta N_{c_{max}}$) which is shown in Fig. 45 is, in general, similar to that of $N_c - N_A$ or ΔN. Most of the values of $\Delta N_{c_{max}}$ are smaller than the corresponding values of ΔN at the cloud edges (Fig. 39). Note the one spectacular value at 8,100' where $\Delta N_{c_{max}}$ is 37N units. This is about three times the values of ΔN at the same altitude.

Downcurrents around the immediate periphery of cumulus most probably account for the very considerable negative $N_1 - N_2$ refractive index differences shown in Fig. 46 just below, in, and above the inversion. The mechanism of downcurrent formation has been described on page 26.

A summary of the preceding data, plus some additional material, is presented in Figs. 47 and 48. Of particular note is the distribution of pass heights which shows: 1) the poor sampling obtained outside of the 8-10,000 foot altitude region (the bar graphs, therefore, largely apply to these levels); 2) occurrence of a few, very sharp gradients (4 per cent of the cases showed maximum transition zone thicknesses of less than 5 feet; the absolute maximum gradient was 2N units per foot); and 3) the common occurrence of dry air surrounding the cloud.

Figure 49 was drawn according to the procedures outlined in Section 6. On this day the cloud temperatures again straddle the ambient temperature in the lower unstable air. Note that the temperature lapse rate

in the ambient air below the inversion follows the dry adiabatic. (No scale correction to the vortex thermometer temperature was necessary on this day. Also, there were insufficient data below 7800' to extend cloud temperatures downward.) This 30 June case differs appreciably from the 19 July case (Fig. 23). On 19 July the lapse rate in the cloud region was close to moist adiabatic.

It has previously been supposed that the temperatures found inside clouds which penetrate substantial inversions are given by the extrapolation of the in-cloud temperature lapse for the region below the inversion. The remarkable feature of this 30 June data is the sharp increase of cloud temperatures above the inversion. Presumably, this means that the cloud as it grows upward is mixing very rapidly with the air immediately surrounding it. More data of this type are needed before a correction for cold cloud temperatures above an inversion can be applied to the method of computing N_C-N_A from radiosonde data.

In Fig. 49 the slope of the dotted curve below the inversion (the curve of maximum dry air temperature just outside cloud) suggests that the source of the warm surrounding air is from the inversion region and not from above. However, if this air mixes with colder air as it descends, its source could have been above the inversion. Theoretical calculations could be made to shed some light on this problem. Tentatively, it seems that the warm air outside the clouds and just above the inversion could have resulted if air from some higher level had descended only some 400 feet.

Figure 50 shows an "average" cloud and "average" refractive-index-change traces for 30 June. The same procedures were used for making this sketch as were used in Fig. 24. Some thirty-five cloud photographs were reviewed before the cloud shape was sketched. The cloud top on this sketch is placed well above the average tops in order to illustrate the type of refractive index traces obtained at the highest level in the tallest clouds. It should be noted that the "average" traces shown in Fig. 50 for the base and top cloud region are based on very meager data. (The values used as a guide in drawing this figure are given in Table 3.)

The principal points of interest in Fig. 50, contrasted with the similar 19 July figure (Fig. 24), are: 1) the great variation with altitude of the gross refractive index change; 2) the small altitude variation of the refractive index gradients; 3) the uniformity of refractive index inside the bubble elements in contrast with that in the edge and top regions of the clouds; 4) the relatively low value of the refractive index of that air adjacent to the cloud at levels above 8,000'; 5) the fairly uniform refractive index trace well away from the cloud at all levels (the lower levels were sampled late in the day; records taken earlier might have shown greater changes).

Our best estimate of the geographic and vertical distribution of clouds over the flight area is shown in Fig. 51. The tendency for clouds

to bunch and form in lines is suggested on the plan view. The density of haze is indicated by the small dots on the cross section. This figure portrays the maximum state of cloud development on 30 June.

Table 3. Average values of cloud parameters from scatter diagram for 30 June 1955

	Pressure Altitude - Thousands of Feet						
	6	7	8	8.6	9.2	10	11
C_D (ft)	1250	1250	1500	4500	2600	3500	1500
X_T (ft)	40	110	220	280	280	300	600
$N_c - N_a$ (N)	2.5	5	7.5	10	24	27	12
ΔN (N)	3.5	5	7	11	29	31	15
$N_1 - N_2$ (N)	0	-1/2	-1/2	-2	-5	-5	+1
ΔN_c (N)	3	2	10	10	12	16	12
X_{min} (ft)	30	35	40	35	20	14	40
Osc (#)	0	0	2	3	3	4	6
$M_x \Delta N_a$	1	2	2 1/2	2 1/2	2 1/2	3	1/2

6.3 Data for 22 June 1955

On 22 June many cloud passes were made through small cumulus clouds over Pikes Peak and adjacent mountains.

The air was, in general, quite dry, as indicated in Fig. 52, but strong heating of the mountain slopes and higher terrain produced sufficient buoyant-convective-bubbles in the 5-8,000 foot layer to enable them to reach the condensation level at 15,000' and form clouds. These clouds formed over and near the mountain peaks, then blew off and evaporated. The radiosonde data shown here may not be quite representative of the mountainous region, as the air over Lowry (on the lee slope) is descending and drying after passage over the Rockies. The predicted ΔN values of over 20N units at 16,000' (Fig. 53) are, therefore, questionable.

Figure 54 is a photograph of one of the clouds penetrated. Successive clouds (bubbles) are growing upward from right to left. The entrance path of the aircraft into the bubble series is marked by an arrow and an X. The record obtained on this pass is shown in Fig. 55. The record indicates a gradual transition on entry, a sharp boundary on exit. This obvious asymmetry needs to be studied further in relation to the wind shear and the stage of the cloud history. We intend to do this as soon as possible. Note that this cloud (as well as the others that we penetrated on this day) is colder than the undisturbed air at some distance from the cloud. The change of 7N units outside to inside the cloud (typical for this day) agrees with the predicted change from the radiosonde data.

6.4 Data for 31 July 1955

The next set of data (Figs. 56-59) illustrates a case where the calculated ΔN values did not agree with the measured values. The Yuma, Arizona temperature-dew point soundings are shown on Fig. 56. This sounding indicates almost saturated air at all levels above 7,000'. The resulting ΔN values, Fig. 57, are quite small. Figure 58 is a photograph taken shortly before entering a group of cumulus congestus clouds near Blythe, California (north of Yuma). Note that the clouds appear in concentrated bunches with broad clear areas in between. Figure 59 shows the record obtained in flying through the clouds pictured in Fig. 58. ΔN values of about 20N units were recorded, as compared with a computed value of 2-4N units. It is obvious that in this case the radiosonde instrument rose through one of the cloud groups and, therefore, gave data which were non-representative of the region as a whole. A method for estimating the representativeness of the radiosonde data for our particular use needs to be developed. A careful scrutiny of the local surface cloud observations at time of balloon release would probably help.

It is of interest to note the temperature of the clouds in Fig. 59. The first three cloudlets constitute a progression from a young warm cloud to a cold and presumably descending cloud. These may be small clouds that built up to the flight path after the cloud picture (Fig. 58) was taken. There are large temperature contrasts in the other, larger clouds which were penetrated later. These temperature effects have quite a large influence on the ΔN cloud-air contrast.

6.5 Data for 24 June 1955

On a flight from Denver to Boston, a belt of cumulus cloud activity was penetrated in the Illinois-Ohio region. Figures 60-63 pertain to the western part of this region. The nearest radiosonde data were from Chanute Field at Rantoul, Illinois. This sounding is plotted in Fig. 60. Here is an example where a modification of the sounding should be considered before a ΔN prediction is made. The layers of dry air which appear on the morning sounding would be expected to disappear with the diurnal convection cycle. The sharp ΔN values up to 33N units, indicated in Fig. 61, are probably

not realistic. The computed ΔN value of 10N units at flight altitude should be compared with the measured value of 6N units. If the narrow, dry layers were not considered, the agreement would be better.

Figure 62 is a photograph of a typical cloud encountered in this region during flight. The traces shown in Fig. 63 were from a cloud on the far side of the one pictured. A sharp entrance into the cloud is indicated by the refractometer trace. The thermometer indicated a warm region immediately on entry and a cold region in the interior and on exit. A marked asymmetry of the cloud shapes is shown by the cloud photograph.

The end of the cumulus cloud region near Toledo consisted of a chaotic mass of cumulus; a large portion of the atmosphere from 7,000 to 15,000' was cloudy. The radiosonde data shown in Fig. 64 indicate an almost saturated atmosphere between 7,000 and 13,000'. The high moisture content is reflected in the small ΔN values shown in Fig. 65. In this case the low values can be trusted. Data from several ground stations, other than that at the radiosonde site, reported broken cloud and one thunderstorm was observed.

Figure 66 is a photograph taken from the middle of this chaotic cloud region. Low cumuli were building into a higher deck of cumuli; wind shear was spreading out the less active and older cloud bubbles. An example of the flight record through the clouds is not shown. It was found after examination of the records that the cloud penetrations could hardly be distinguished from the clear air fluctuations. The cloud to clear air ΔN values were only a few N units and they were in agreement with the calculated values.

7. Summary

The material presented in this report can best be summarized in tabular and diagrammatic form. Table 4 summarizes the data pertaining to gross refractive index changes between cloud and air.

One can see from Table 4 that, on the whole, there is reasonable agreement between predicted values of ΔN and the calculated values. Meteorological reasons for the few deviations from agreement have been suggested in the text.

The detailed data on the character of the refractive index trace through and around clouds are most concisely summarized by the two "average" cloud sketches, Figs. 24 and 50.

Estimates of the spatial distribution of clouds in the area of the flight are summarized in Table 5.

8. Conclusions

Analysis and study of the limited data obtained to date are incomplete and conclusions are, of a necessity, tentative.

The fluctuations of refractive index in and around clouds are qualitatively explainable, using existing hypotheses of cloud physics and dynamics. The total change in index from inside to outside the cloud agrees well with theory; the index values and gradients found within the transition zone, within the cloud, and in the near regions surrounding cloud are explained only by our personal combination of the ideas of convection that appear most appropriate.

At present, a good theory of cumulus convection does not exist. It is hoped that further work on present and future data will help establish the governing mechanisms and refine our explanation of the causes of refractive index fluctuations.

Table 4. Gross refractive index changes; cloud-clear air

Date	Location	Altitude in 1,000'	Av. Temp. Dry Air	Meas. ΔN	Calc. ΔN	Remarks
7-19-55	NE Tucson	13 to 16	-1	10*	10	Little if any inhibition of convection by inversions
		16 to 19	5	11*	12	
		19 to 20	-9	11	8	
6-30-55	NW Boston	7.5 to 8.8	8°C	8*	14	Radiosonde in clearer region than flight
		8.8 to 10	8°C	24*	20	Inversion with very dry air above
		10 to 11	7°C	20	22	
6-22-55	Pikes Peak Denver	18	-9	7	9	
7-31-55	Ariz. - Cal.	16	2	20	3	A radiosonde ascent through a cloud
6-24-55	Ill. - Ind.	11	0	6	10	Nonrepresentative dry layers on radiosonde
6-24-55	Michigan	11	-2	0-5	3	

*NOTE: Measured values starred are approximate averages for a large number of cases. Those not starred are for only a few cases.

Table 5. Table of estimated cloud coverage and dimensions

		19 July 1955	30 June 1955	22 June 1955	31 July 1955	24 June 1955	
1.	Time of flight	1330-1530 MST	1330-1530 EDT	0900-1000 MST	1600-1630 MST	1525-1535 EDT	1550-1600 EDT
2.	Location	Area 15-50 mi. NE of Tucson	Area 25-50 mi. NW of Boston	Area 50-100 mi SW of Denver	Vicinity Blythe Calif.	Vicinity South Bend -Goshen	Vicinity Toledo
3.	Air mass	mT	mT	mod. cP	mT	$\frac{mT}{mod\ cP}$	$\frac{mT}{mod\ cP}$
4.	Average total cumulus coverage from nearest ground weather observing station (%)	SCTD to BRKN	17	0*		SCTD	BRKN
5.	Average cumulus cloud coverage observed in flight (%)	28	12	5	10	20	80
6.	Average cumulus cloud coverage at mid-altitude observed in flight (%)	12	8	4	7	8	25
7.	Average cumulus cloud coverage at 20,000 ft (excluding cirrus anvils) observed in flight (%)	1	0	1	1	0	< 1
8.	Average cloud base altitude (ft)	12,000	6,000	15,500	10,500	6,500	6,500
9.	Average top altitude of typical cloud (ft)	19,000	11,000	19,500	20,000	10,500	14,000
10.	Average top altitude of highest 10% of typical clouds (ft)	20,000	11,500	20,500	24,000	12,000	17,000
11.	Typical cloud size (horizontal) (ft)	6,000	3,500	3,500	7,000	3,500	4,000
12.	Average distance between edges of neighboring clouds or cloud bunches (miles)	3	2	4	5	2	1

Remarks: * few clouds over mountains; SCTD, 10-50%; BRKN, 60-90%.

ACKNOWLEDGMENTS

The work presented herein represents the integrated efforts of a considerable number of individuals and groups. Each contribution is sincerely appreciated; however, all cannot be separately acknowledged.

Special reference is made to the efforts of Mr. Alfred A Spatola, of the Geophysics Research Directorate, who accomplished or assisted with much of the data analysis, drafted all the figures, and served as an indispensable member of the project aircraft crew. Likewise, S/Sgt. Robert H. Garner, T/Sgt. Frederick M. Towles, and A/1C Marvin M. Gehr, also of GRD, deserve particular note for maintaining the instruments, assisting with the data analysis, and manning project positions aboard the aircraft.

Group credit is given to the pilots and crews who flew the aircraft, and to those persons, especially Capt. Richard Francey, who helped design the special instrumentation required for this project, and to those members of the Air Force Cambridge Research Center who installed this instrumentation.

REFERENCES AND SHORT BIBLIOGRAPHY

1. Austin, J. M., "A Note on Cumulus Growth in a Nonsaturated Environment," J. Meteor. 5, 103-107, 1948.

2. Austin, J. M. and A. Fleisher, "A Thermodynamic Analysis of Cumulus Convection," J. Meteor. 5, 240-243, 1948.

3. Austin, J. M., "Cumulus Convection and Entrainment," Compendium Meteor., 694-701, 1950.

4. Bjerknes, J., "Saturated Adiabatic Ascent of Air Through a Dry-Adiabatically Descending Environment," Q. J. Roy. Met. Soc. 64, 325, 1938.

5. Bunker, A. F., "Diffusion, Entrainment and Frictional Drag Associated with Nonsaturated, Buoyant Air Parcels Rising Through a Turbulent Air Mass," J. Meteor. 10, 212-218, 1953.

6. Byers, H. R. and R. R. Braham, Jr., The Thunderstorm, U.S. Gov't Print. Off., Washington, 282 pp., 1949.

7. Crain, C. M. and A. P. Deam, "Measurement of Tropospheric Index of Refraction Profiles with an Airplane Carried Direct Reading Refractometer," EERL, Univ. of Texas Report No. 54, 1951.

8. Enenstein, N. H., "The Effect of Water Droplets on the Index of Refraction," Proceedings, Symposium on Tropospheric Wave Propagation, U.S. Navy Electronics Laboratory Report No. 173, p. 52, 1948.

9. Houghton, H. G. and H. E. Cramer, "A Theory of Entrainment in Convective Currents," J. Meteor. 8, 95-102, 1951.

10. James, D. G., "Fluctuations of Temperature Below Cumulus Clouds," Q. J. Roy. Met. Soc. 79, 425, 1953.

11. Ludlam, F. H. and R. S. Scorer, "Convection in the Atmosphere," Q. J. Roy. Met. Soc. 79, 317-342, 1953 (Review article with extensive bibliography).

12. Ludlam, F. H., "The Subcloud Layer over Land," Q. J. Roy. Met. Soc. 79, 430, 1953.

13. Malkus, J. S., "Effects of Wind Shear on Some Aspects of Convection," Transactions A.G.U. 30, 19-25, 1949.

14. Malkus, J. S., "Cumulus, Thermals and Wind," Soaring 13, 6, 1949.

PRECEDING PAGE BLANK-NOT FILMED

15 Malkus, J. S , "The Birth and Death of a Cumulus," Weatherwise 3, 56-59, 1950.

16. Malkus, J. S., "Recent Advances in the Study of Convective Clouds and Their Interaction with the Environment," Tellus 4, 71, 1952.

17 Malkus, J. S. and R. S. Scorer, "The Erosion of Cumulus Towers," J. Meteor. 12, 43-57, 1954.

18. Murgatroyd, R. J., "Cloud Physics at the Meteorological Research Flight," Archiv für Meteorologie, Geophysik und Bioklimatologie Wien, Series A, Vol 8, No. 3, 1955.

19. Packer, L. S., "Vortex Free Air Thermometer," Final Report No. 1H-775, Cornell Aeronautical Laboratory (Contract No. A(s)51-852c), Buffalo, N. Y., p 2, 1 April 1953.

20. Petterssen, S., Weather Analysis and Forecasting, McGraw-Hill, N. Y., 1940

21. Petterssen, S , E. Knighting, R. W. James and N. Herlafson, "Convection in Theory and Practice," Geofys. Publ., 16, No. 10, Oslo, 1945.

22. Rainey, R. G., "Observations on the Structure of Cumulus Clouds," Q. J. Roy. Met. Soc. 73, 446 1952

23. Scorer, R S. and F. H. Ludlam, "Bubble Theory of Penetrative Convection," Q. J. Roy. Met. Soc. 79, 94-104, 1953.

24. Scorer, R. S., "Report of Meeting on 17 February 1956," Weather 11, 122-123, 1956.

25. Stommel, H., "Entrainment of Air into a Cumulus Cloud," J. Meteor. 4, 91-94, 1947.

26. Vonnegut, B., "Vortex Thermometer for Measuring True Air Temperature and True Air Speeds," Rev. Sci Instrum. 21, 136-141, 1950.

27. Welch, L., "Thermals as Seen by Glider Pilots," Q. J. Roy. Met. Soc. 79, 429, 1953.

28. Woodcock, A. H. and J. Wyman, "Convection over the Sea," Ann. N. Y. Acad. Sci. 48, 749, 1947.

29. Yates, A. H., "Atmospheric Convection, the Structure of Thermals Below Cloud Base," Q. J. Roy. Met. Soc. 79, 420-424, 1953.

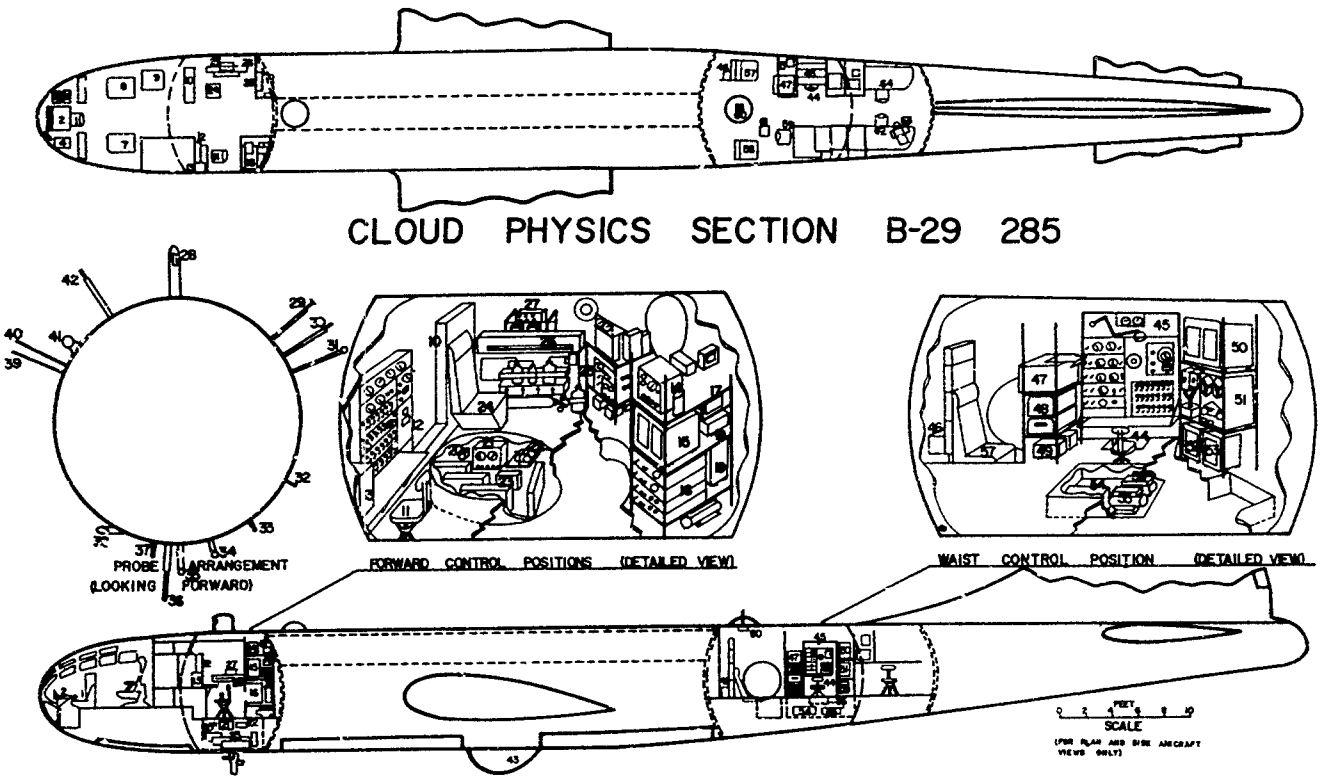
CLOUD PHYSICS SECTION B-29 285
PROBE ARRANGEMENT (LOOKING FORWARD)
FORWARD CONTROL POSITIONS (DETAILED VIEW)
WAIST CONTROL POSITION (DETAILED VIEW)
SCALE

FIGURE 37

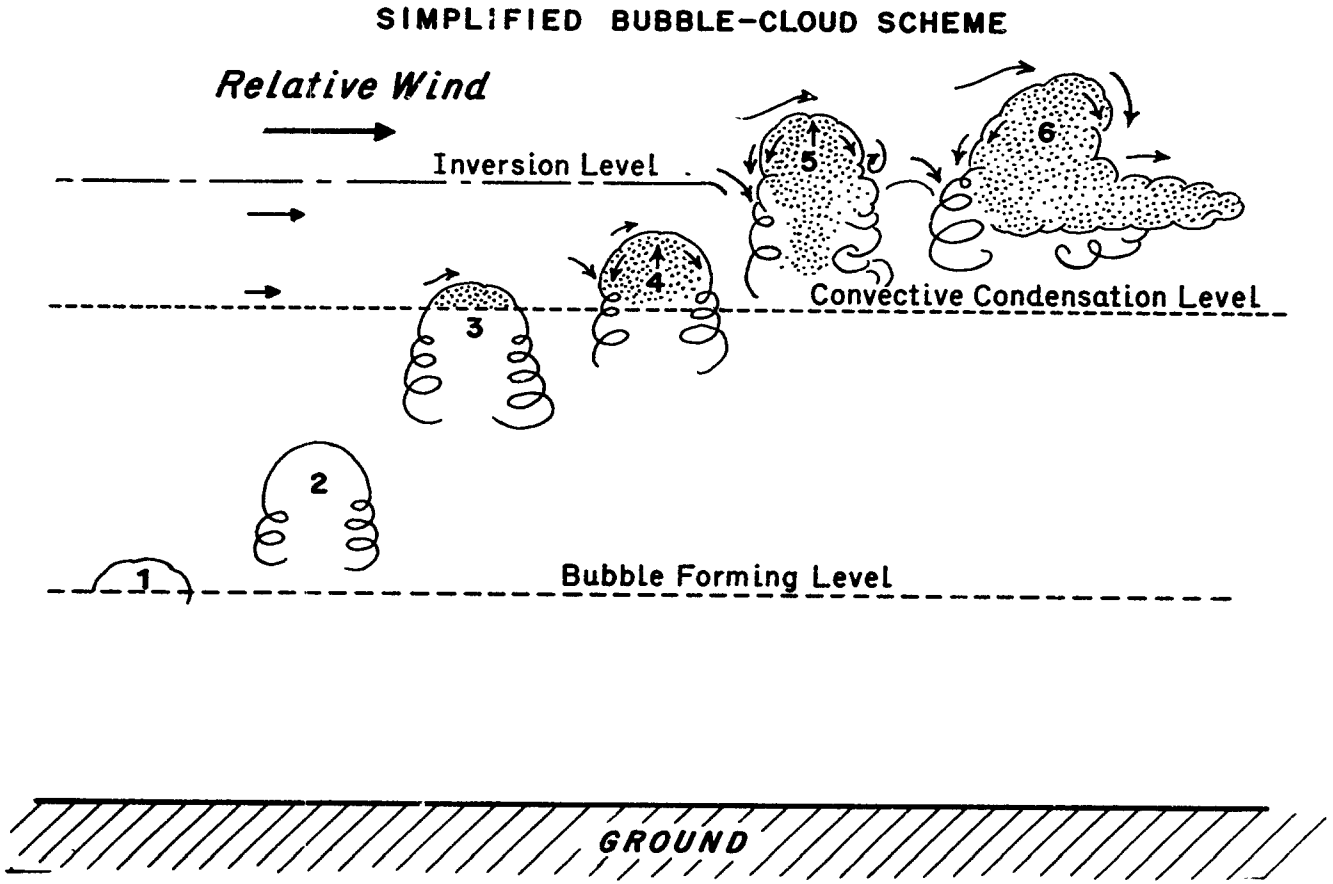
SIMPLIFIED BUBBLE-CLOUD SCHEME
Relative Wind
Inversion Level
Convective Condensation Level
Bubble Forming Level
GROUND
1
2
3
4
5
6

FIGURE 2

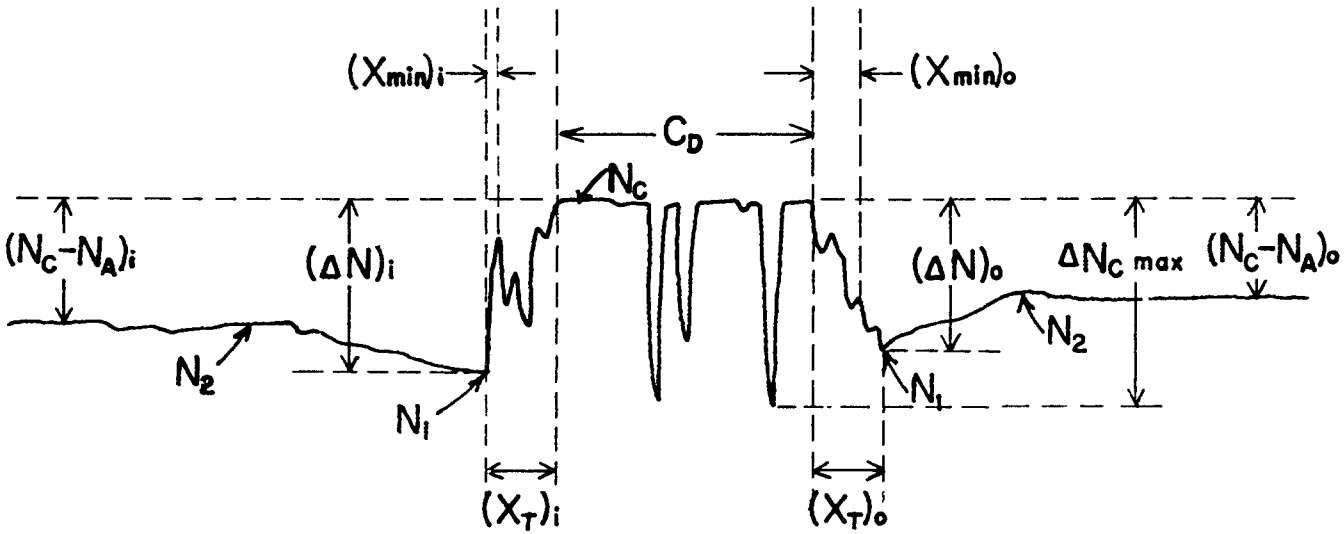

GRAPHICAL PRESENTATION OF PARAMETERS AND SYMBOLS USED FOR CLOUD-PASS DATA

FIGURE 3

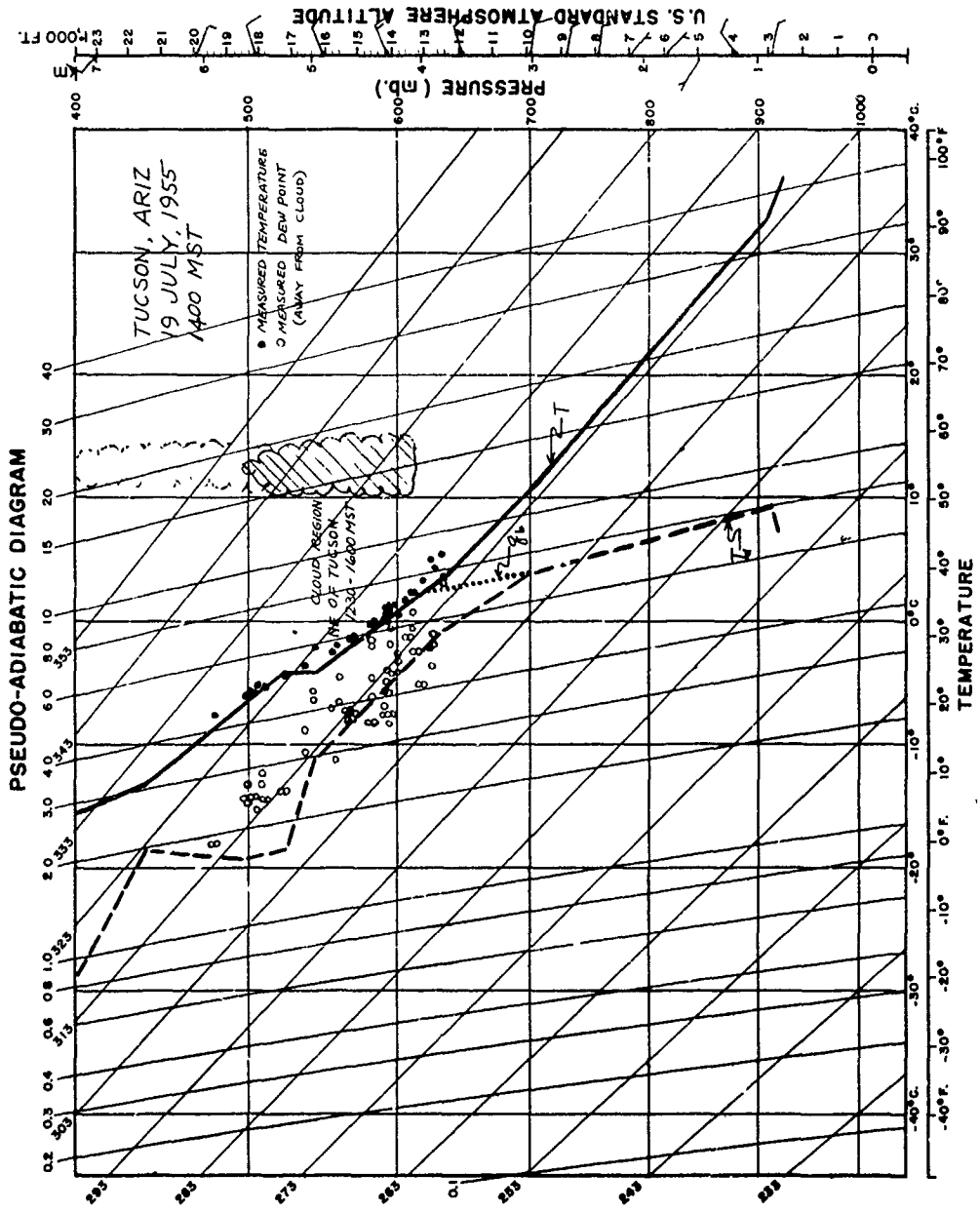
TUCSON, ARIZ
19 JULY, 1955
1400 MST
● MEASURED TEMPERATURES
○ MEASURED DEW POINT
(AWAY FROM CLOUD)
CLOUD REGION
TIME OF TUCSON
1230 - 1600 MST
PSEUDO-ADIABATIC DIAGRAM
PRESSURE (mb.)
U.S. STANDARD ATMOSPHERE ALTITUDE
1000 FT.
TEMPERATURE
R-T
T-S

FIGURE 4

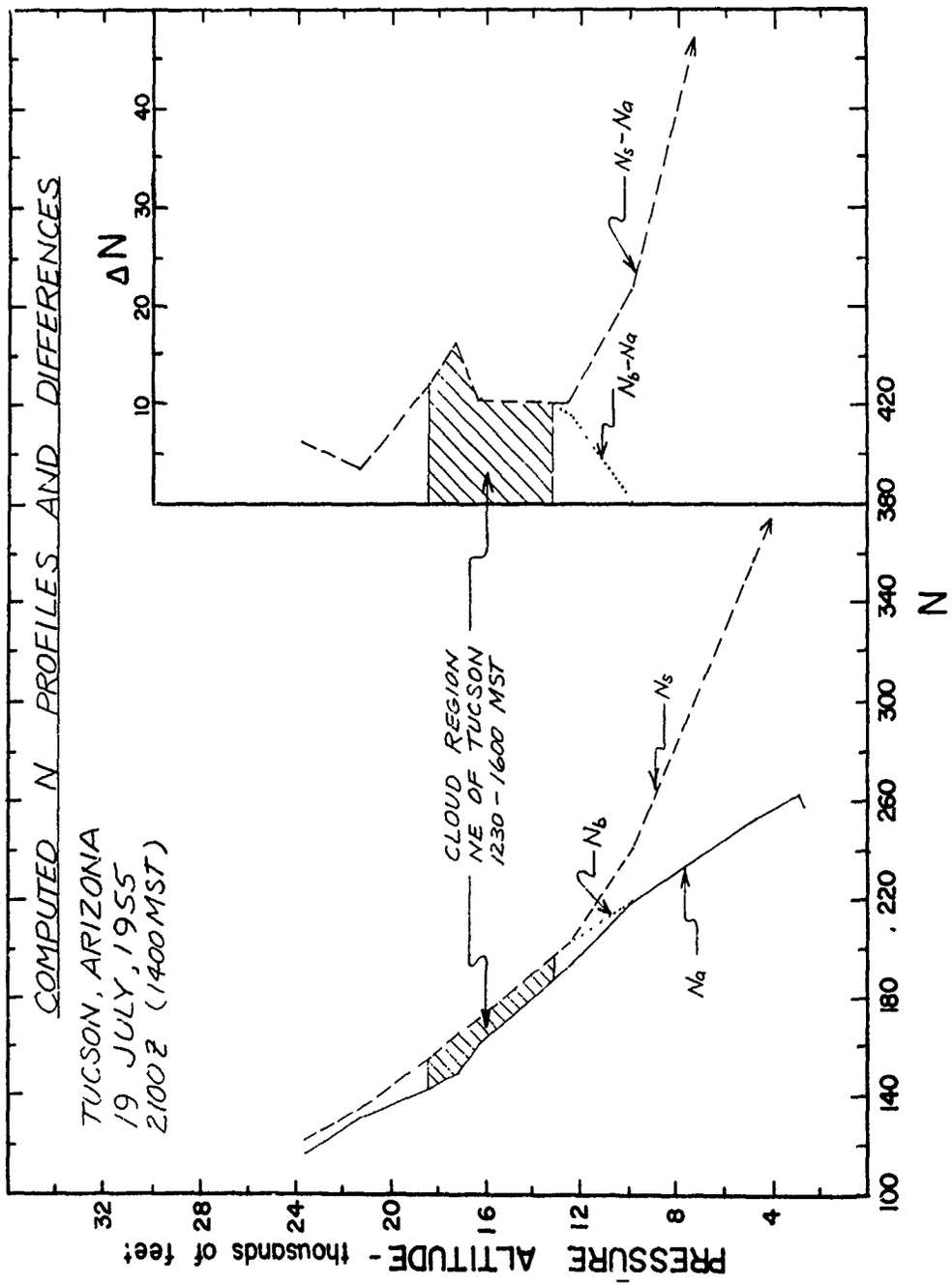
COMPUTED N PROFILES AND DIFFERENCES
TUCSON, ARIZONA
19 JULY, 1955
2100Z (1400MST)
CLOUD REGION
NE OF TUCSON
1230 - 1600 MST
Na
Nb
Ns
Ns-Na
Nb-Na
ΔN
PRESSURE ALTITUDE - thousands of feet
N
100
140
180
220
260
300
340
380
420
4
8
12
16
20
24
28
32
10
20
30
40

FIGURE 5

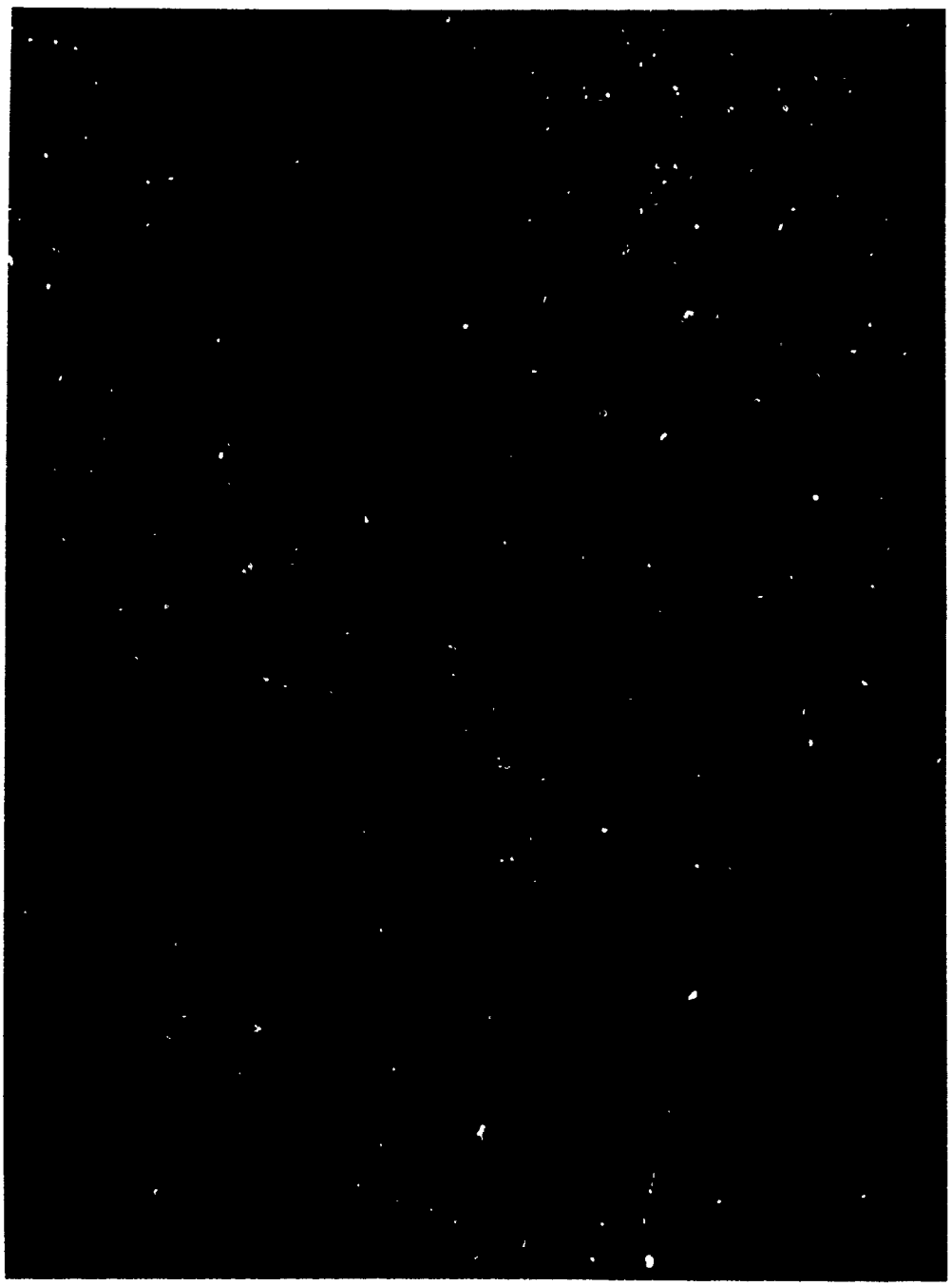

FIGURE 6

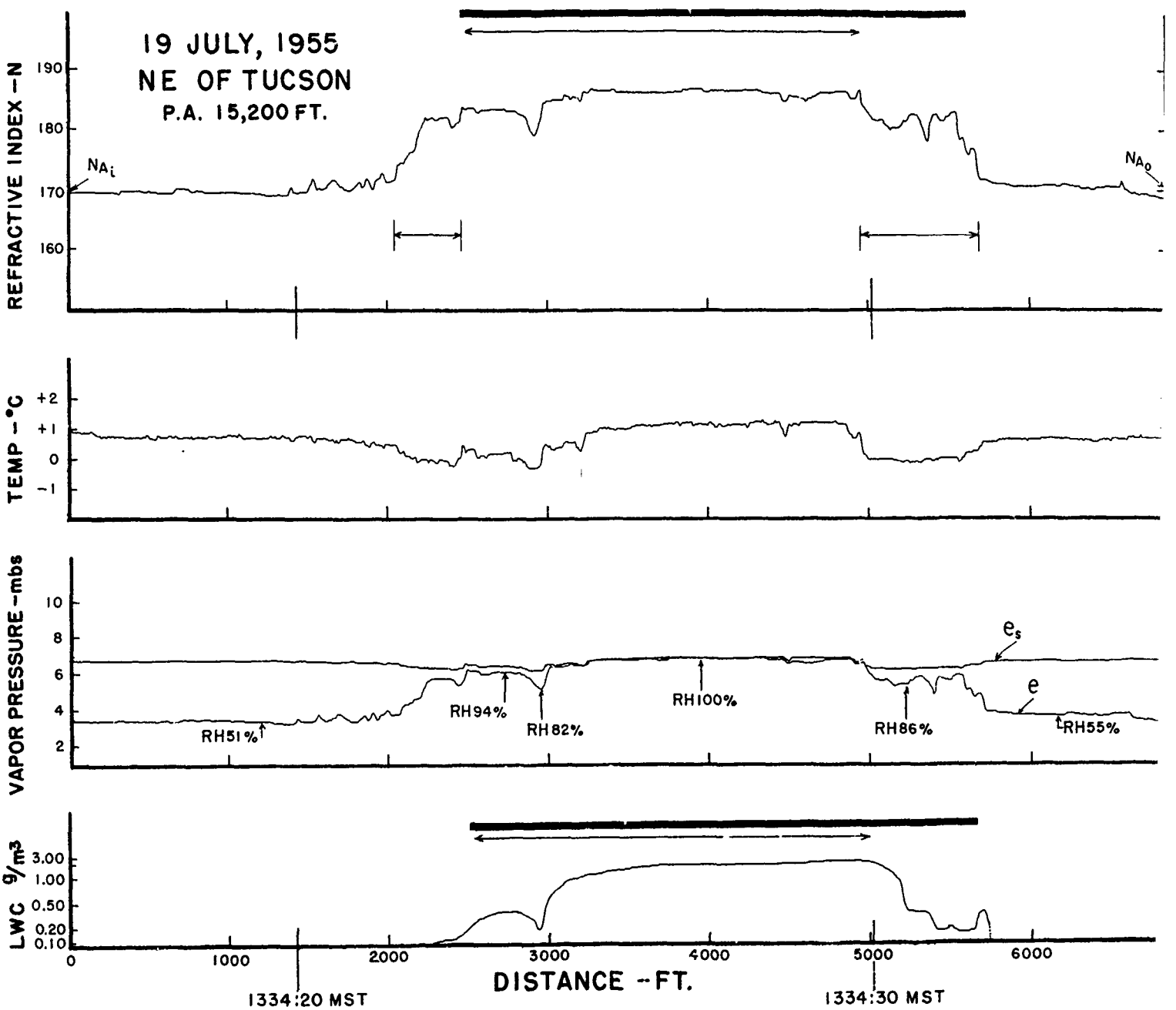

Figure 7.

The Murray Printing Company, Wakefield, Mass., 2-11-57 — 1000

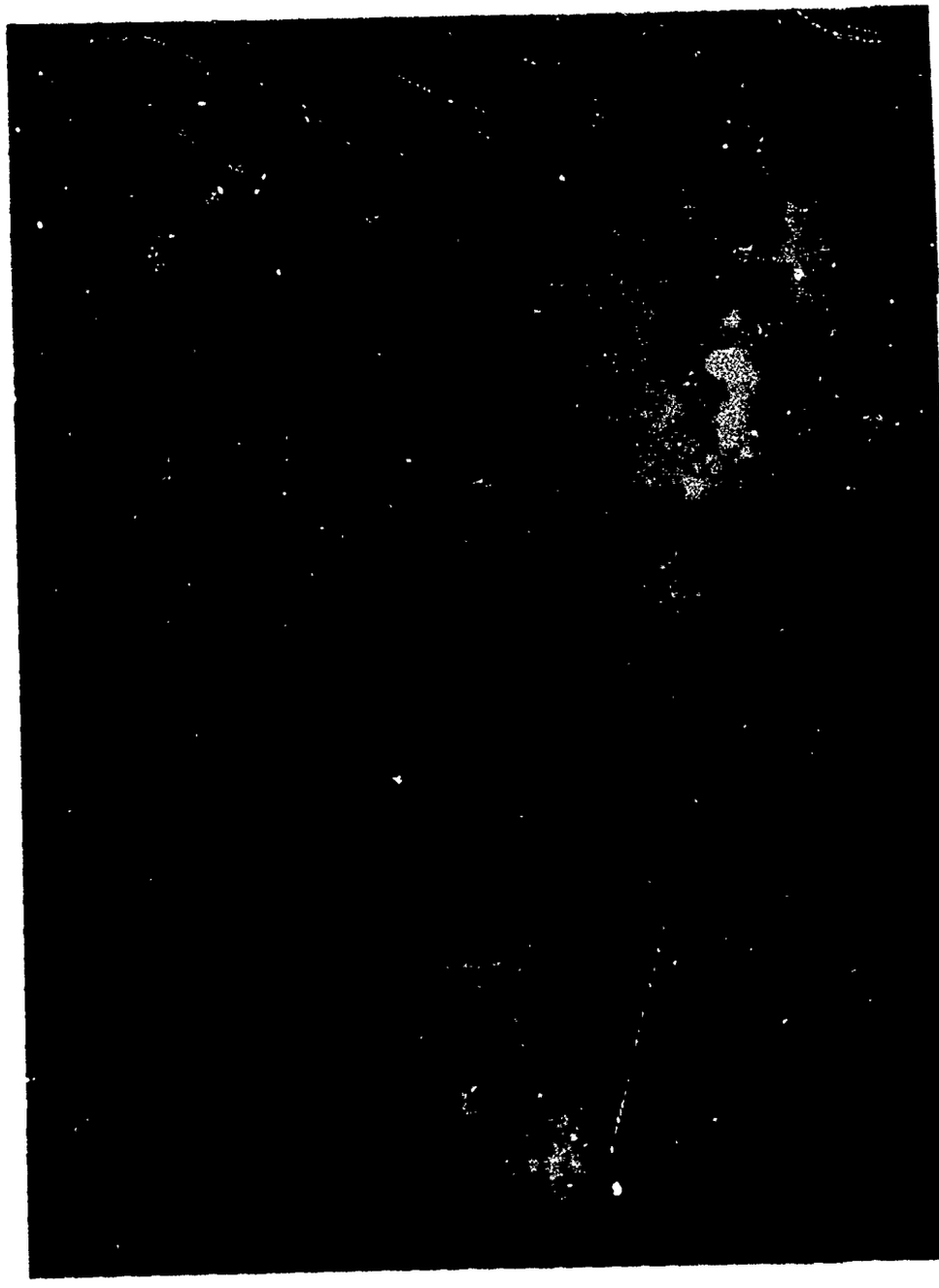

FIGURE 8

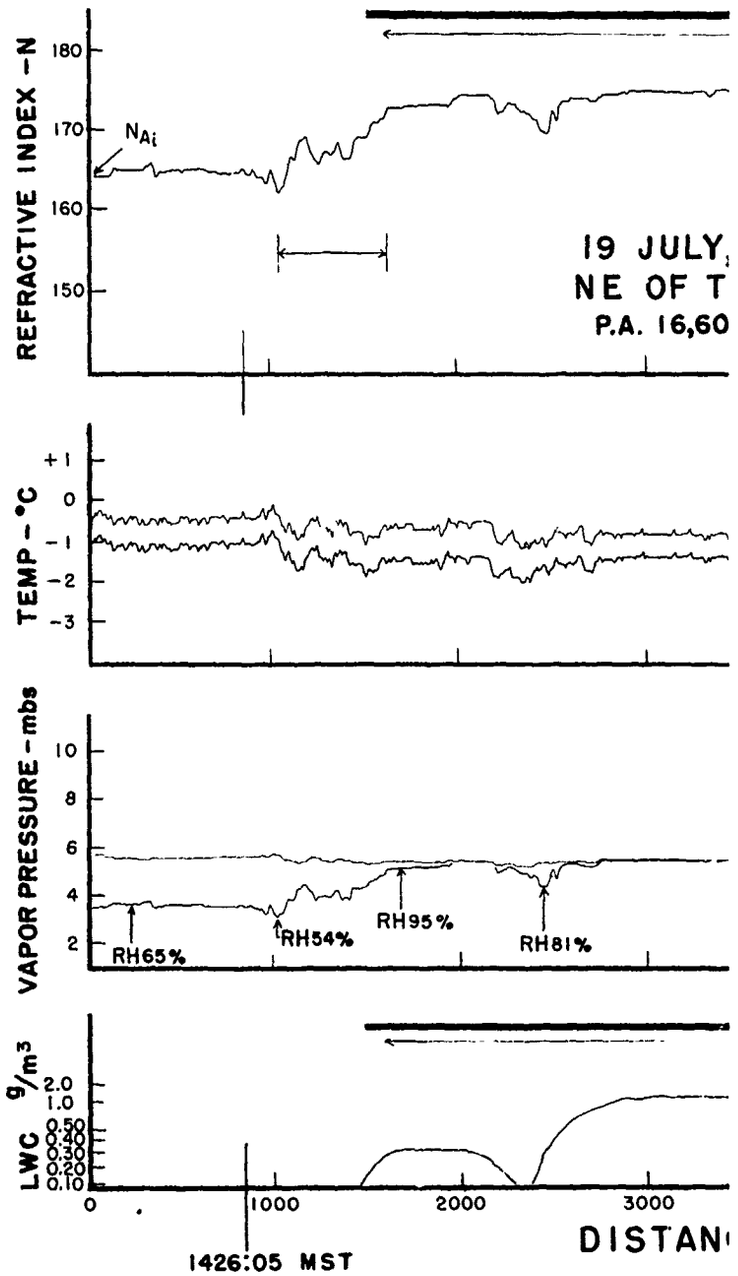

Figure 9.

The Murray Printing Company, Wakefield, Mass., 2-11-57 --- 1000

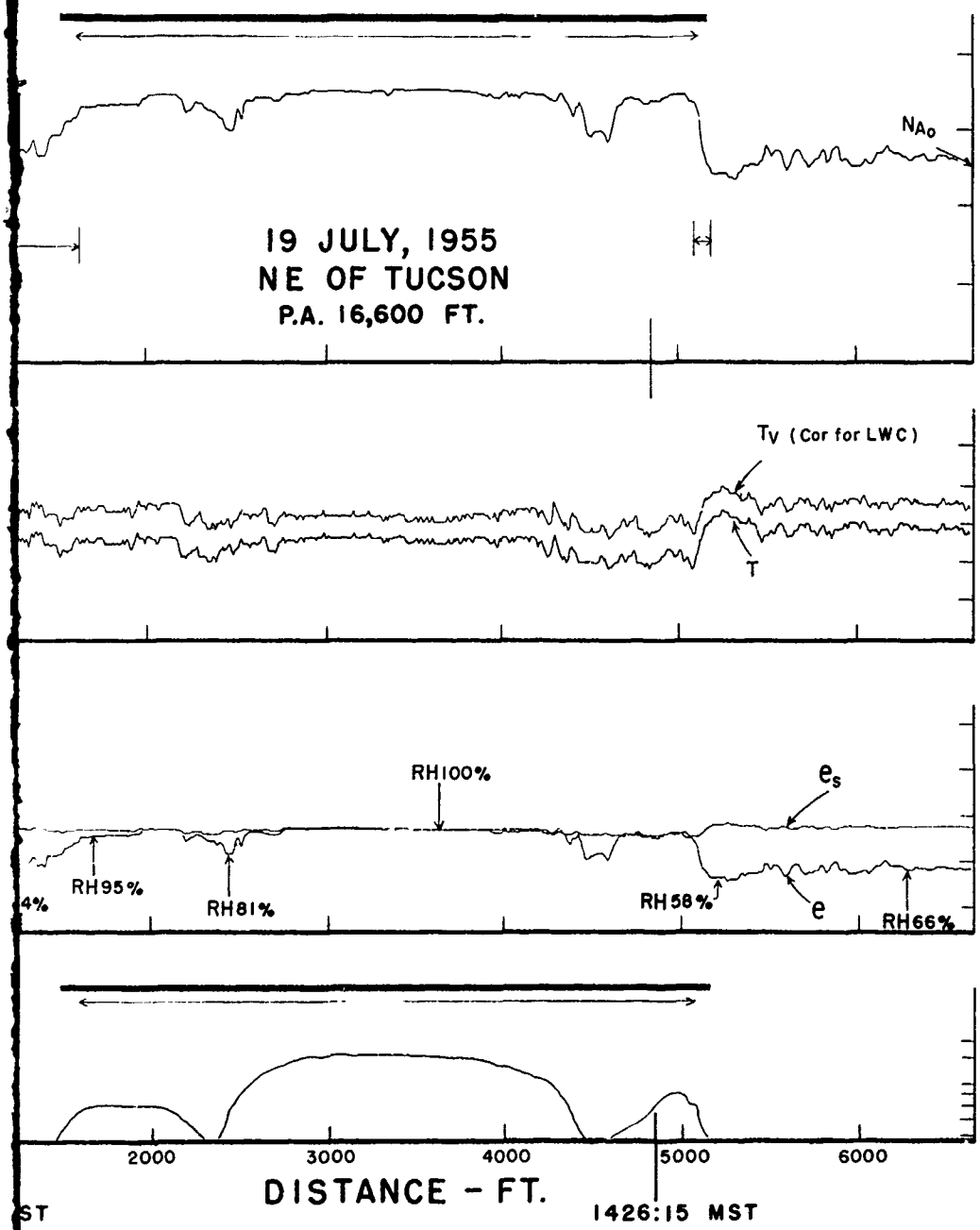
N_{Ao}
19 JULY, 1955
NE OF TUCSON
P.A. 16,600 FT.
T_V (Cor for LWC)
T
RH100%
e_s
RH95%
RH81%
RH58%
e
RH66%
2000
3000
4000
5000
6000
DISTANCE - FT.
1426:15 MST

Figure 9.

FIGURE 10

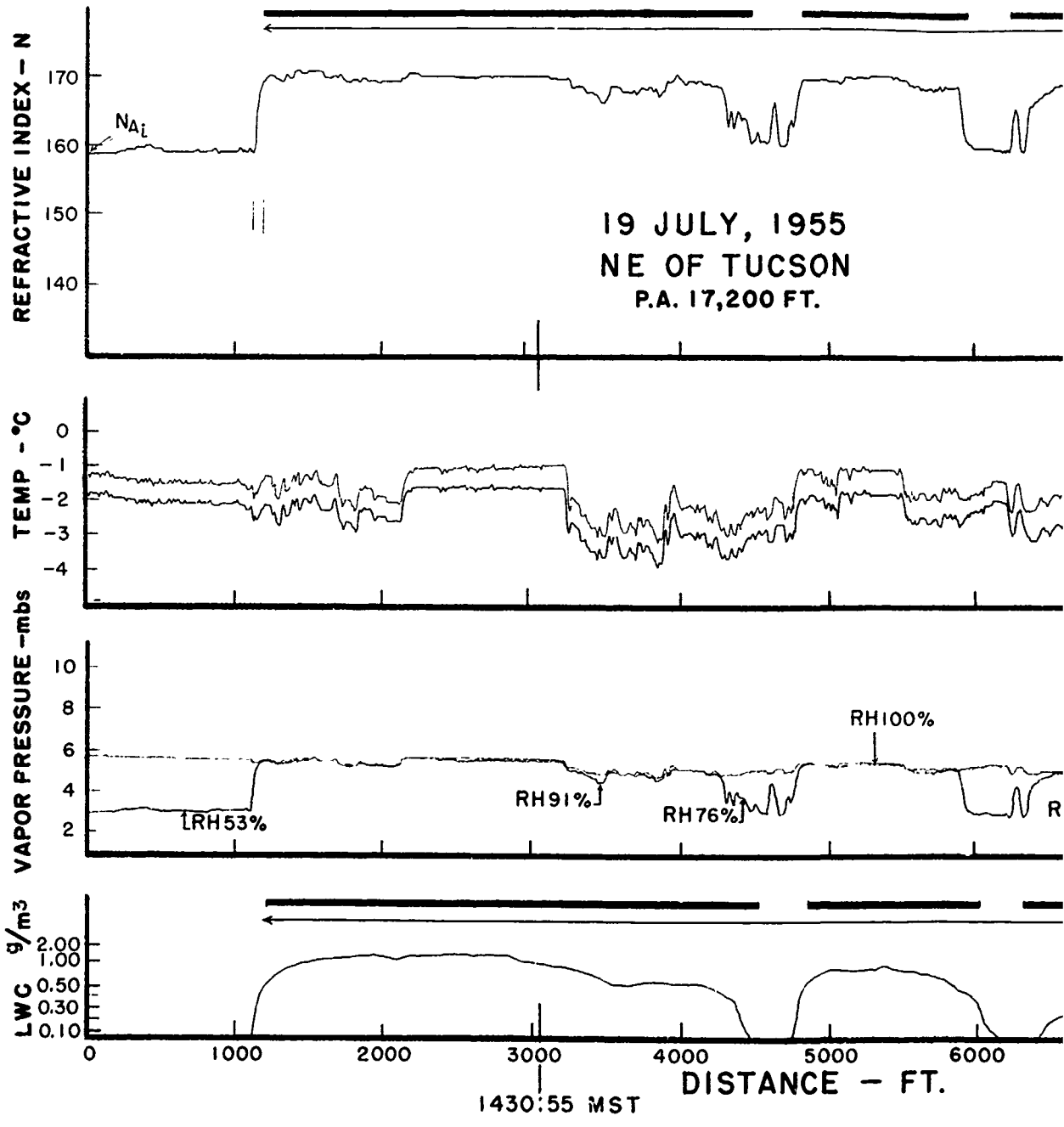

Figure 11.

The Murray Printing Company, Wakefield, Mass., 2-11-57 -- 1000

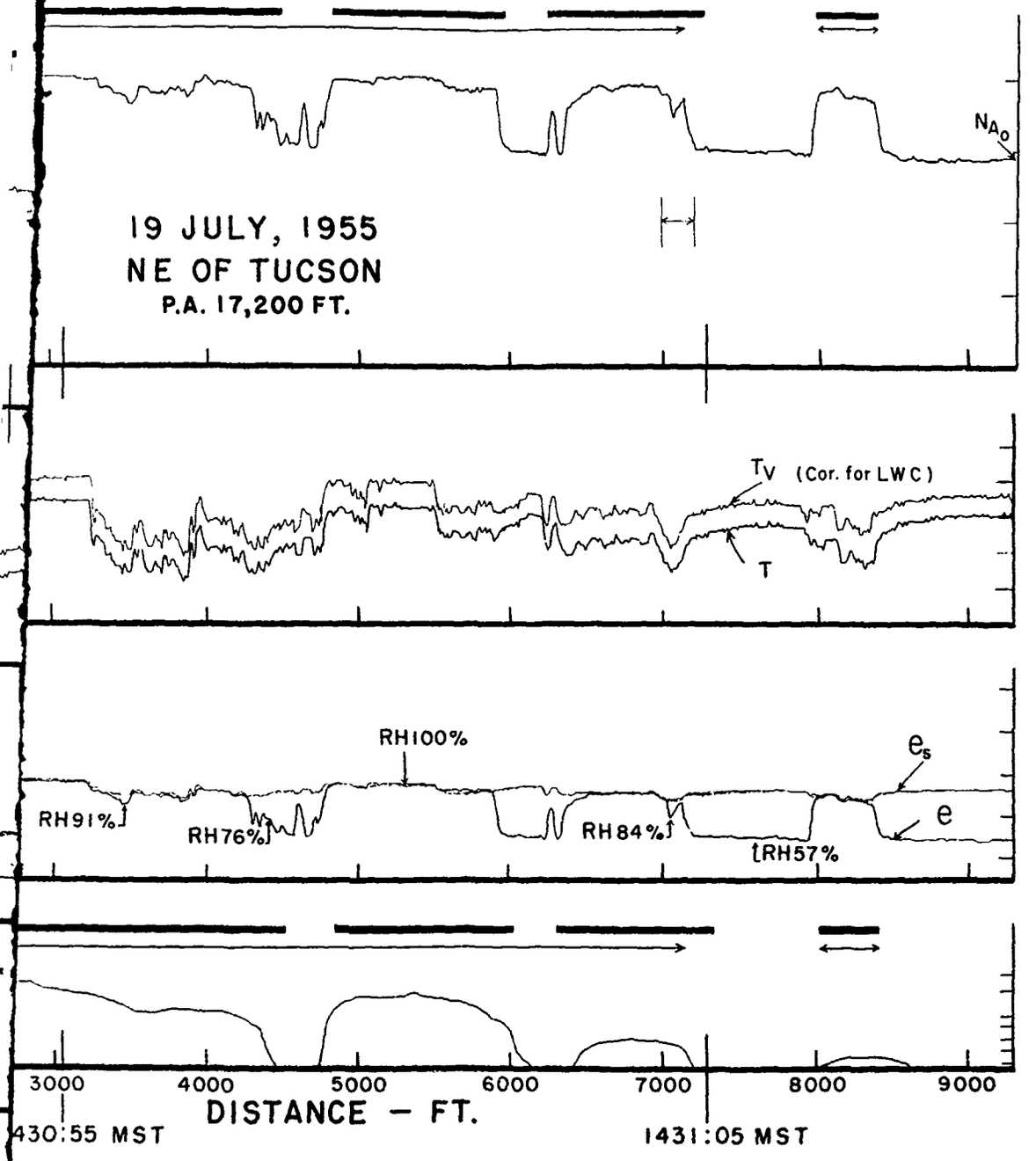
19 JULY, 1955
NE OF TUCSON
P.A. 17,200 FT.
N_{A_0}
T_V (Cor. for LWC)
T
RH100%
e_s
e
RH91%
RH76%
RH84%
RH57%
3000
4000
5000
6000
7000
8000
9000
DISTANCE – FT.
1430:55 MST
1431:05 MST

Figure 11.

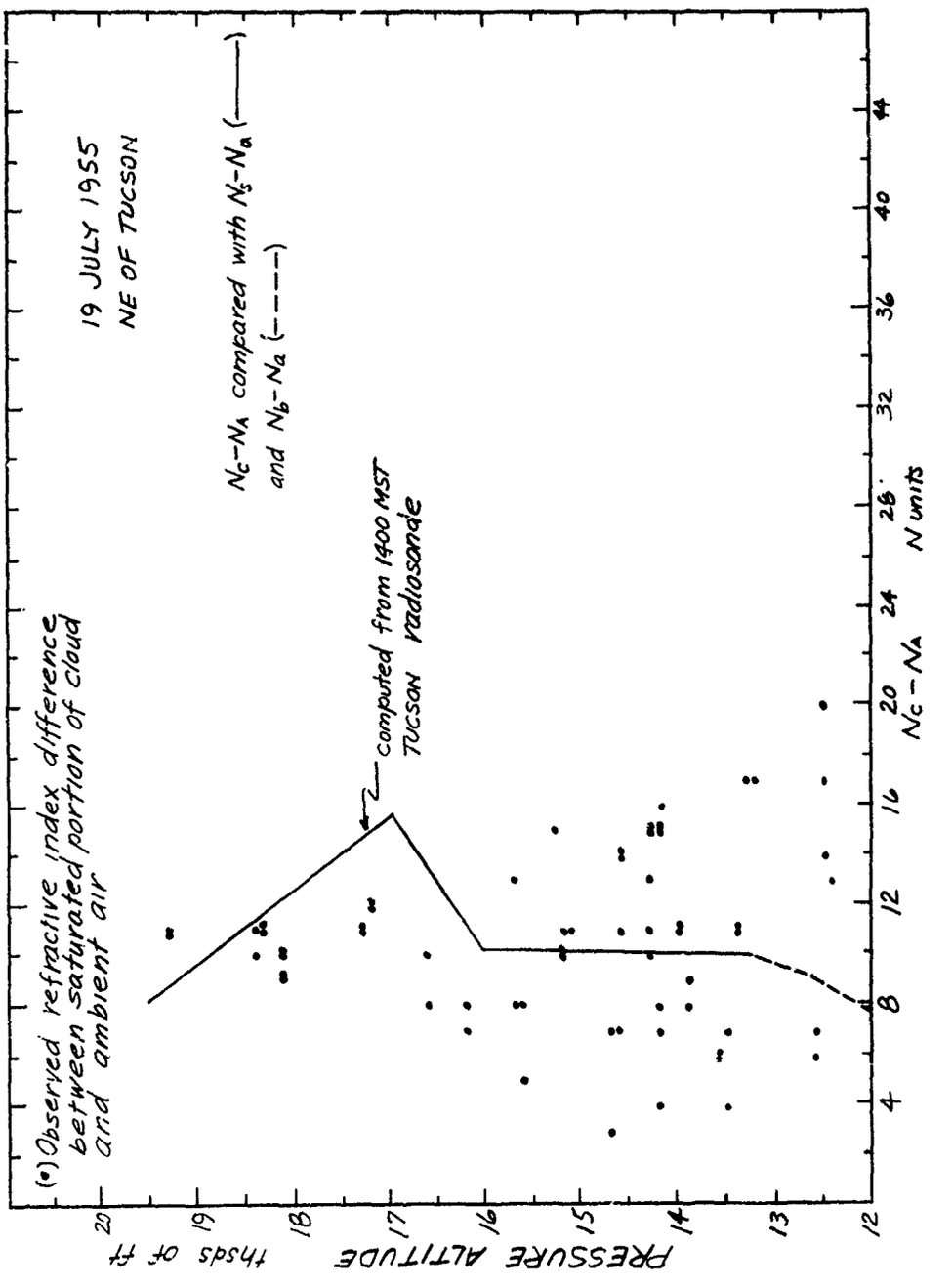
(•) Observed refractive index difference between saturated portion of cloud and ambient air
19 JULY 1955
NE OF TUCSON
N_c-N_A compared with N_5-N_a (——)
and N_b-N_a (- - - -)
computed from 1400 MST
TUCSON radiosonde
PRESSURE ALTITUDE
thsds of ft
20
19
18
17
16
15
14
13
12
4
8
12
16
20
24
28
32
36
40
44
N_c-N_A
N units

FIGURE 12

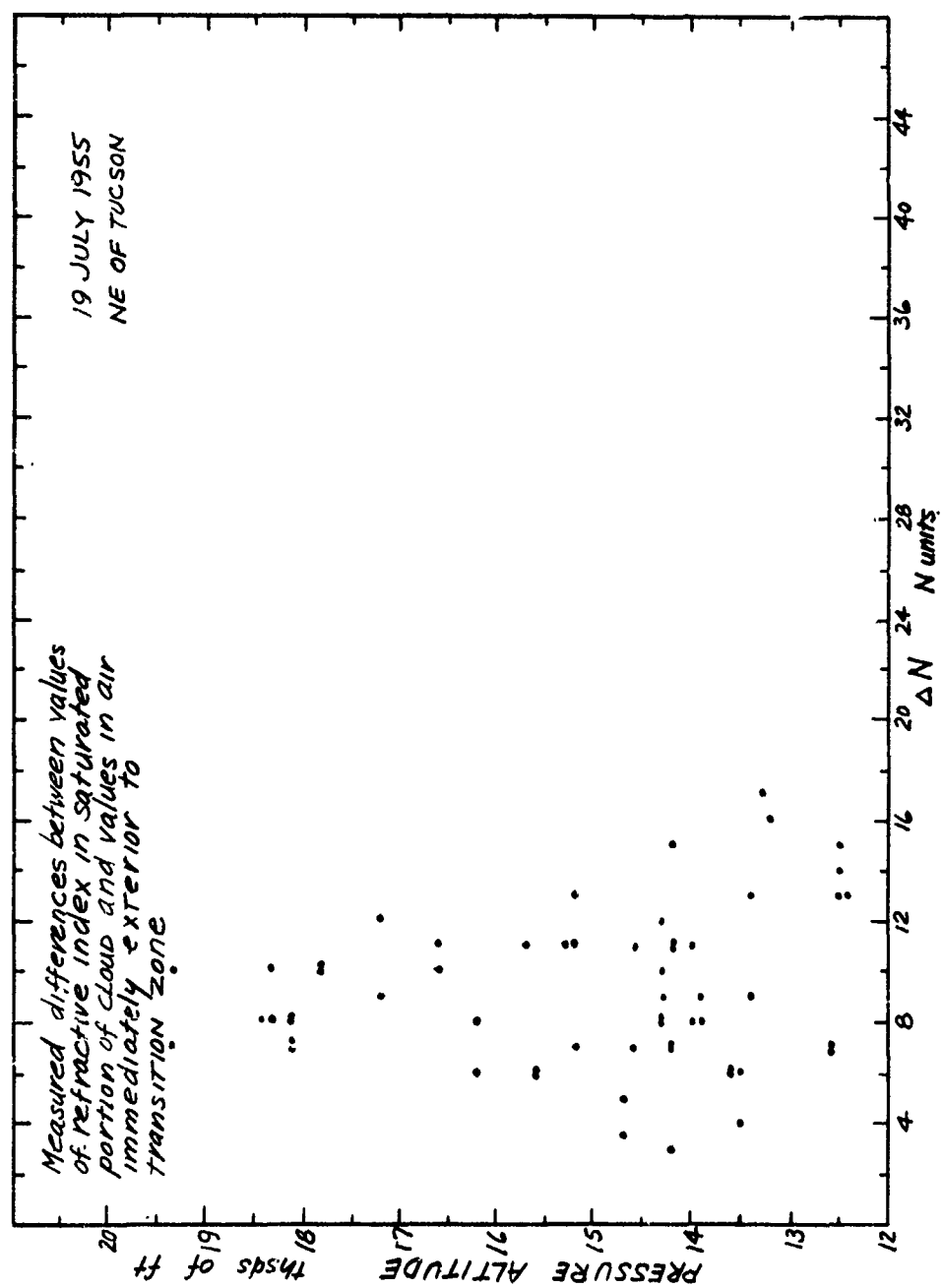

FIGURE 13

U.S. BUREAU OF RECLAMATION
USWRC LIBRARY

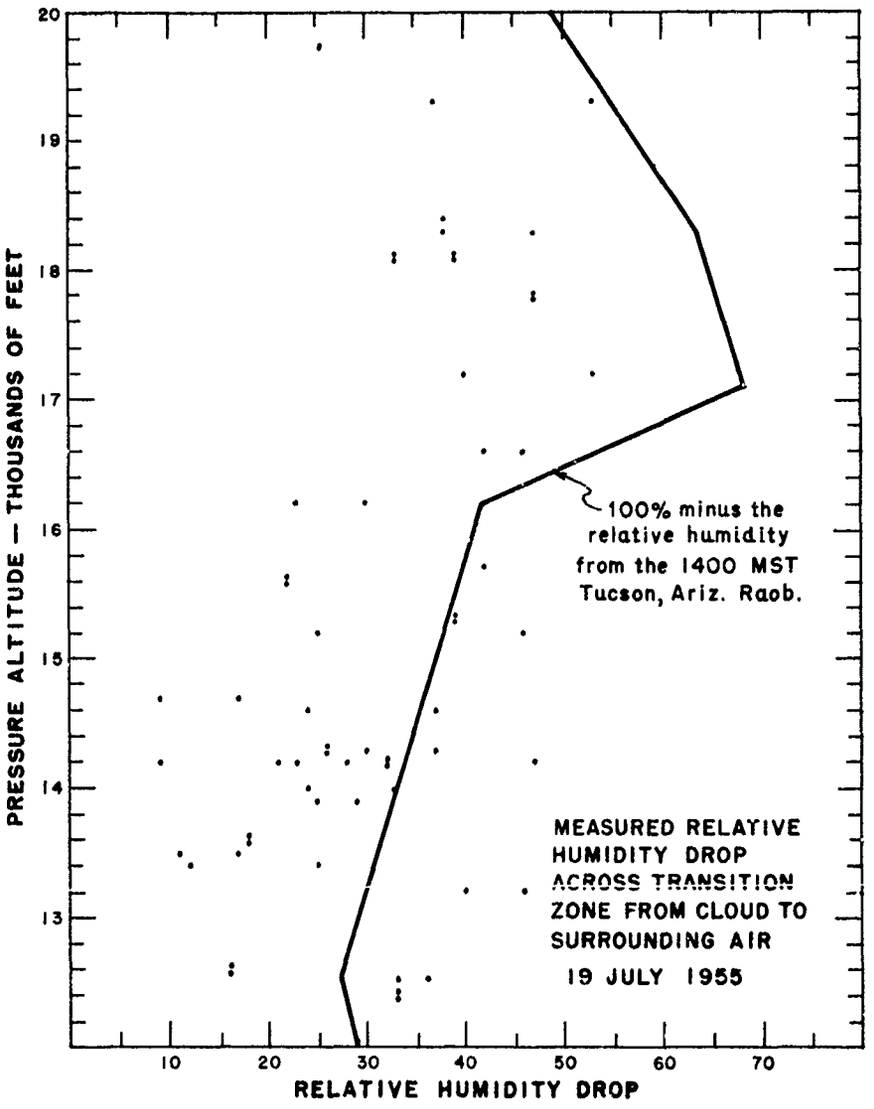
PRESSURE ALTITUDE — THOUSANDS OF FEET
20
19
18
17
16
15
14
13
10
20
30
40
50
60
70
RELATIVE HUMIDITY DROP
100% minus the relative humidity from the 1400 MST Tucson, Ariz. Raob.
MEASURED RELATIVE HUMIDITY DROP ACROSS TRANSITION ZONE FROM CLOUD TO SURROUNDING AIR
19 JULY 1955

FIGURE 14

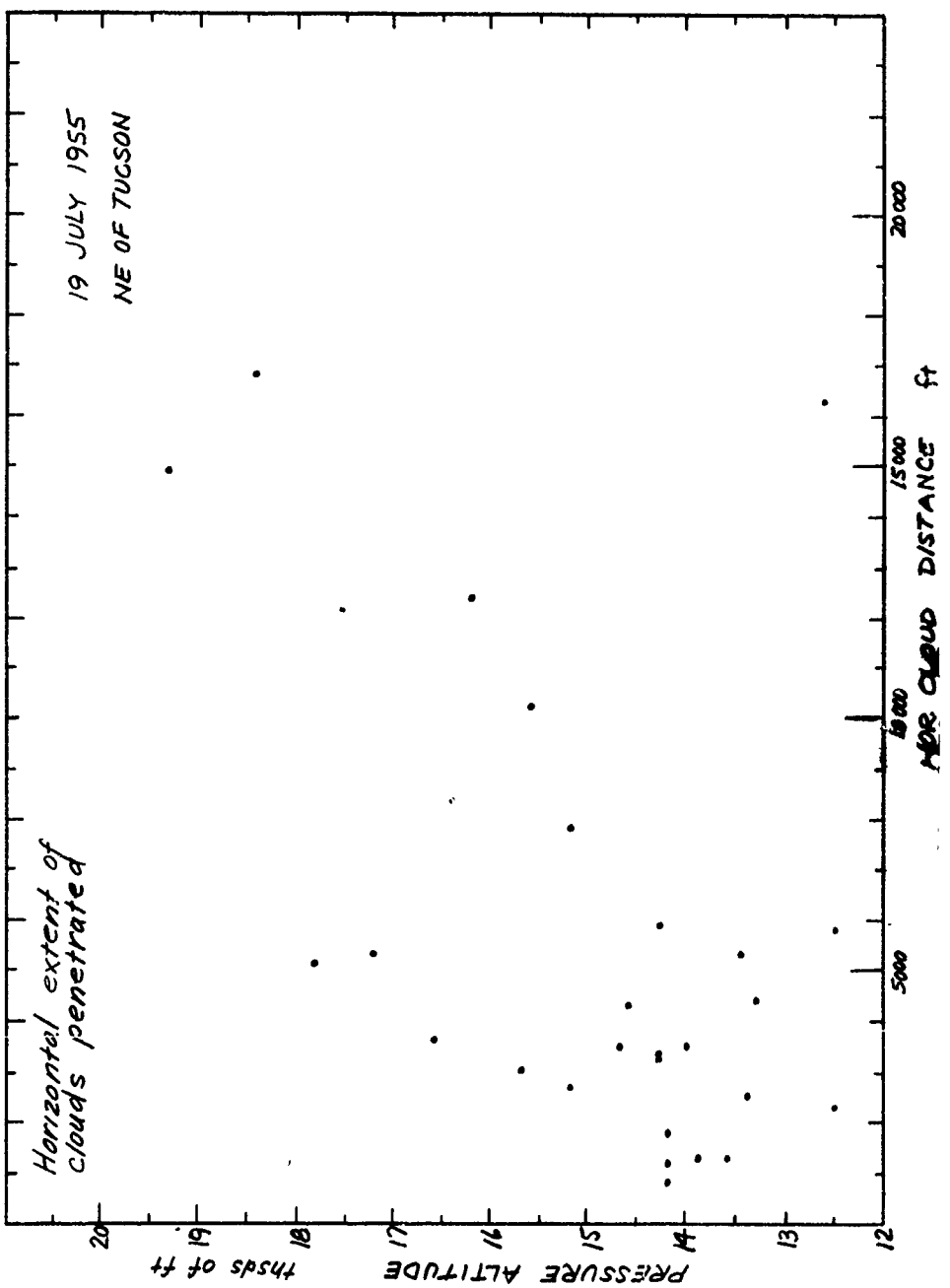
Horizontal extent of clouds penetrated
19 JULY 1955
NE OF TUCSON
PRESSURE ALTITUDE
thsds of ft
20
19
18
17
16
15
14
13
12
5000
10000
15000
20000
NOR CLOUD DISTANCE ft

FIGURE 15

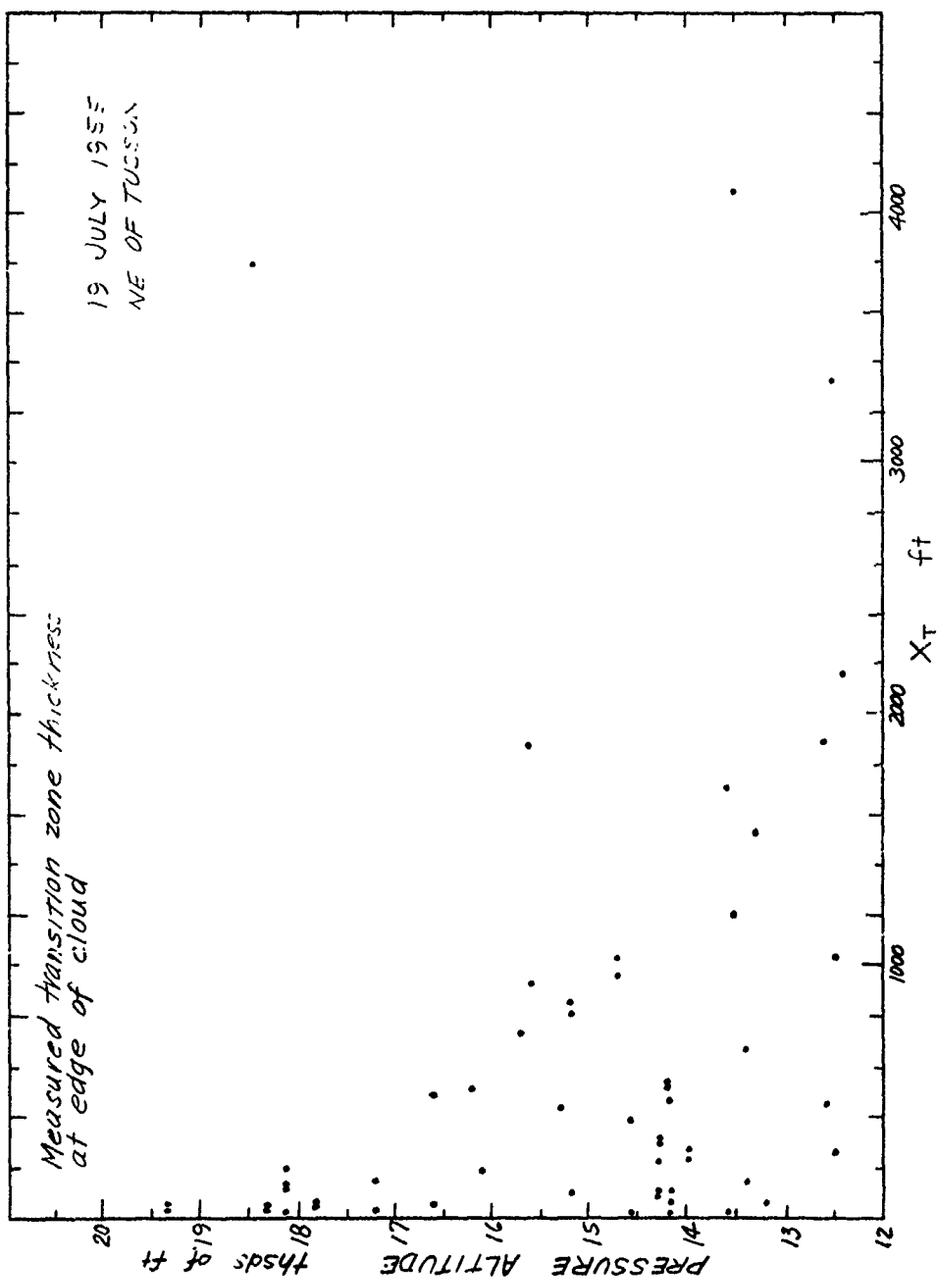
19 JULY 1955
NE OF TUCSON
Measured transition zone thickness
at edge of cloud
PRESSURE ALTITUDE
thsds of ft
20
19
18
17
16
15
14
13
12
1000
2000
3000
4000
X_T ft

FIGURE 16

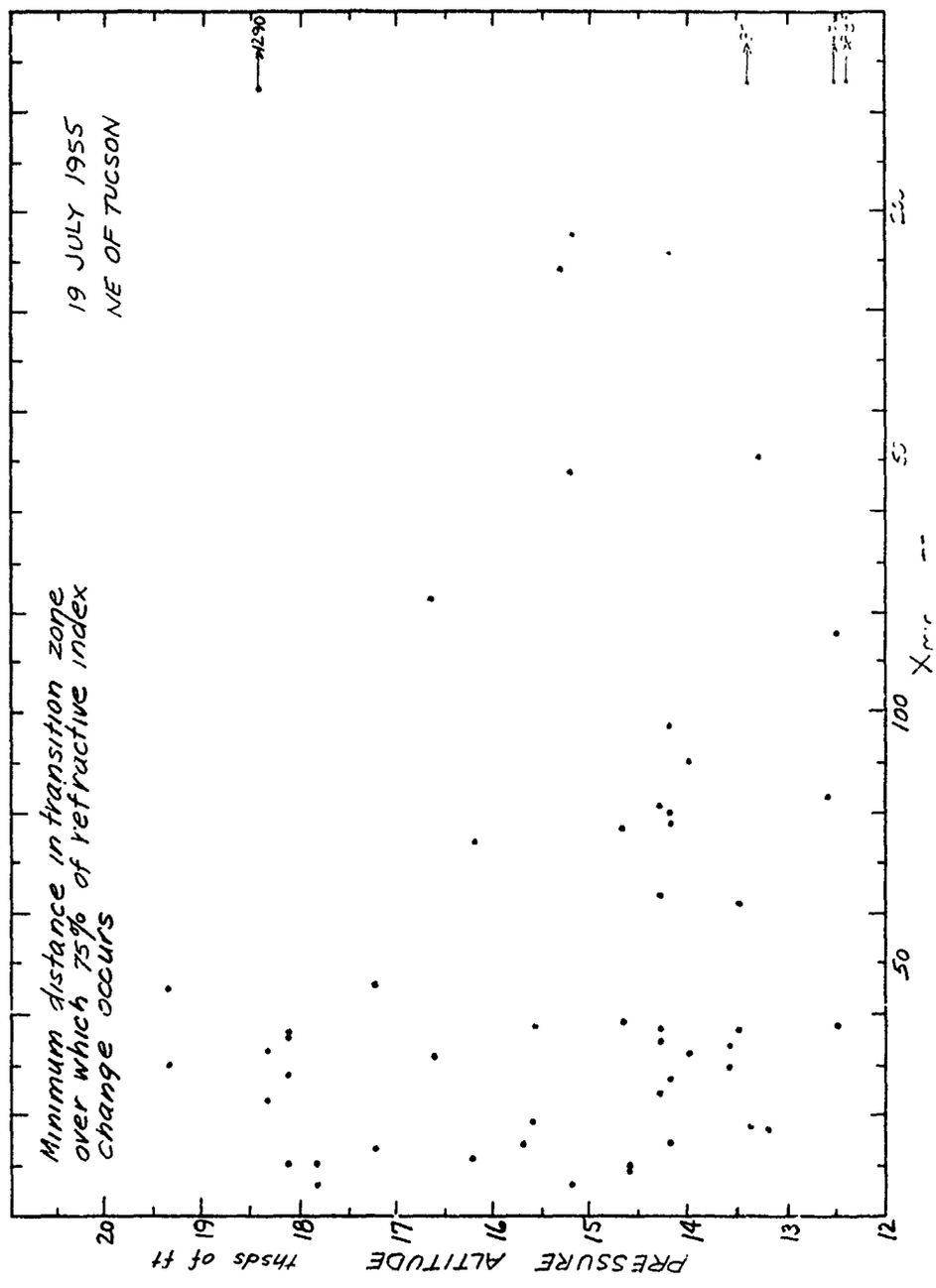
Minimum distance in transition zone over which 75% of refractive index change occurs
19 JULY 1955
NE OF TUCSON
PRESSURE ALTITUDE
thsds of ft
20
19
18
17
16
15
14
13
12
50
100

FIGURE 17

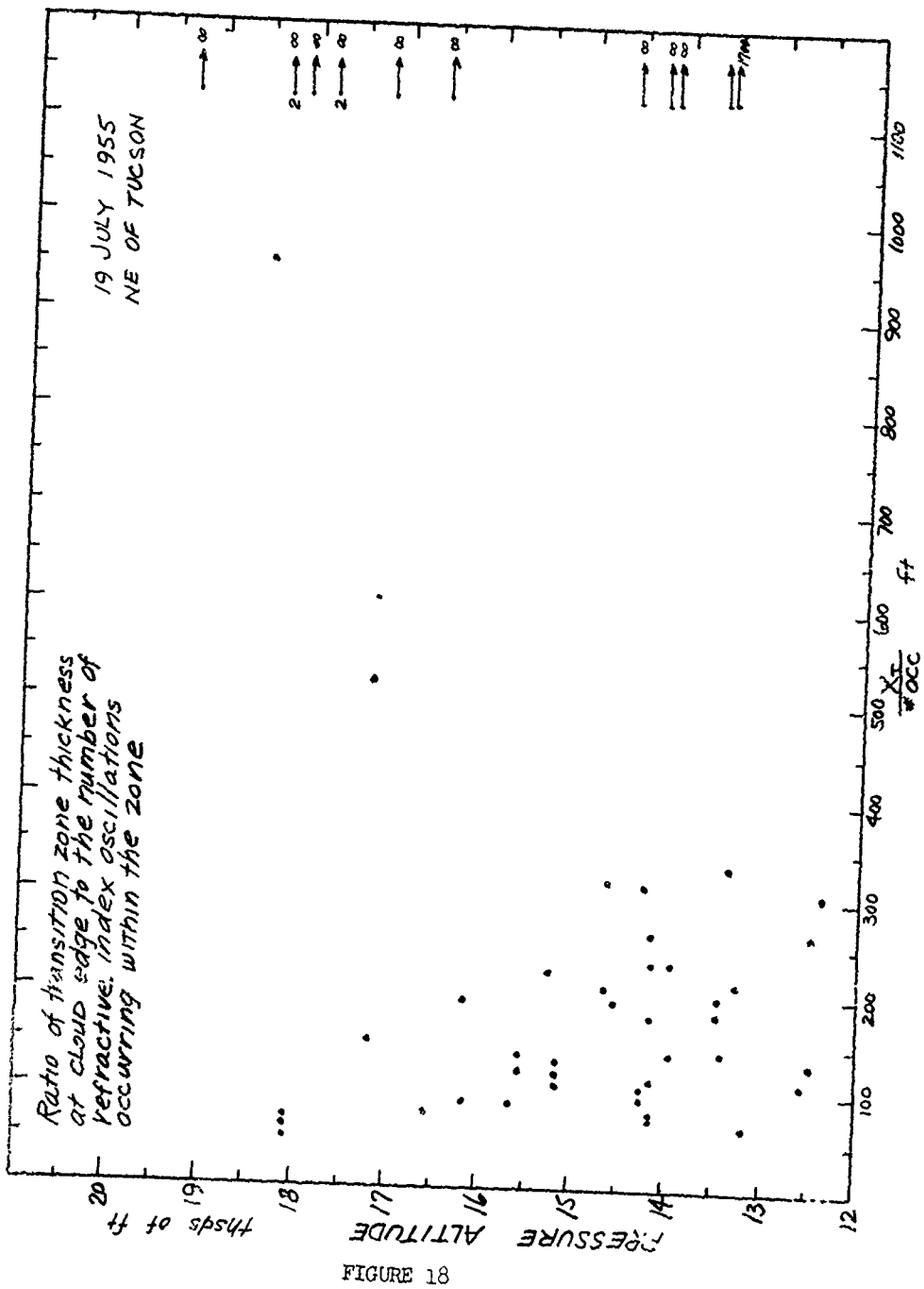
Ratio of transition zone thickness
at cloud edge to the number of
refractive index oscillations
occurring within the zone
19 JULY 1955
NE OF TUCSON
PRESSURE ALTITUDE
thsds of ft
ft
$\frac{\Delta z}{\#OCC}$

FIGURE 18

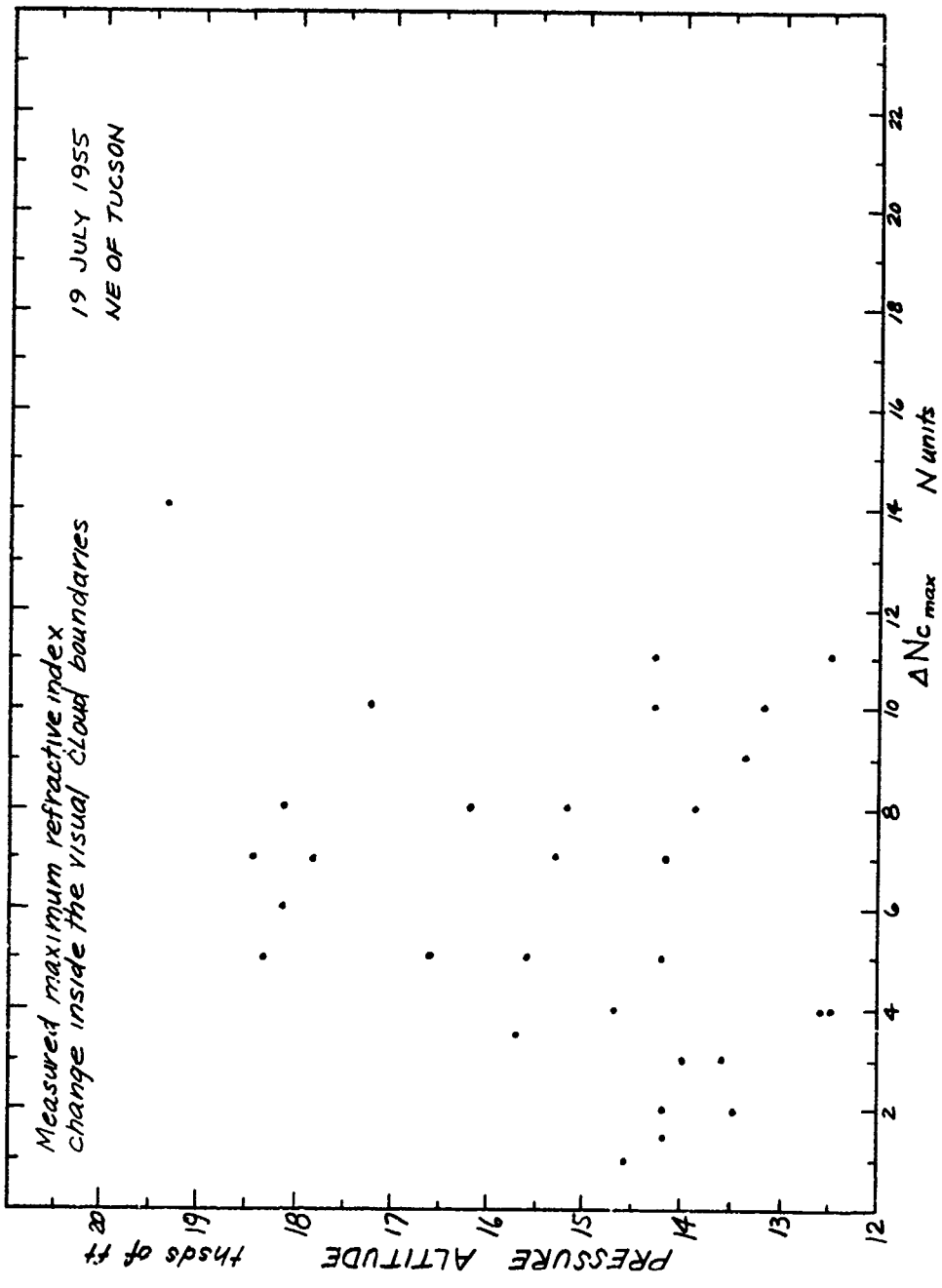
Measured maximum refractive index
change inside the visual cloud boundaries
19 JULY 1955
NE OF TUCSON
PRESSURE ALTITUDE
thsds of ft
ΔNc max
N units

FIGURE 19

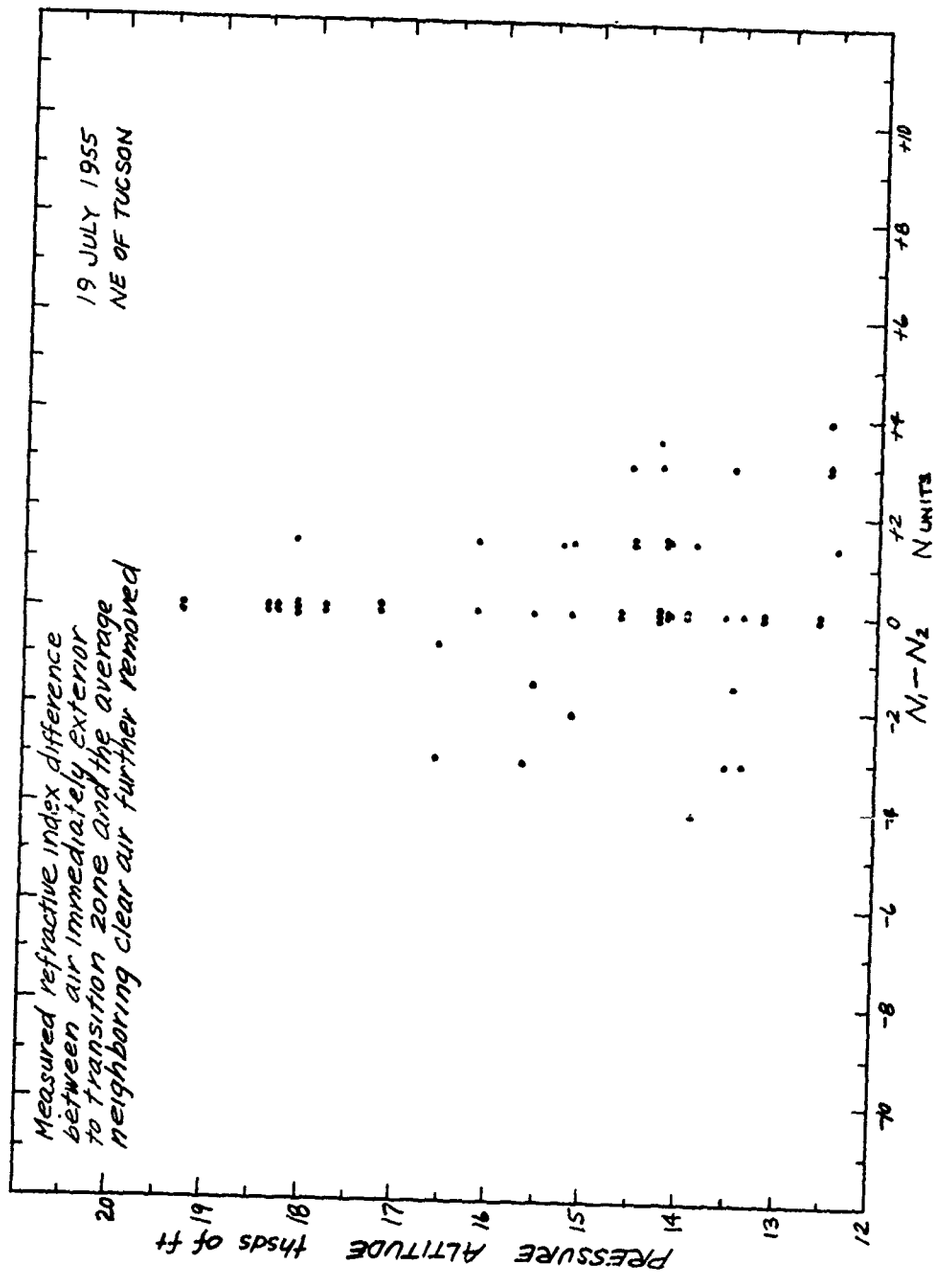
Measured refractive index difference between air immediately exterior to transition zone and the average neighboring clear air further removed
19 JULY 1955
NE OF TUCSON
PRESSURE ALTITUDE thsds of ft
20
19
18
17
16
15
14
13
12
-10
-8
-6
-4
-2
0
+2
+4
+6
+8
+10
N1 − N2 N UNITS

FIGURE 20

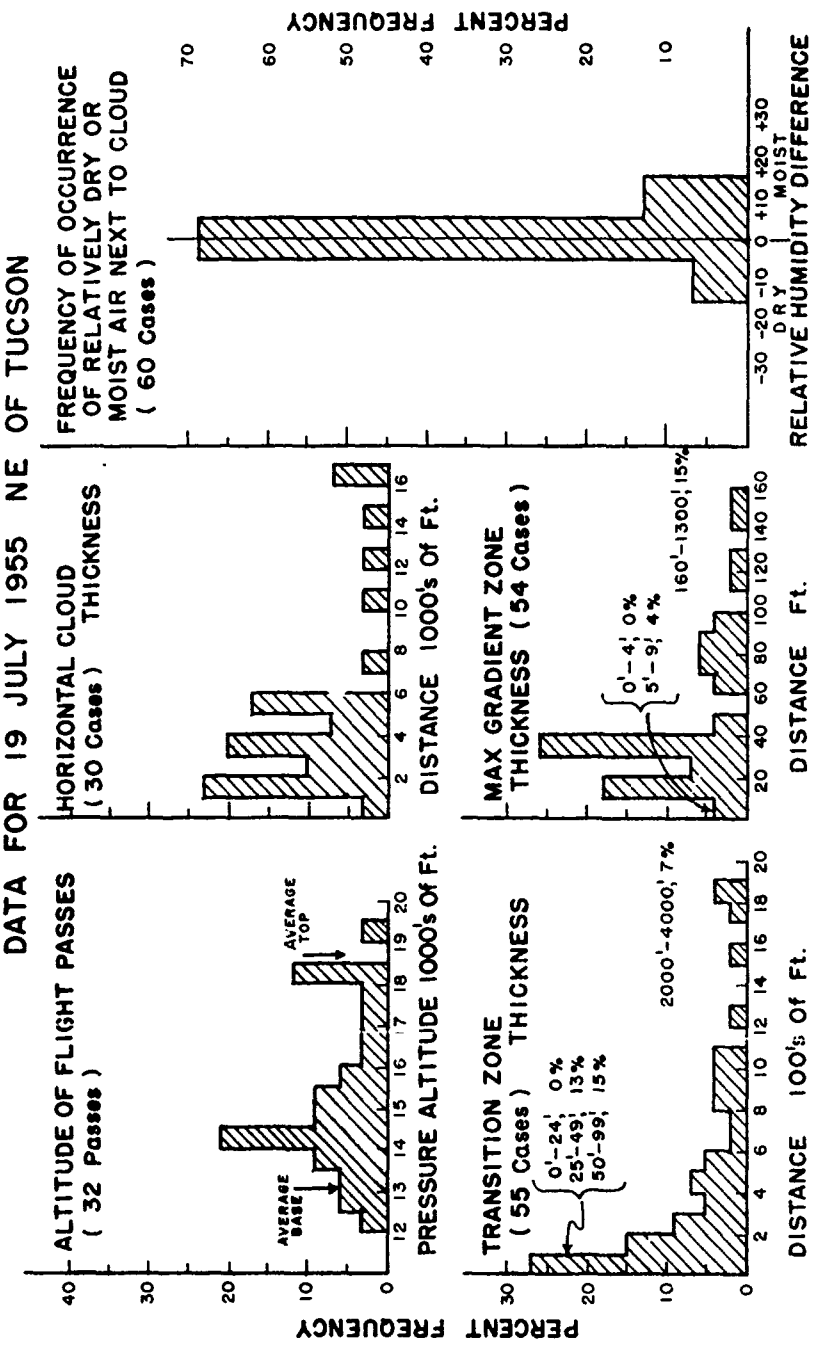
DATA FOR 19 JULY 1955 NE OF TUCSON
ALTITUDE OF FLIGHT PASSES
(32 Passes)
AVERAGE BASE
AVERAGE TOP
PRESSURE ALTITUDE 1000's Of Ft.
HORIZONTAL CLOUD
(30 Cases) THICKNESS
DISTANCE 1000's Of Ft.
FREQUENCY OF OCCURRENCE
OF RELATIVELY DRY OR
MOIST AIR NEXT TO CLOUD
(60 Cases)
DRY
MOIST
RELATIVE HUMIDITY DIFFERENCE
TRANSITION ZONE
(55 Cases) THICKNESS
0'-24'; 0%
25'-49'; 13%
50'-99'; 15%
2000'-4000'; 7%
DISTANCE 100's Of Ft.
MAX GRADIENT ZONE
THICKNESS (54 Cases)
0'-4'; 0%
5'-9'; 4%
160'-1300'; 15%
DISTANCE Ft.
PERCENT FREQUENCY
PERCENT FREQUENCY

FIGURE 21

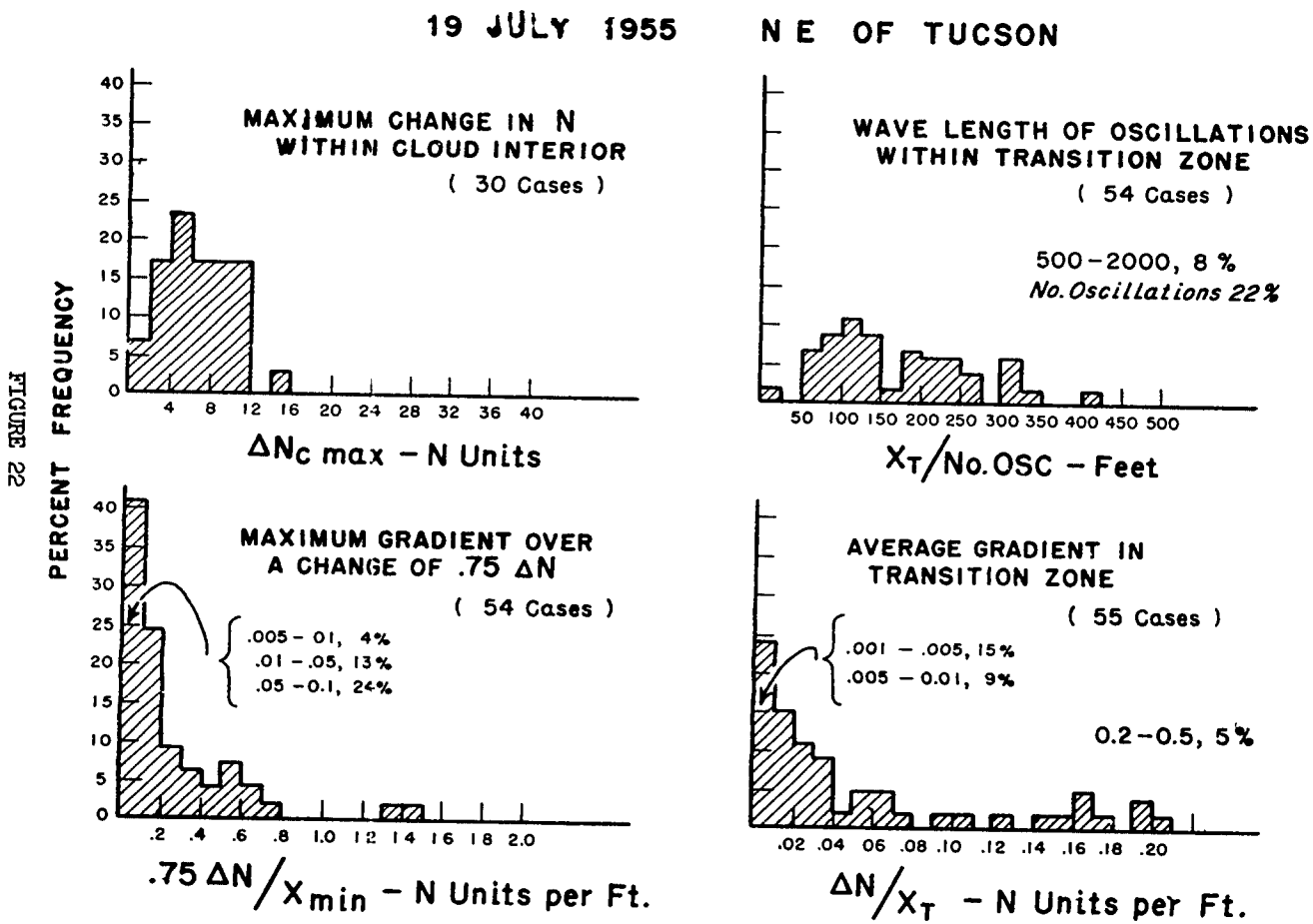
19 JULY 1955
N E OF TUCSON
MAXIMUM CHANGE IN N
WITHIN CLOUD INTERIOR
(30 Cases)
PERCENT FREQUENCY
ΔNc max – N Units
WAVE LENGTH OF OSCILLATIONS
WITHIN TRANSITION ZONE
(54 Cases)
500–2000, 8 %
No. Oscillations 22%
XT/No. OSC – Feet
MAXIMUM GRADIENT OVER
A CHANGE OF .75 ΔN
(54 Cases)
.005 – 01, 4%
.01 – .05, 13%
.05 – 0.1, 24%
.75 ΔN/Xmin – N Units per Ft.
AVERAGE GRADIENT IN
TRANSITION ZONE
(55 Cases)
.001 – .005, 15%
.005 – 0.01, 9%
0.2–0.5, 5%
ΔN/XT – N Units per Ft.

FIGURE 22

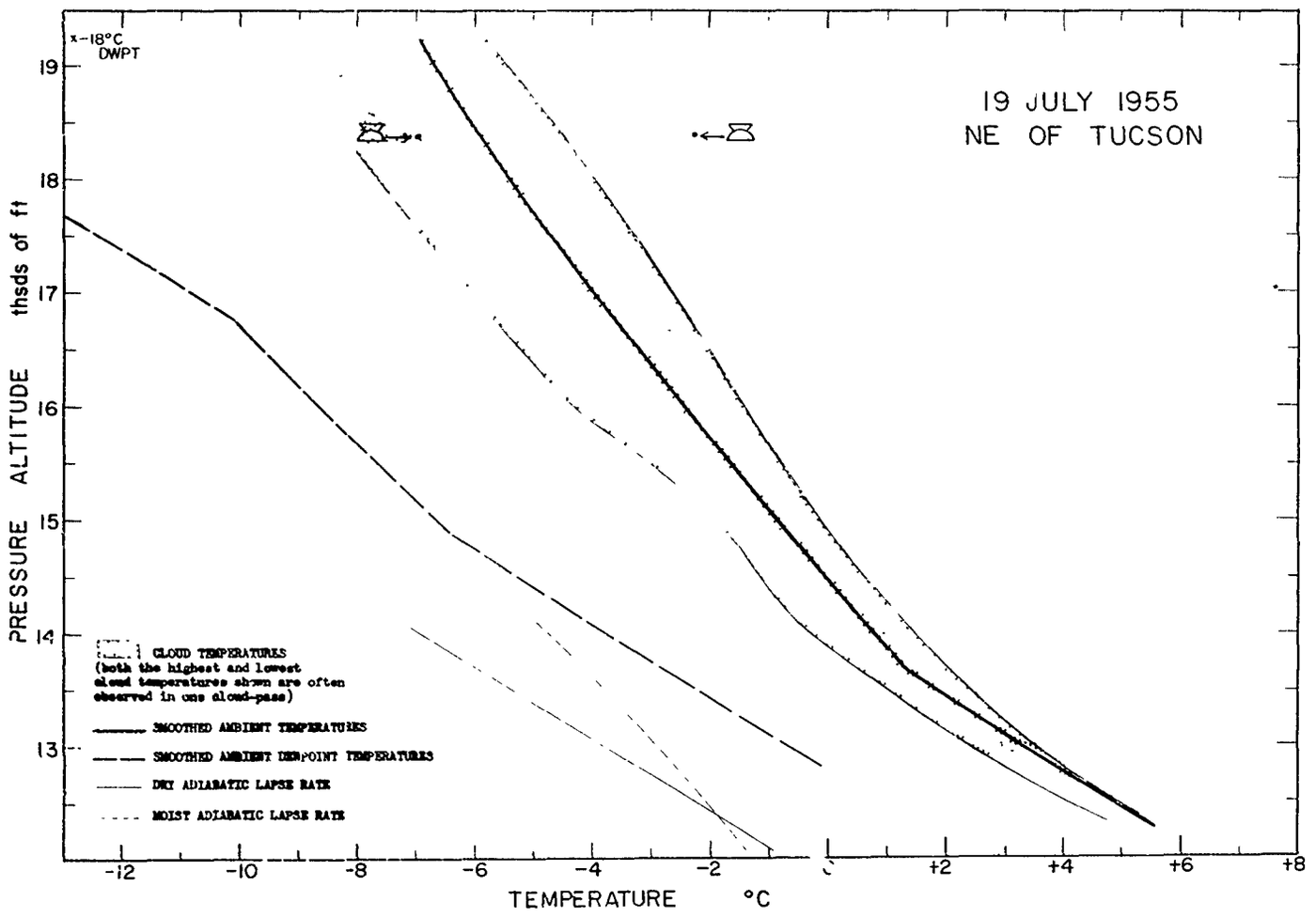
x-18°C
DWPT
19 JULY 1955
NE OF TUCSON
PRESSURE ALTITUDE thsds of ft
19
18
17
16
15
14
13
CLOUD TEMPERATURES
(both the highest and lowest
cloud temperatures shown are often
observed in one cloud-pass)
SMOOTHED AMBIENT TEMPERATURES
SMOOTHED AMBIENT DEW-POINT TEMPERATURES
DRY ADIABATIC LAPSE RATE
MOIST ADIABATIC LAPSE RATE
-12
-10
-8
-6
-4
-2
+2
+4
+6
+8
TEMPERATURE °C

FIGURE 23

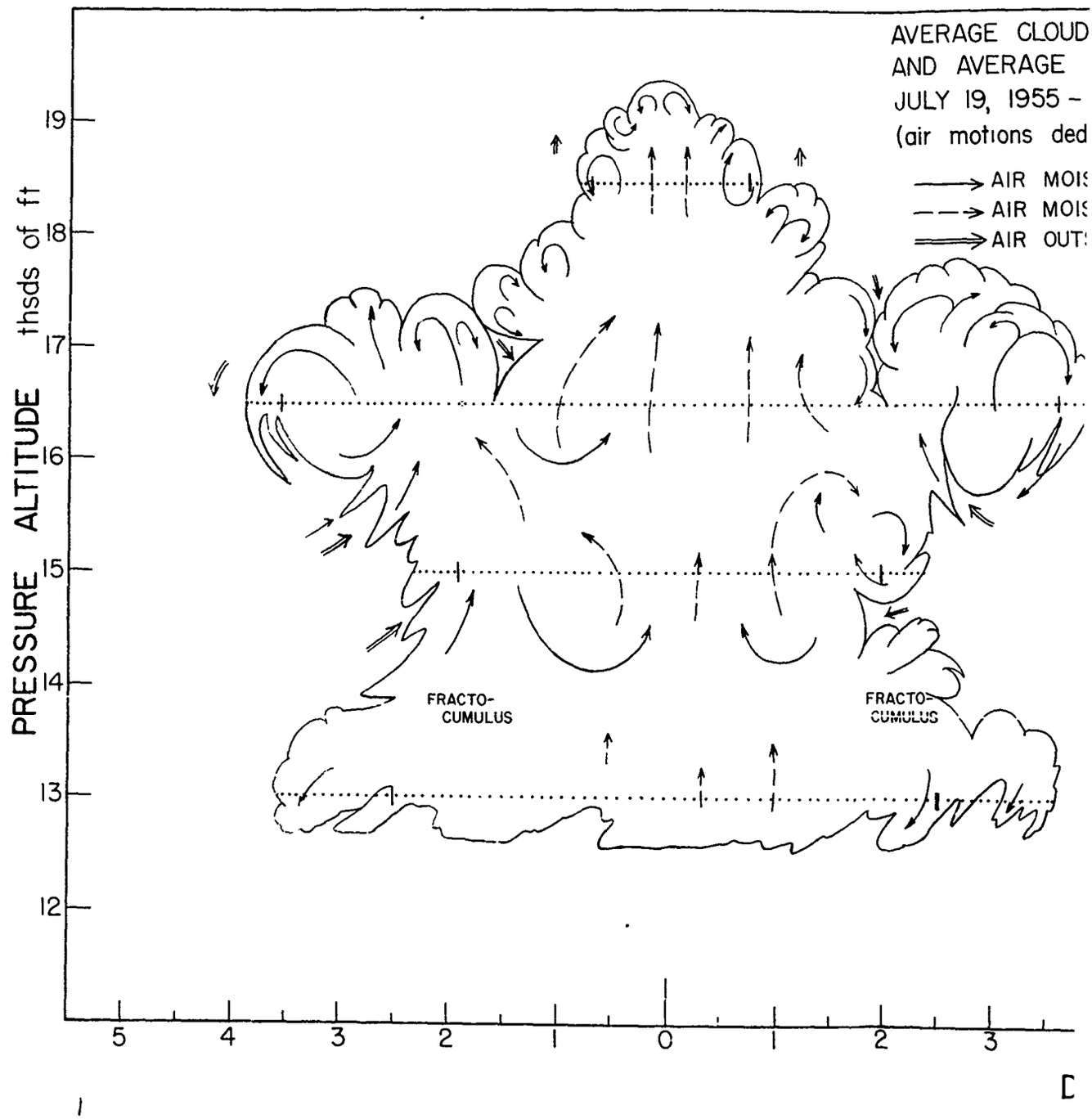

The Murray Printing Company, Wakefield, Mass., 2-11-57 --- 1000

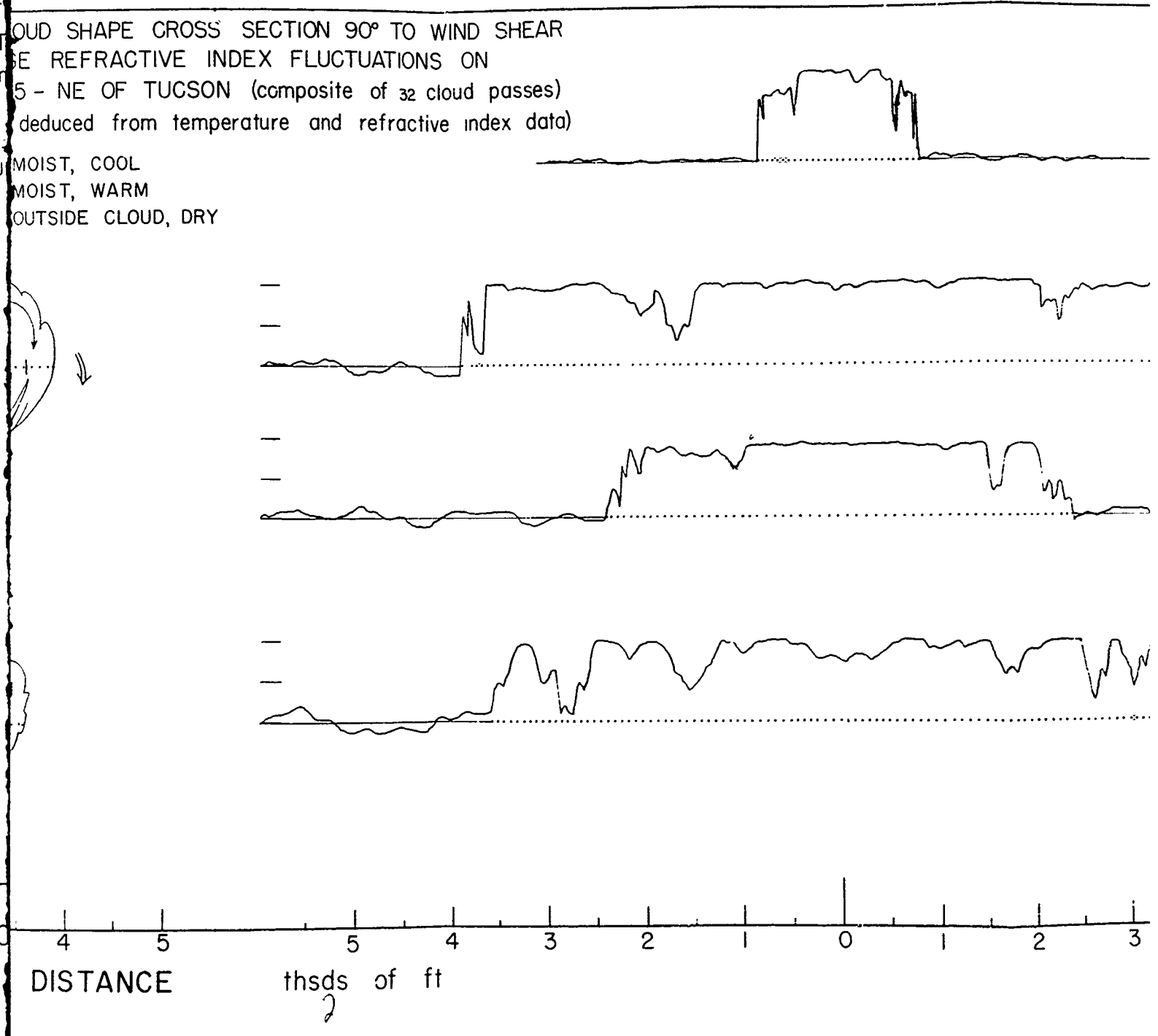
OUD SHAPE CROSS SECTION 90° TO WIND SHEAR
E REFRACTIVE INDEX FLUCTUATIONS ON
5 - NE OF TUCSON (composite of 32 cloud passes)
deduced from temperature and refractive index data)
MOIST, COOL
MOIST, WARM
OUTSIDE CLOUD, DRY
4
5
5
4
3
2
1
0
1
2
3
DISTANCE
thsds of ft

Figure 24.

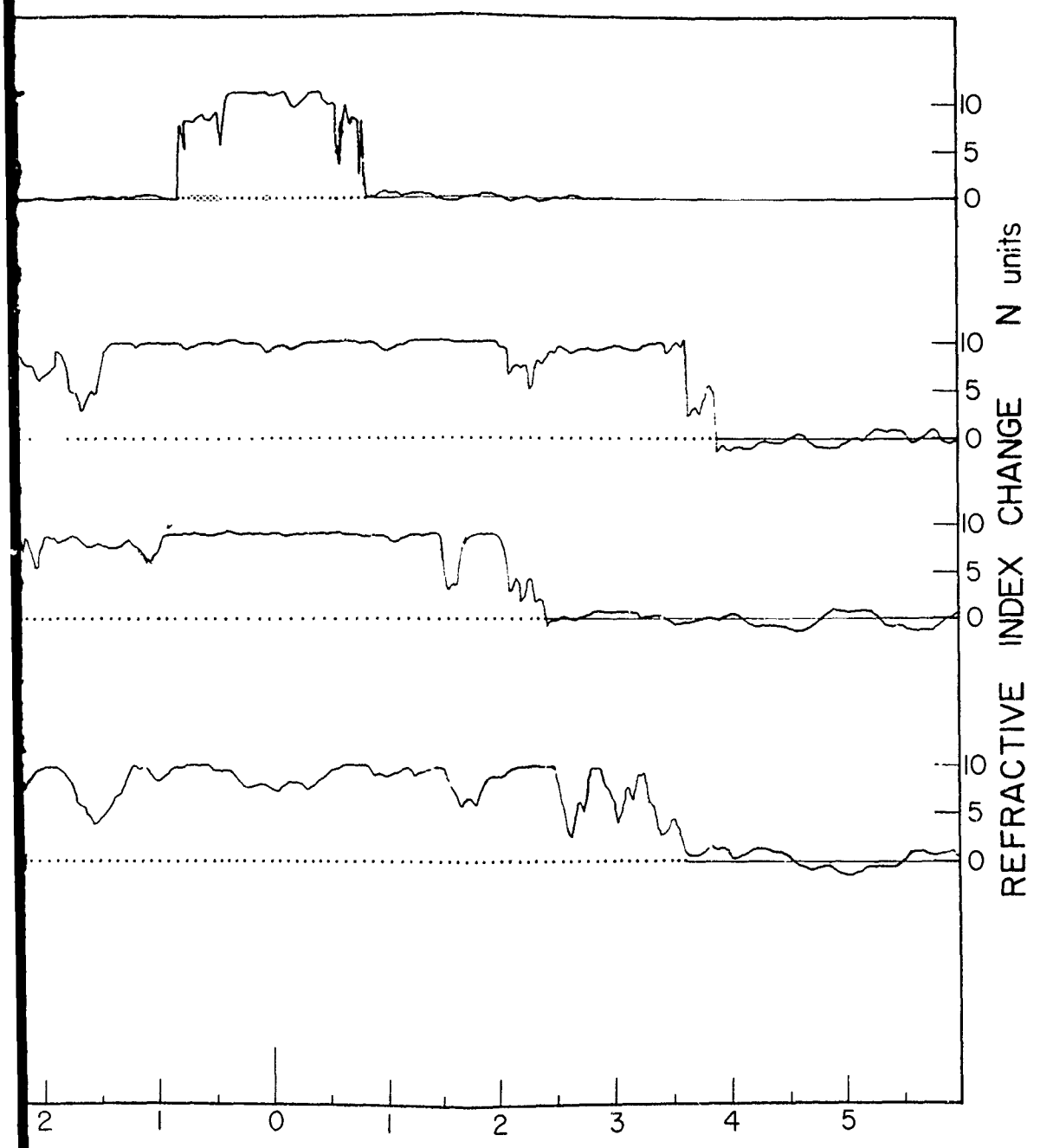
10
5
0
10
5
0
10
5
0
10
5
0
REFRACTIVE INDEX CHANGE N units
2
1
0
1
2
3
4
5

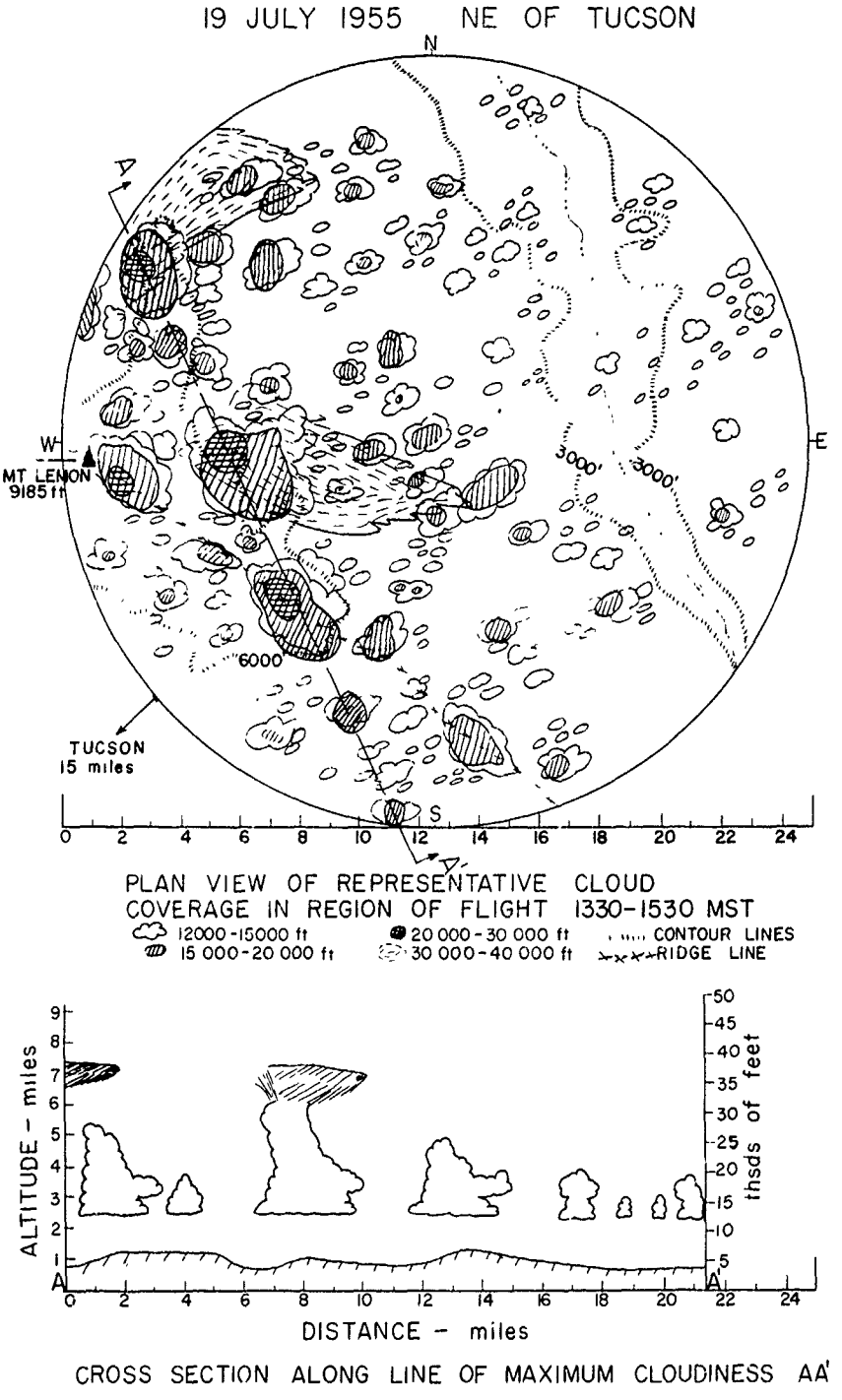
19 JULY 1955 NE OF TUCSON
N
W
E
S
A
A'
MT LEMON
9185ft
TUCSON
15 miles
3000'
3000'
6000'
0 2 4 6 8 10 12 14 16 18 20 22 24
PLAN VIEW OF REPRESENTATIVE CLOUD
COVERAGE IN REGION OF FLIGHT 1330-1530 MST
12000-15000 ft
15 000-20 000 ft
20 000-30 000 ft
30 000-40 000 ft
CONTOUR LINES
RIDGE LINE
ALTITUDE - miles
thsds of feet
DISTANCE - miles
CROSS SECTION ALONG LINE OF MAXIMUM CLOUDINESS AA'

Figure 25

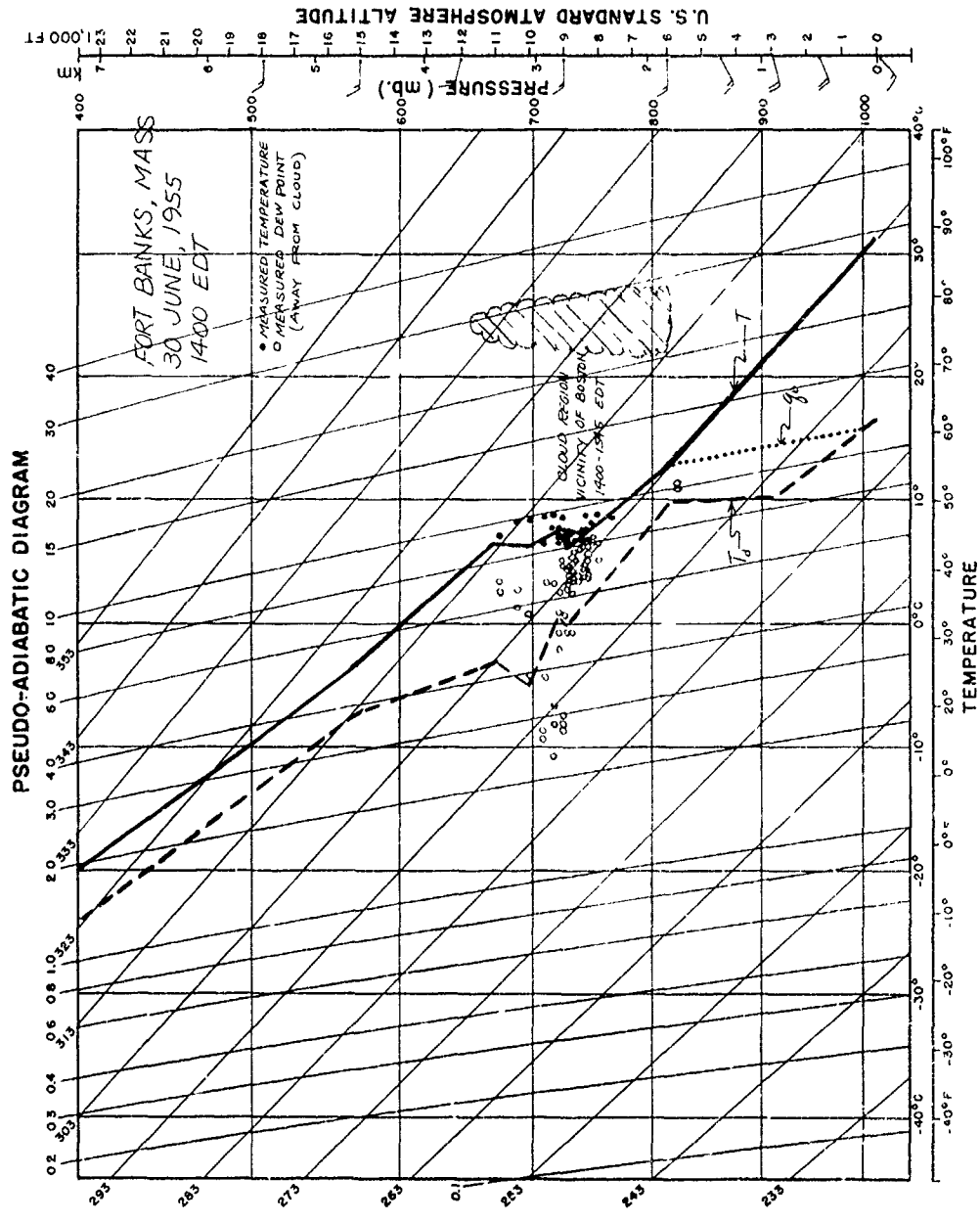
U.S. STANDARD ATMOSPHERE ALTITUDE
PRESSURE (mb.)
PSEUDO-ADIABATIC DIAGRAM
TEMPERATURE
FORT BANKS, MASS
30 JUNE, 1955
1400 EDT
• MEASURED TEMPERATURE
○ MEASURED DEW POINT
(AWAY FROM CLOUD)
CLOUD REGION
VICINITY OF BOSTON
1400-1500 EDT

FIGURE 26

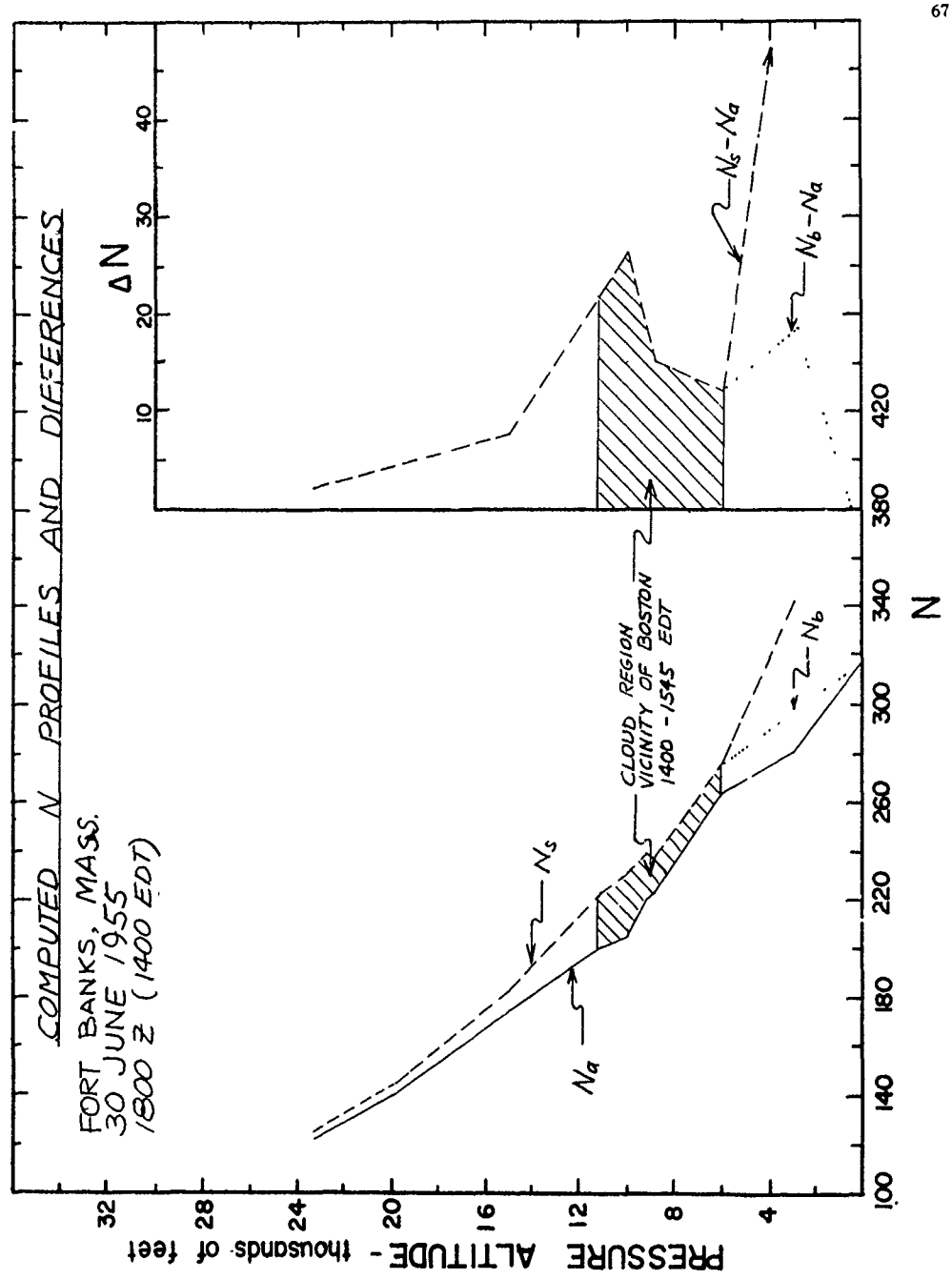
COMPUTED N PROFILES AND DIFFERENCES
FORT BANKS, MASS.
30 JUNE 1955
1800 Z (1400 EDT)
PRESSURE ALTITUDE - thousands of feet
N
ΔN
N_a
N_s
N_b
$N_s - N_a$
$N_b - N_a$
CLOUD REGION
VICINITY OF BOSTON
1400 - 1545 EDT

FIGURE 27

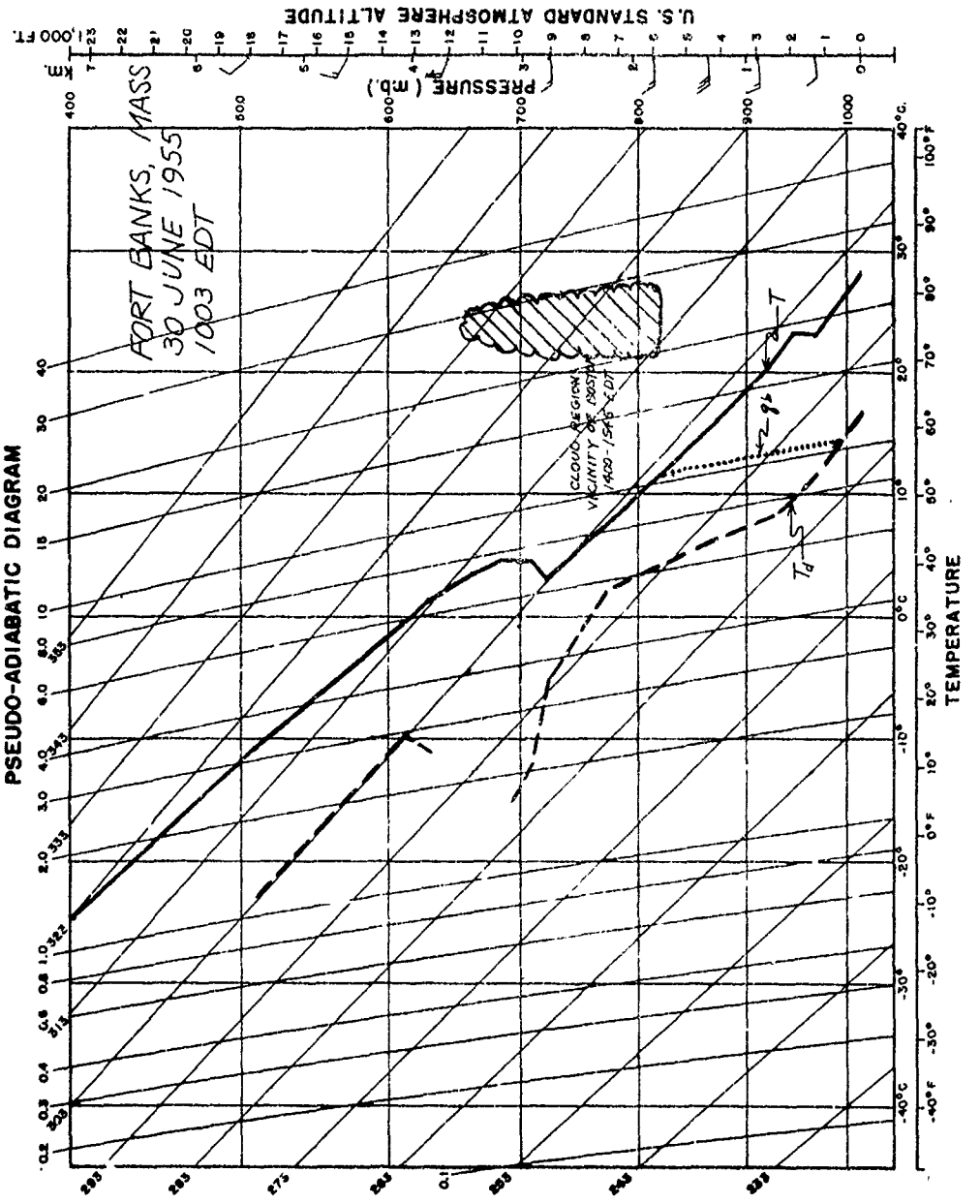
PSEUDO-ADIABATIC DIAGRAM
U.S. STANDARD ATMOSPHERE ALTITUDE
PRESSURE (mb.)
TEMPERATURE
FORT BANKS, MASS
30 JUNE 1955
1003 EDT
CLOUD REGION
VICINITY OF BOSTON
1420 / SAS EDT
T
Td

FIGURE 28

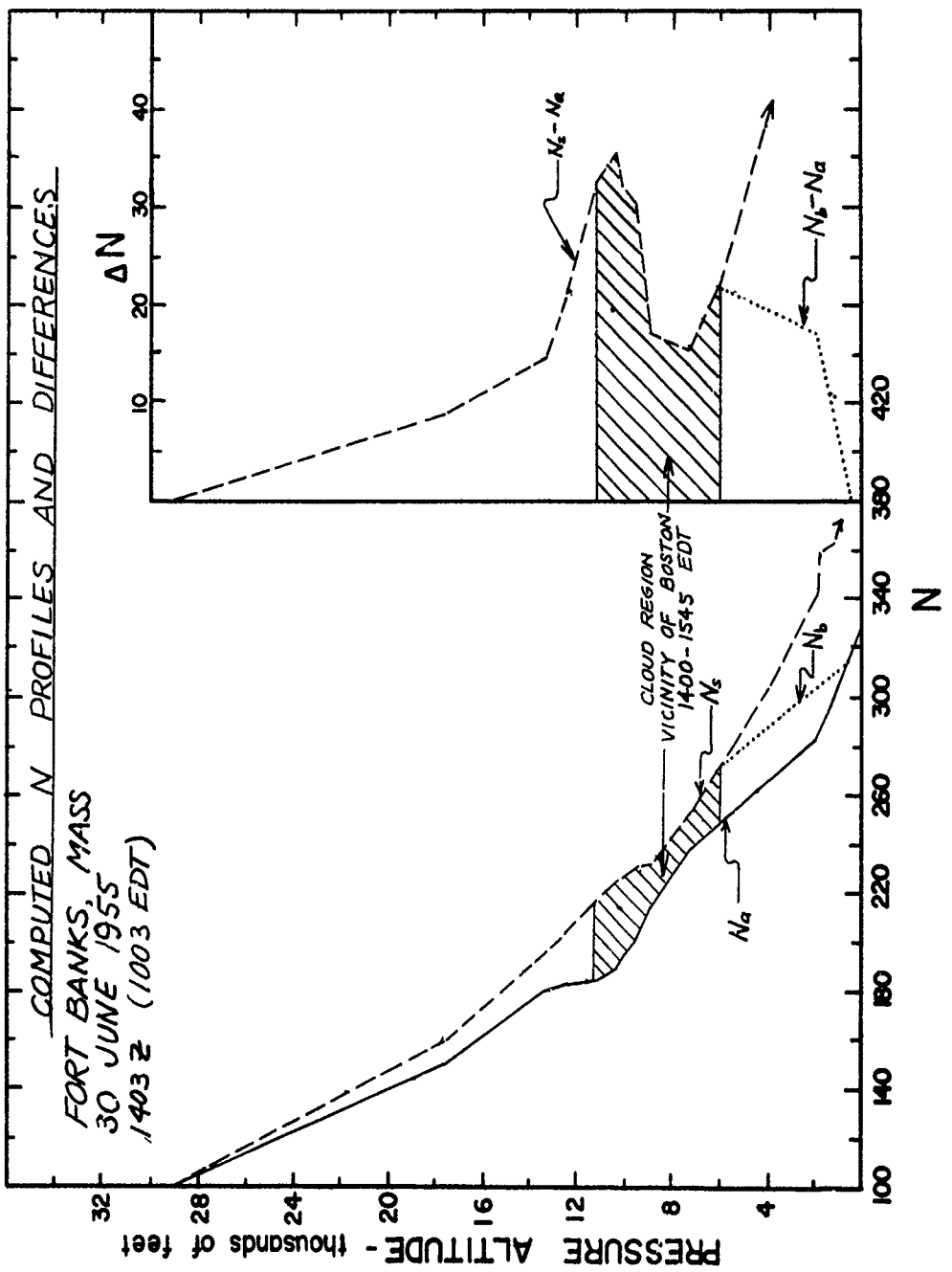
COMPUTED N PROFILES AND DIFFERENCES
FORT BANKS, MASS
30 JUNE 1955
1403 Z (1003 EDT)
PRESSURE ALTITUDE - thousands of feet
N
ΔN
CLOUD REGION
VICINITY OF BOSTON
1400-1545 EDT
Ns
Na
Nb
Ns-Na
Nb-Na

FIGURE 29

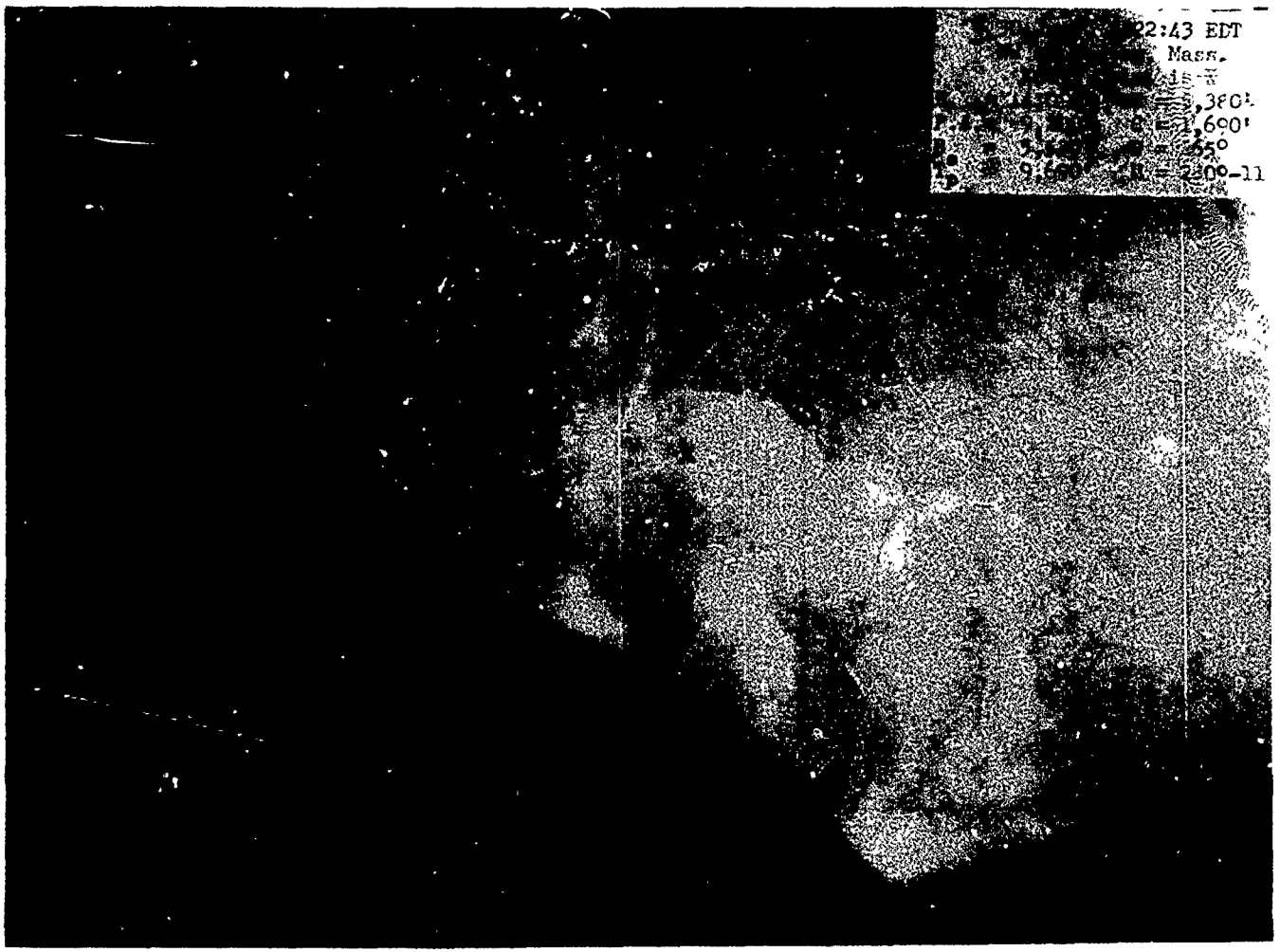

FIGURE 30

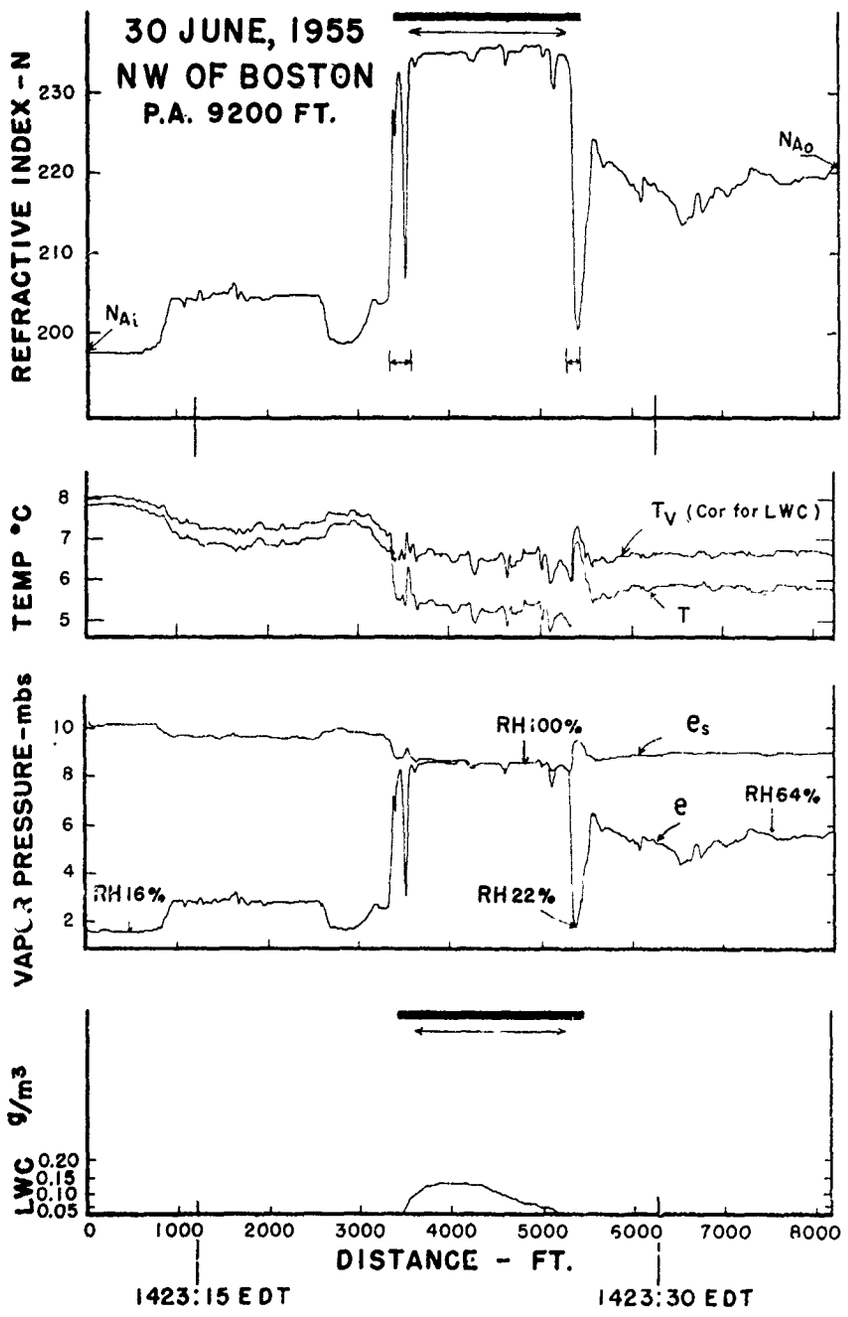
30 JUNE, 1955
NW OF BOSTON
P.A. 9200 FT.
REFRACTIVE INDEX - N
230
220
210
200
N_{Ai}
N_{Ao}
TEMP °C
8
7
6
5
T_V (Cor for LWC)
T
VAPOR PRESSURE-mbs
10
8
6
4
2
RH 100%
e_s
e
RH 64%
RH 16%
RH 22%
LWC g/m³
0.20
0.15
0.10
0.05
0
1000
2000
3000
4000
5000
6000
7000
8000
DISTANCE - FT.
1423:15 EDT
1423:30 EDT

FIGURE 31

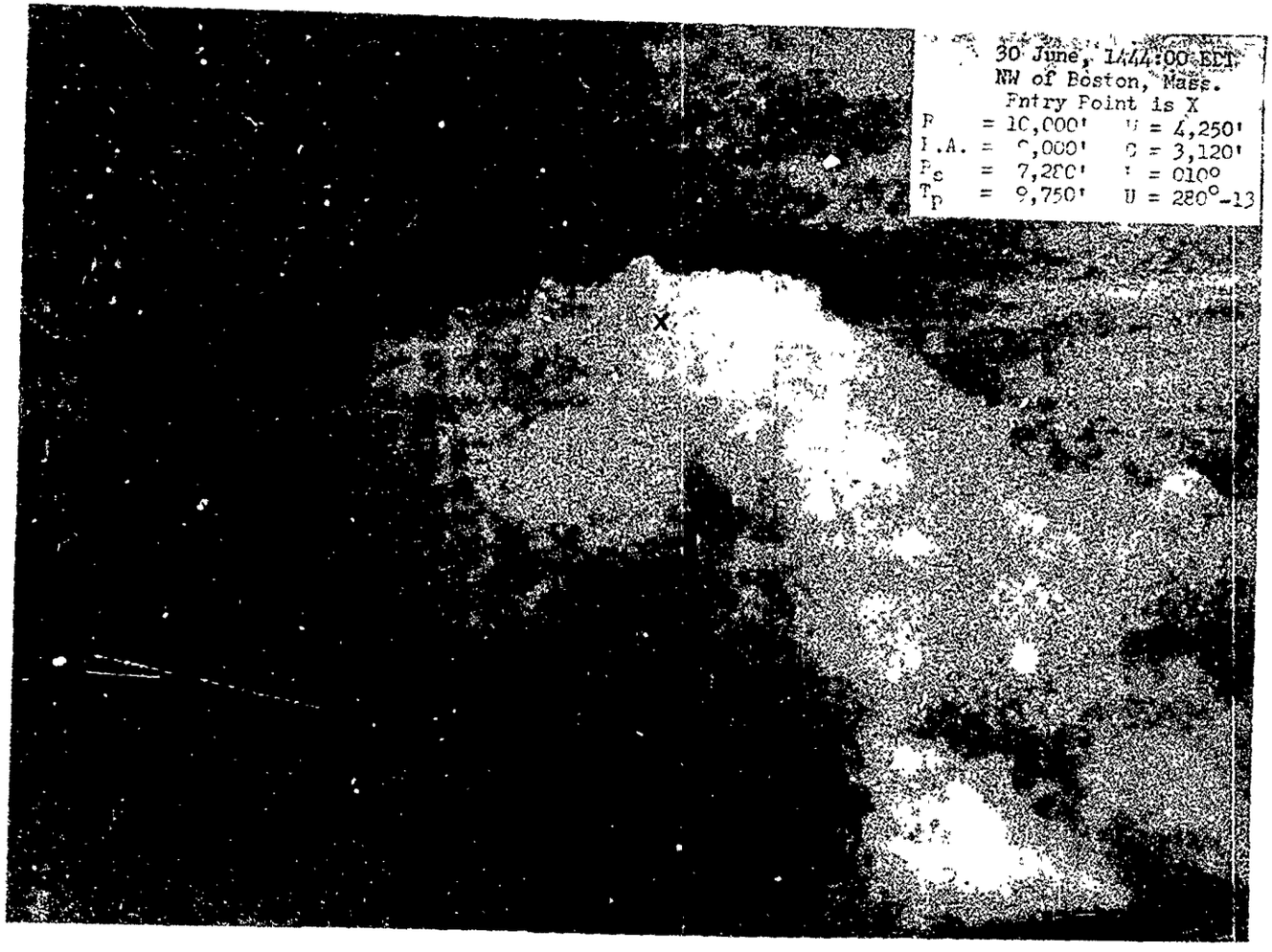
30 June, 1444:00 EDT
NW of Boston, Mass.
Entry Point is X
P = 10,000' U = 4,250'
I.A. = 0,000' D = 3,120'
Pc = 7,200' ' = 010°
Tp = 9,750' U = 280°-13
X

FIGURE 32

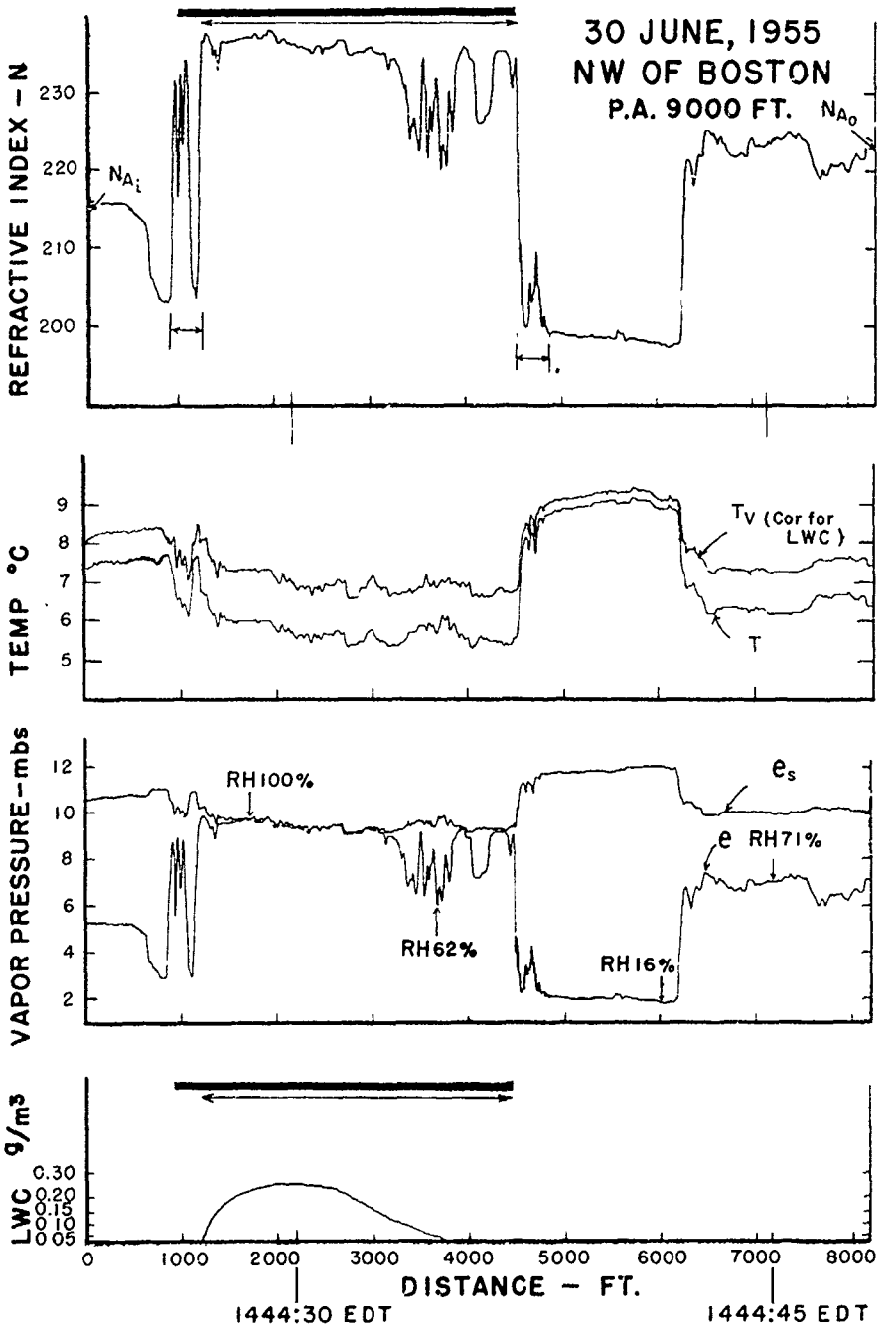
30 JUNE, 1955
NW OF BOSTON
P.A. 9000 FT.
REFRACTIVE INDEX - N
230
220
210
200
N_{A_i}
N_{A_0}
TEMP °C
9
8
7
6
5
T_V (Cor for LWC)
T
VAPOR PRESSURE-mbs
12
10
8
6
4
2
RH100%
e_s
e RH71%
RH62%
RH16%
LWC g/m³
0.30
0.20
0.15
0.10
0.05
0
1000
2000
3000
4000
5000
6000
7000
8000
DISTANCE - FT.
1444:30 EDT
1444:45 EDT

FIGURE 33

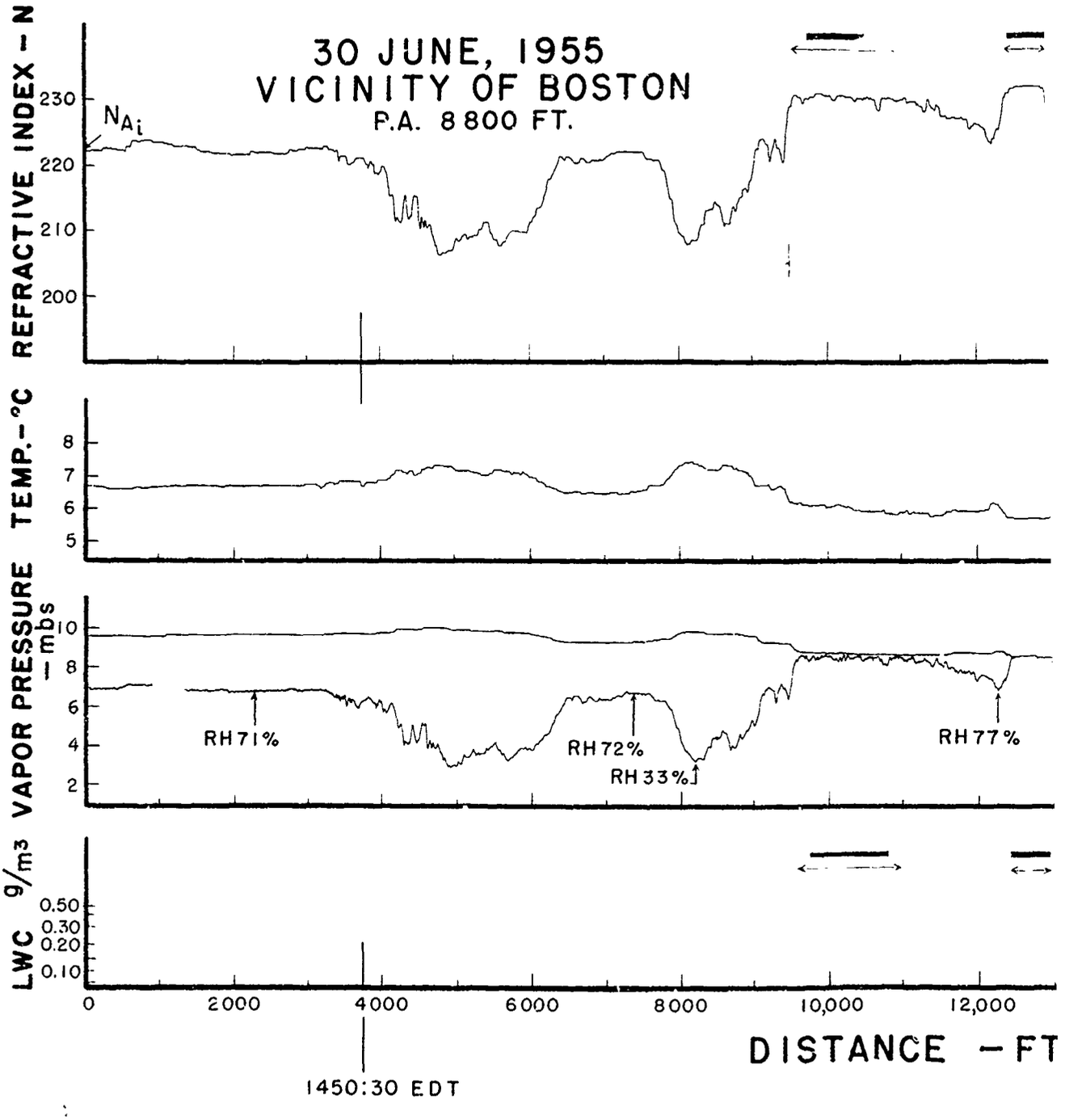

Figure 34.

The Murray Printing Company, Wakefield, Mass., 2-11-57 --- 1000

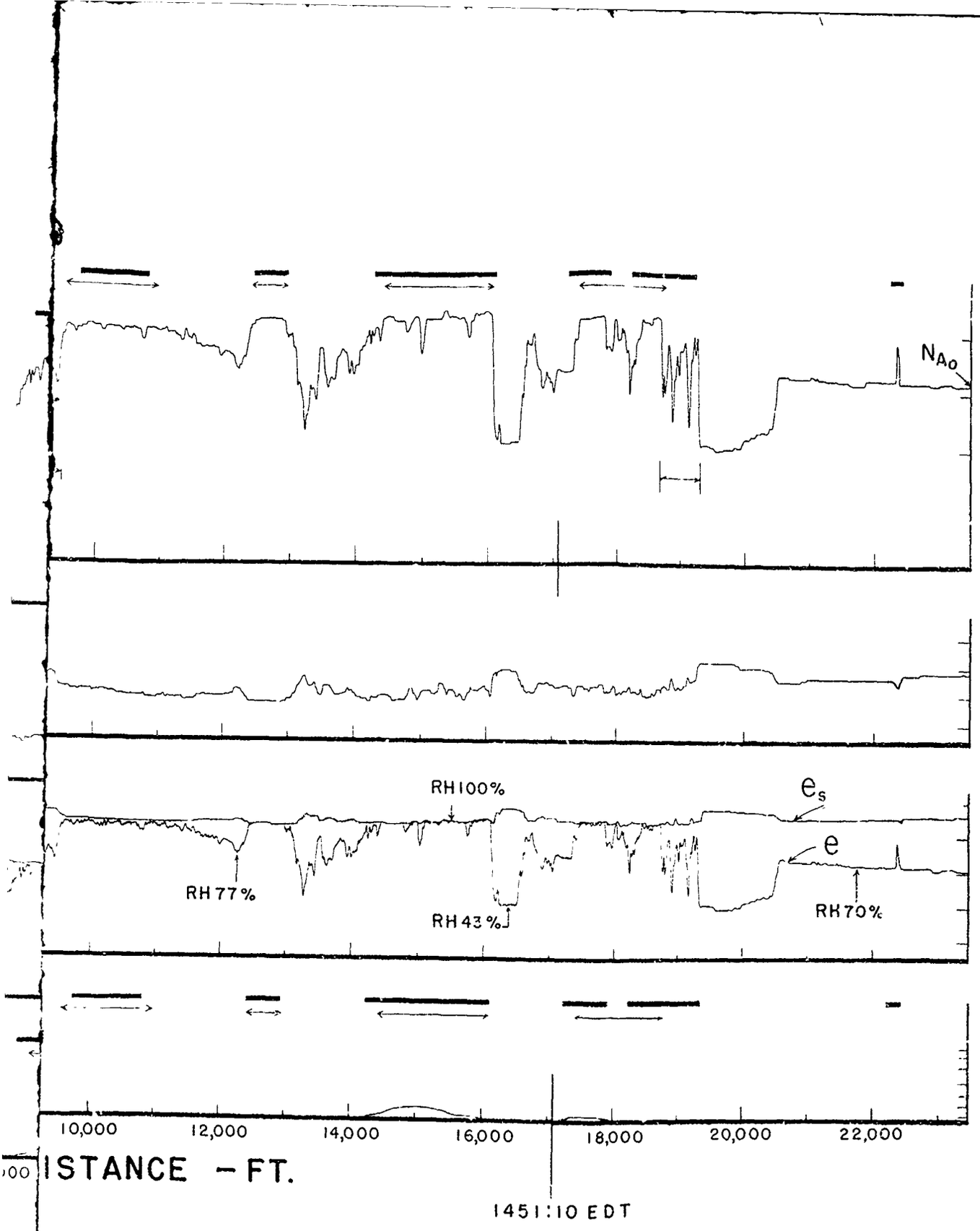
N_{Ao}
RH100%
e_s
e
RH 77%
RH 43%
RH 70%
10,000
12,000
14,000
16,000
18,000
20,000
22,000
ISTANCE - FT.
1451:10 EDT

Figure 34.

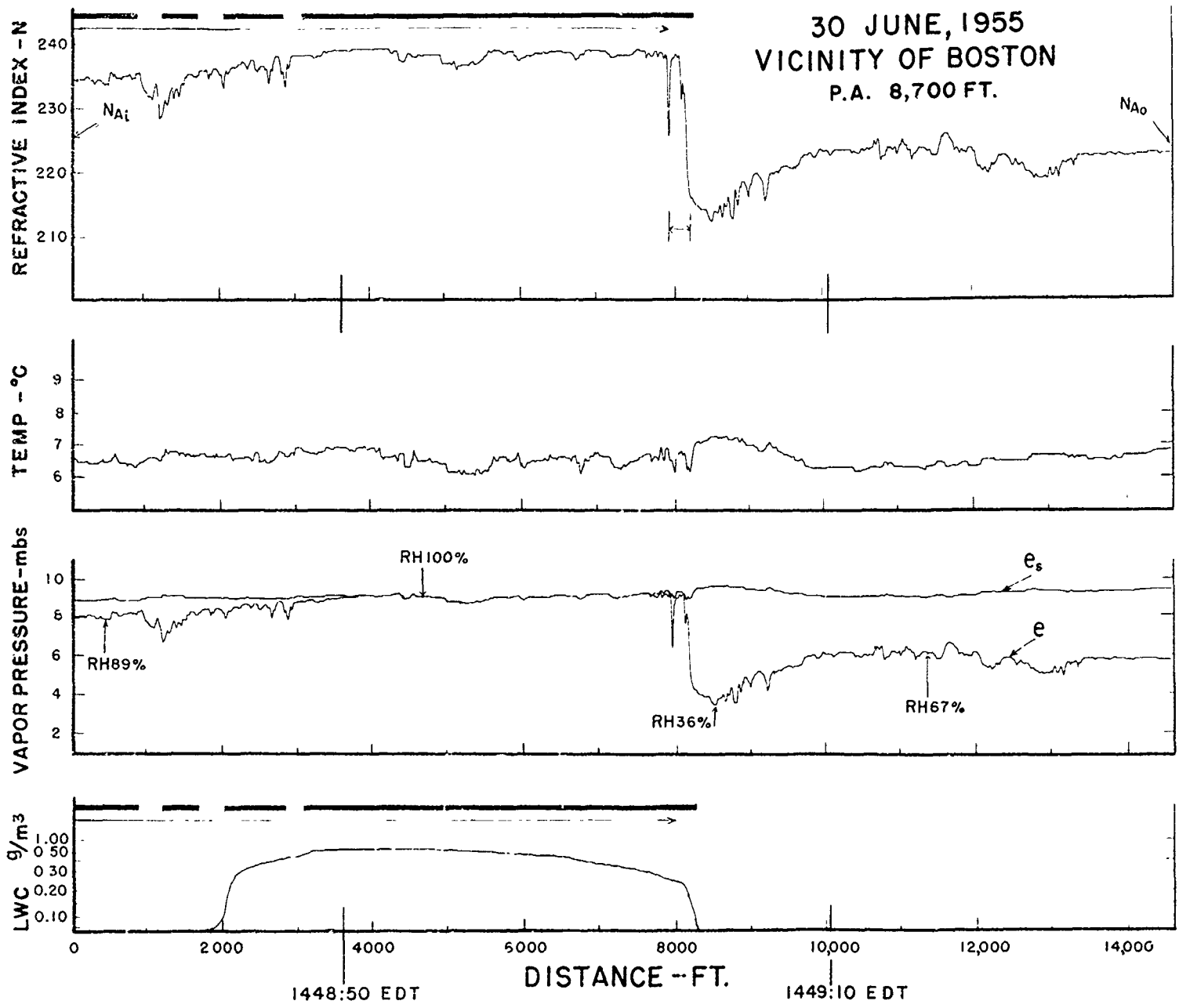

Figure 35.

The Murray Printing Company, Wakefield, Mass., 2-11-57 --- 1000

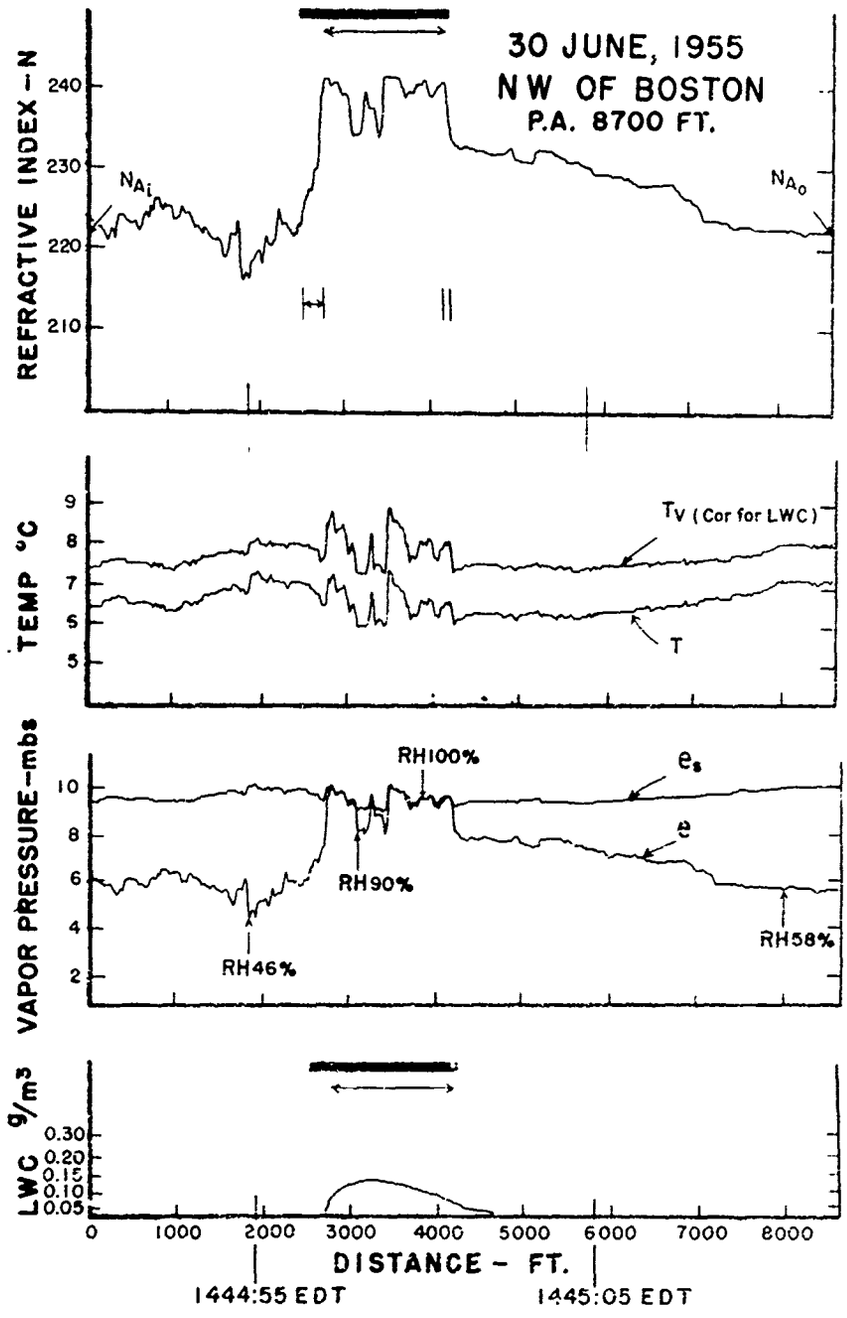
30 JUNE, 1955
NW OF BOSTON
P.A. 8700 FT.
REFRACTIVE INDEX - N
240
230
220
210
N_{A_i}
N_{A_o}
TEMP °C
9
8
7
6
5
T_V (Cor for LWC)
T
VAPOR PRESSURE-mbs
10
8
6
4
2
RH100%
e_s
e
RH90%
RH46%
RH58%
LWC g/m³
0.30
0.20
0.15
0.10
0.05
0
1000
2000
3000
4000
5000
6000
7000
8000
DISTANCE - FT.
1444:55 EDT
1445:05 EDT

FIGURE 36

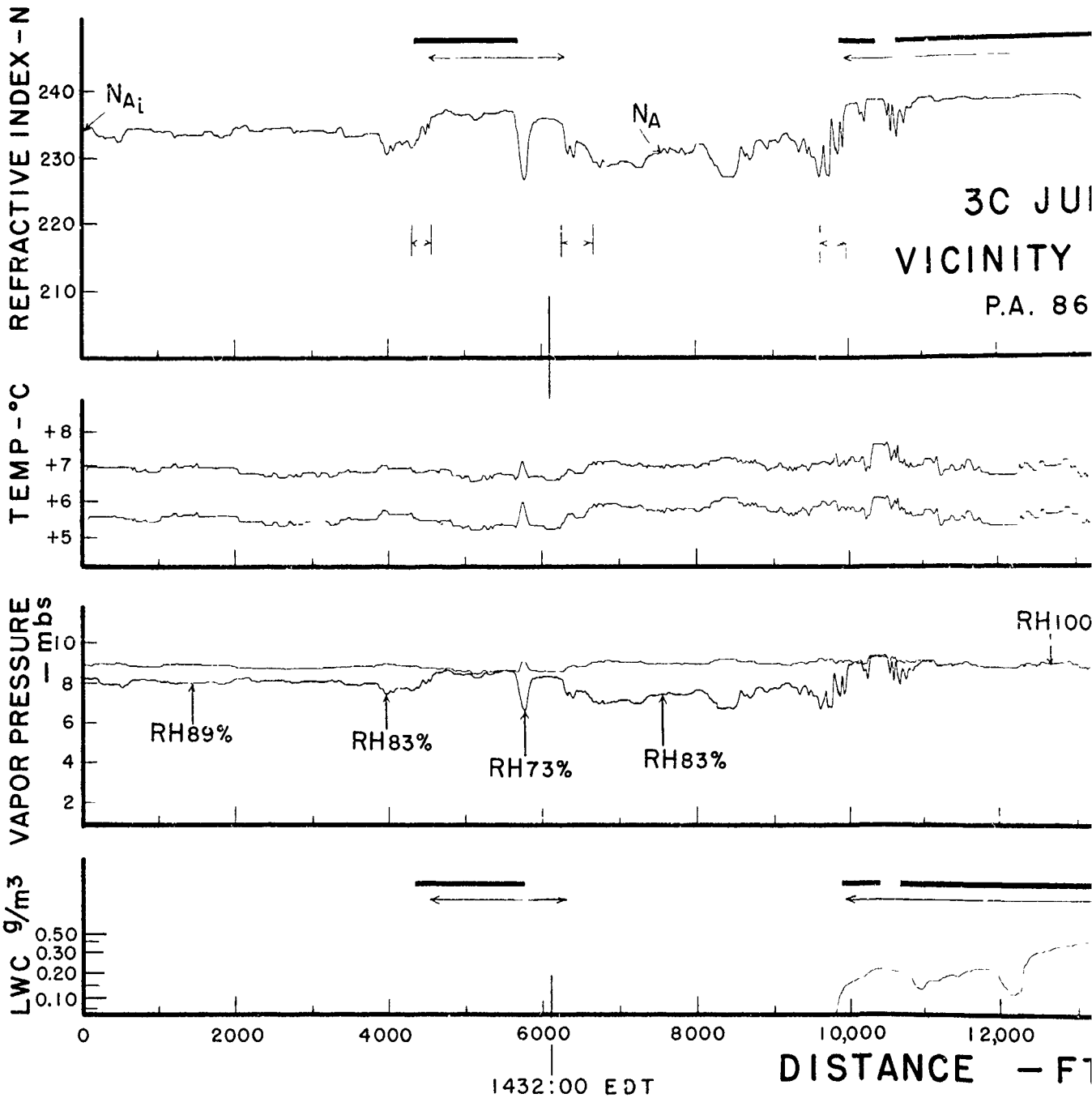

Figure 37.

The Murray Printing Company, Wakefield, Mass., 2-11-57 --- 1000

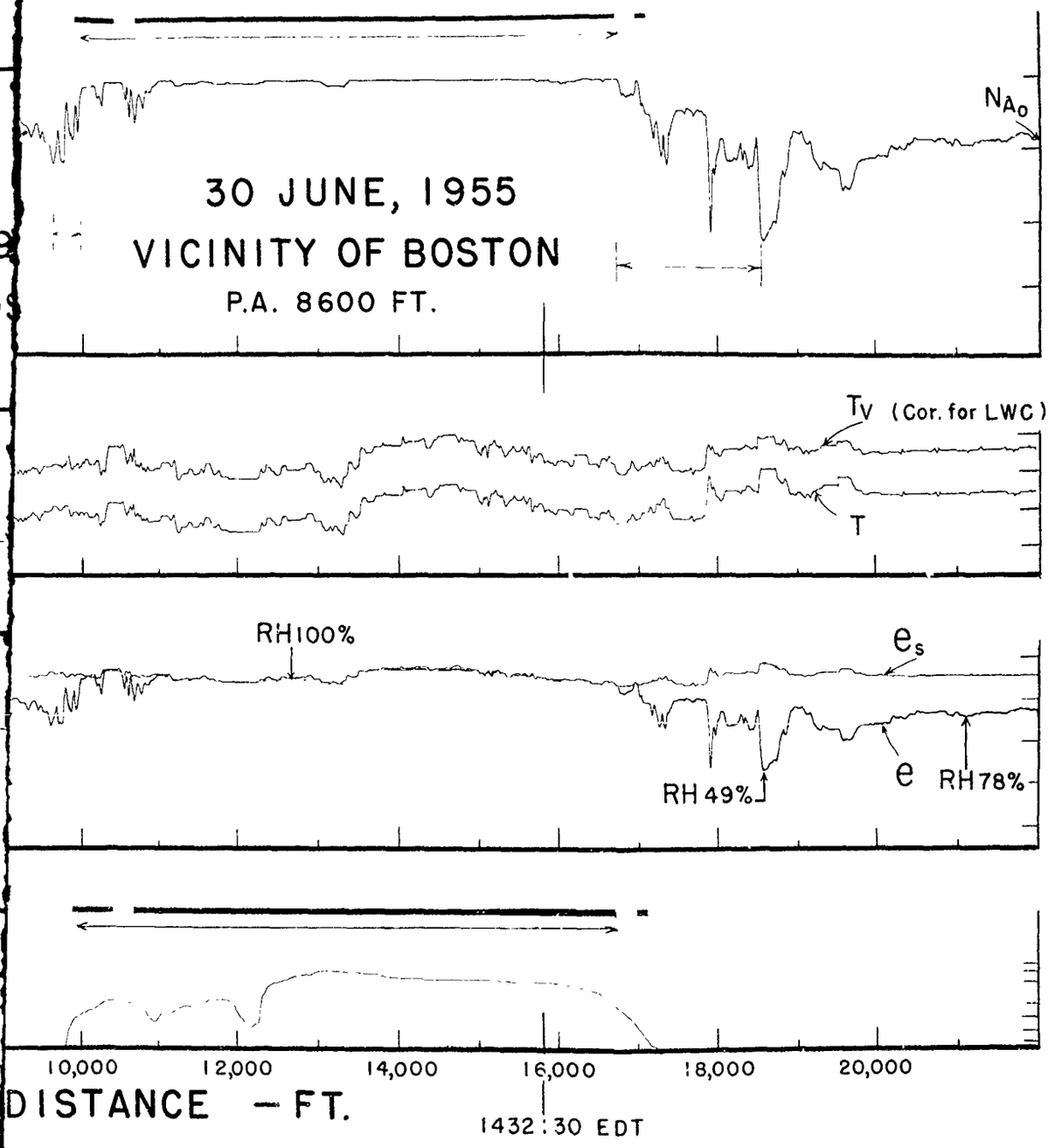
30 JUNE, 1955
VICINITY OF BOSTON
P.A. 8600 FT.
N_{A_0}
T_V (Cor. for LWC)
T
RH100%
e_s
e
RH 49%
RH 78%
10,000
12,000
14,000
16,000
18,000
20,000
DISTANCE — FT.
1432:30 EDT

Figure 37.

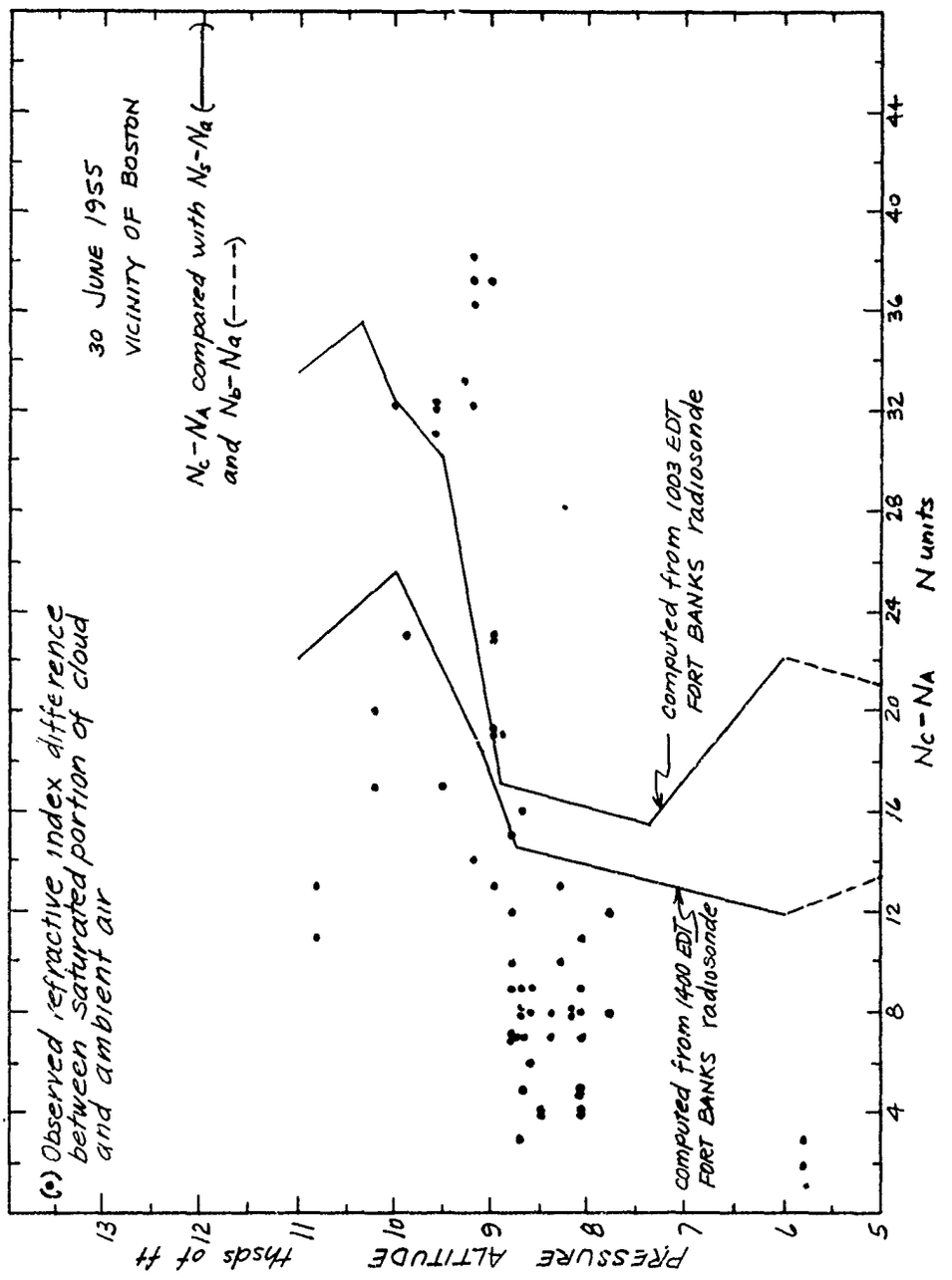
(•) Observed refractive index difference between saturated portion of cloud and ambient air
30 JUNE 1955
VICINITY OF BOSTON
$N_c - N_A$ compared with $N_s - N_a$ (——)
and $N_b - N_a$ (- - - -)
computed from 1003 EDT FORT BANKS radiosonde
computed from 1400 EDT FORT BANKS radiosonde
PRESSURE ALTITUDE thsds of ft
$N_c - N_A$ N units

FIGURE 38

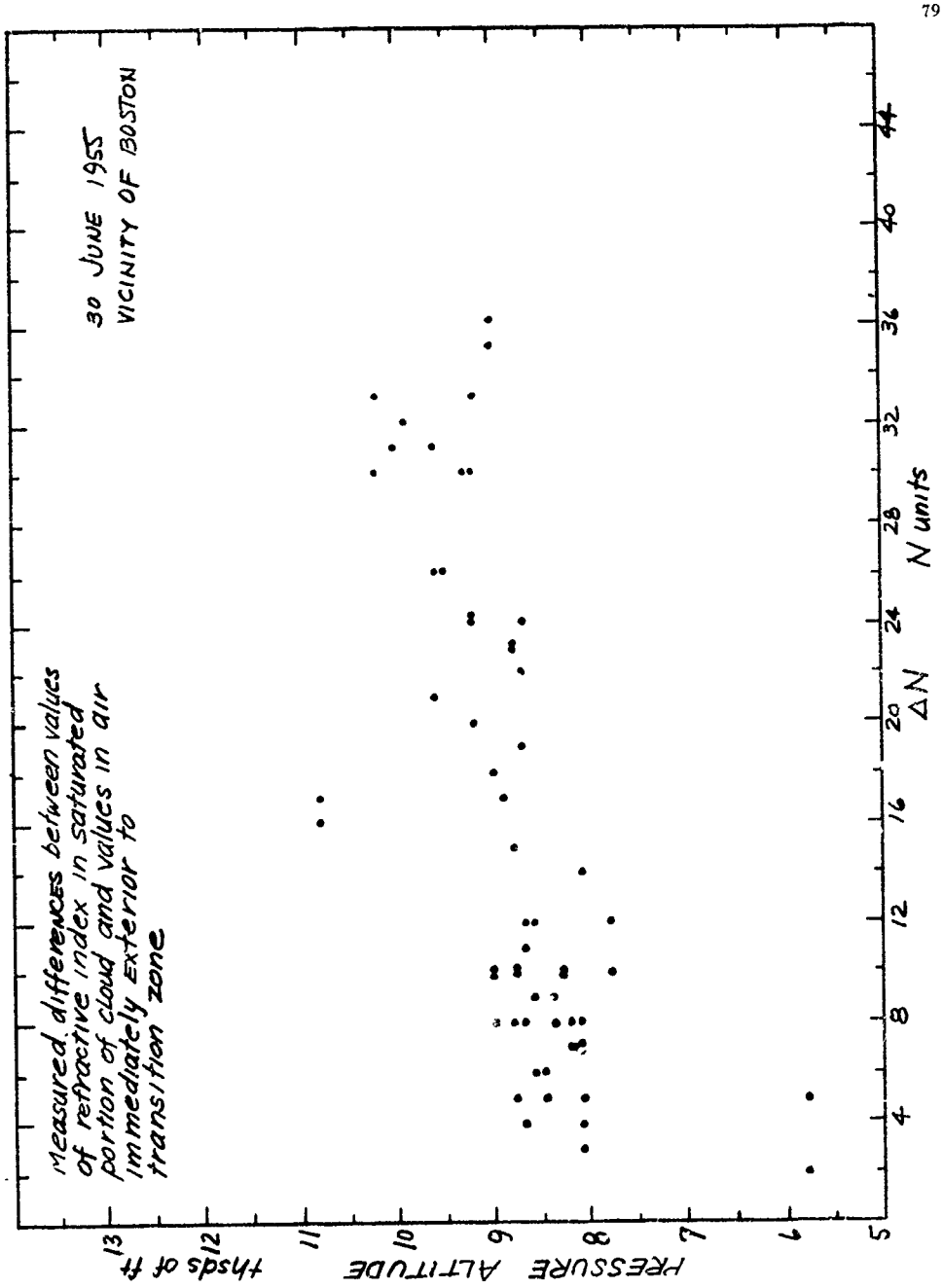
Measured differences between values of refractive index in saturated portion of cloud and values in air immediately exterior to transition zone
30 JUNE 1955
VICINITY OF BOSTON
PRESSURE ALTITUDE
thsds of ft
ΔN N units

FIGURE 39

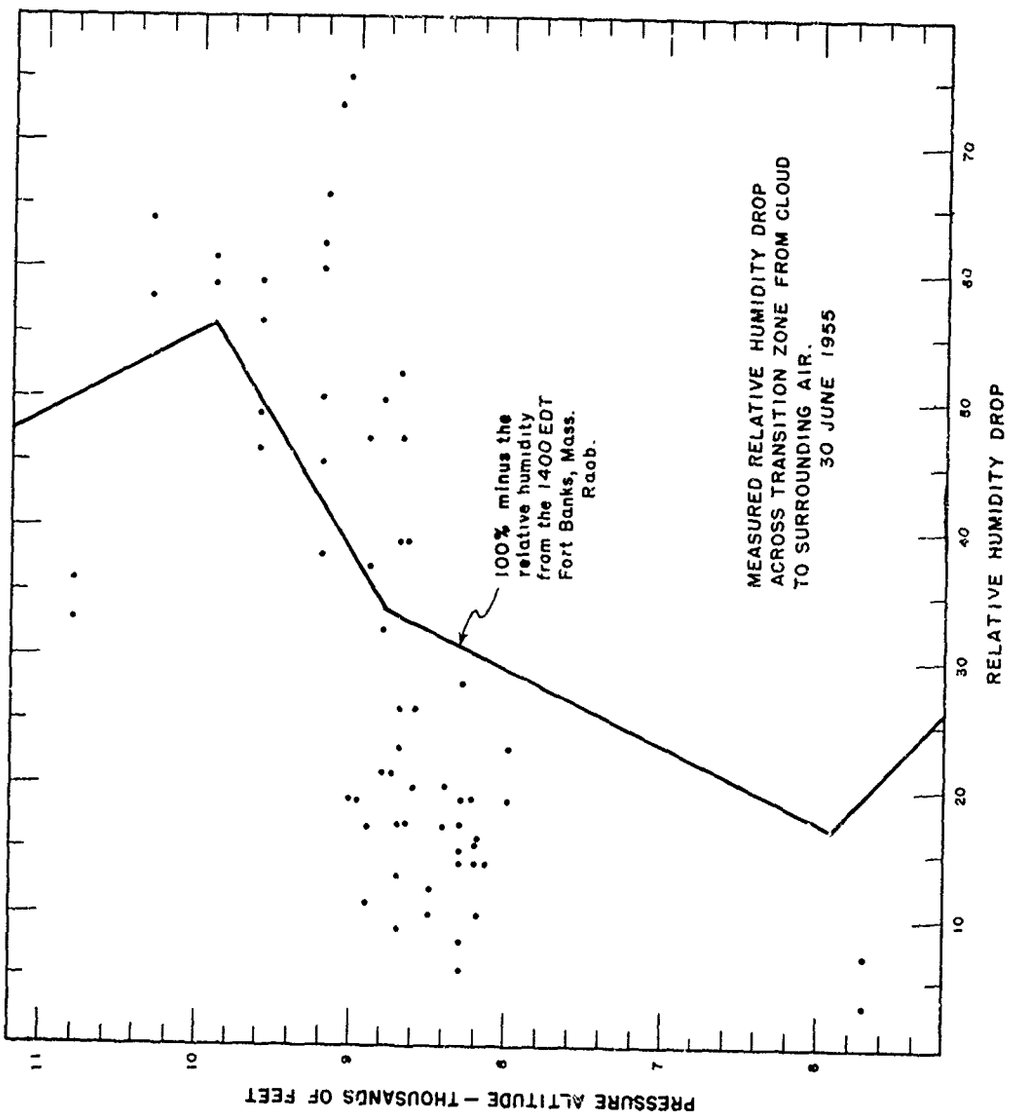
MEASURED RELATIVE HUMIDITY DROP
ACROSS TRANSITION ZONE FROM CLOUD
TO SURROUNDING AIR.
30 JUNE 1955
100% minus the
relative humidity
from the 1400 EDT
Fort Banks, Mass.
Raab.
RELATIVE HUMIDITY DROP
PRESSURE ALTITUDE – THOUSANDS OF FEET

FIGURE 40

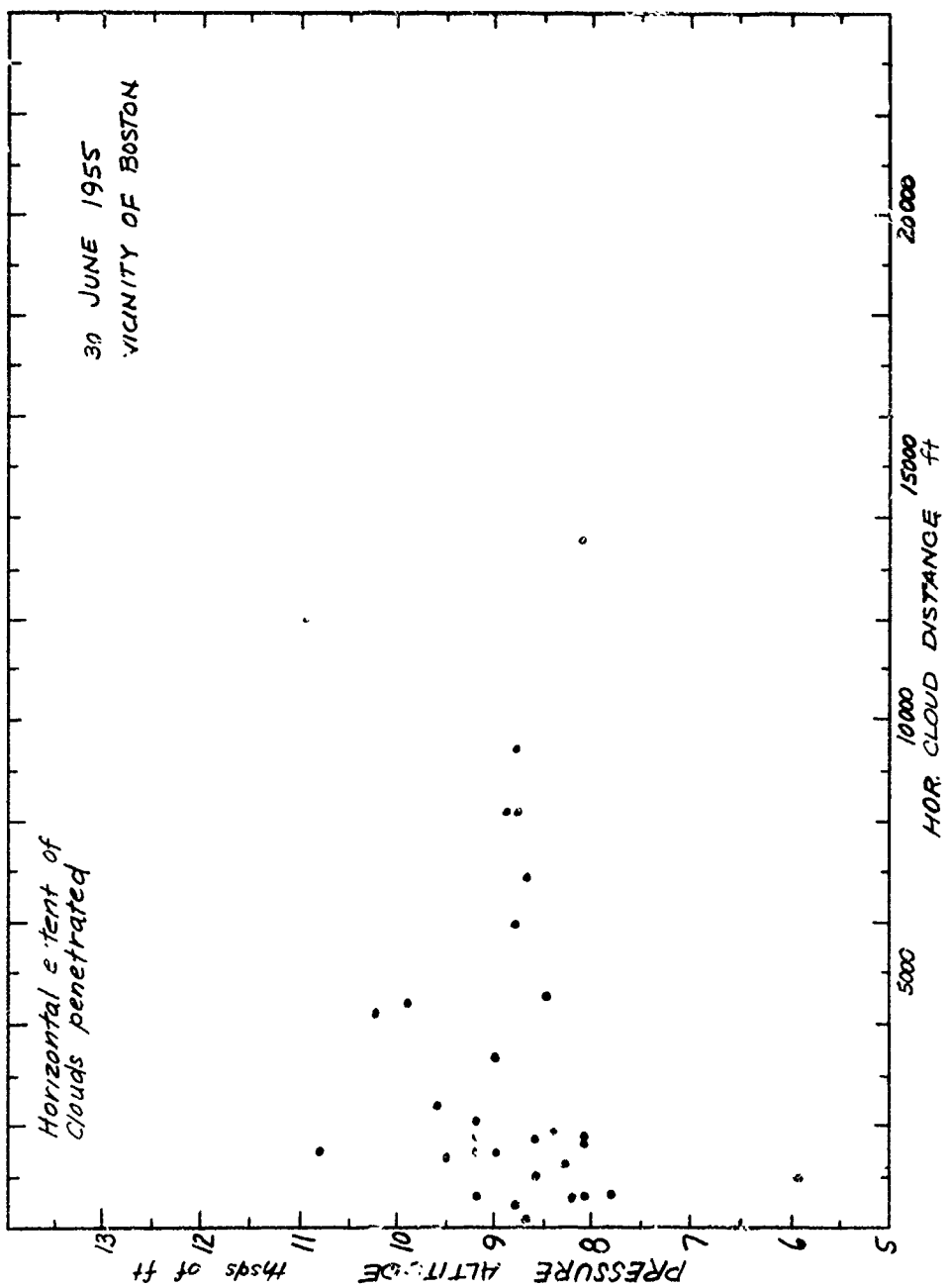
30 JUNE 1955
VICINITY OF BOSTON
Horizontal extent of
Clouds penetrated
PRESSURE ALTITUDE thsds of ft
13
12
11
10
9
8
7
5
5000
10000
15000
20000
HOR. CLOUD DISTANCE ft

FIGURE 41

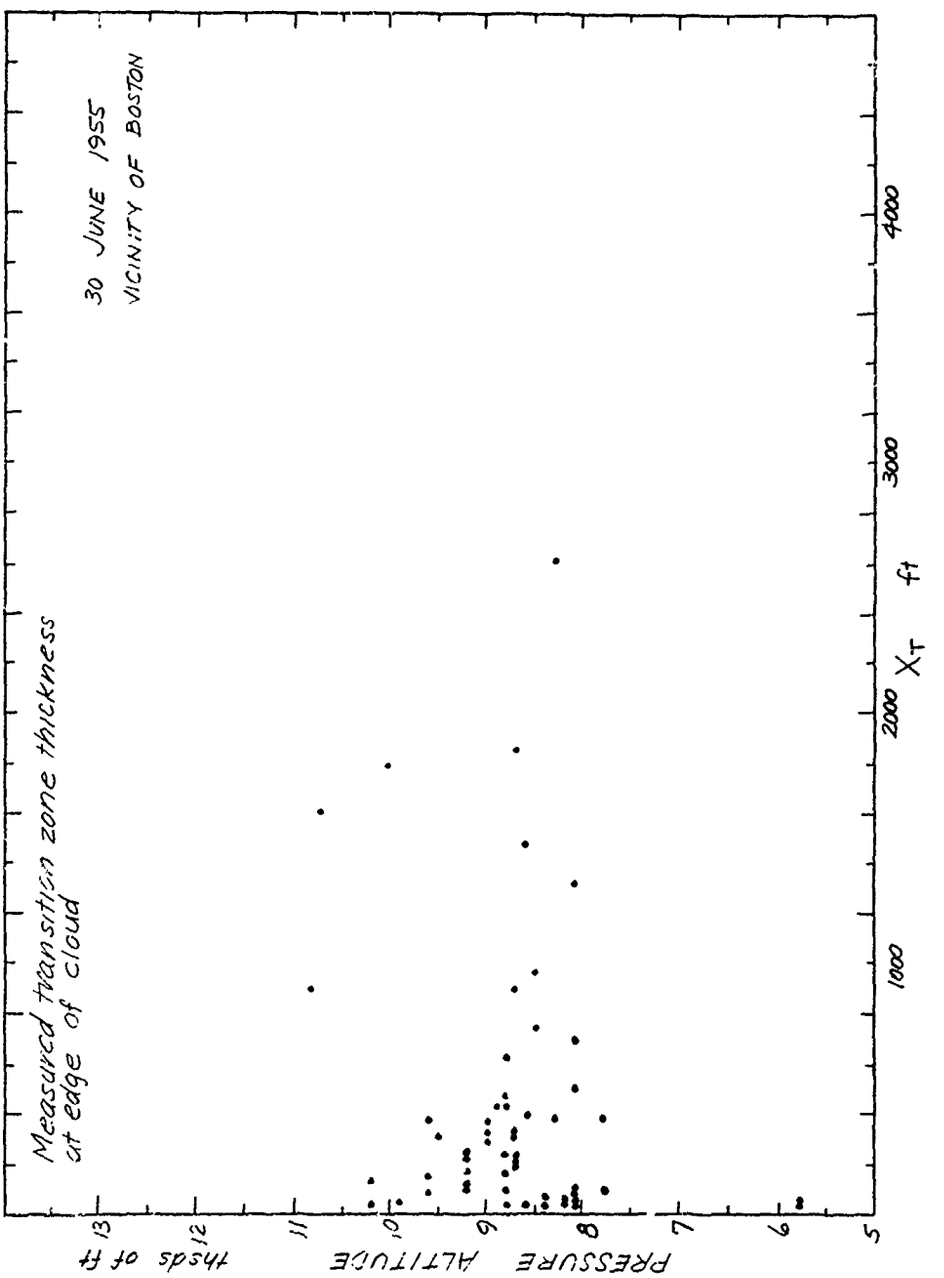
Measured transition zone thickness
at edge of cloud
30 JUNE 1955
VICINITY OF BOSTON
PRESSURE ALTITUDE
thsds of ft
13
12
11
10
9
8
7
6
5
1000
2000
3000
4000
X_T ft

FIGURE 42

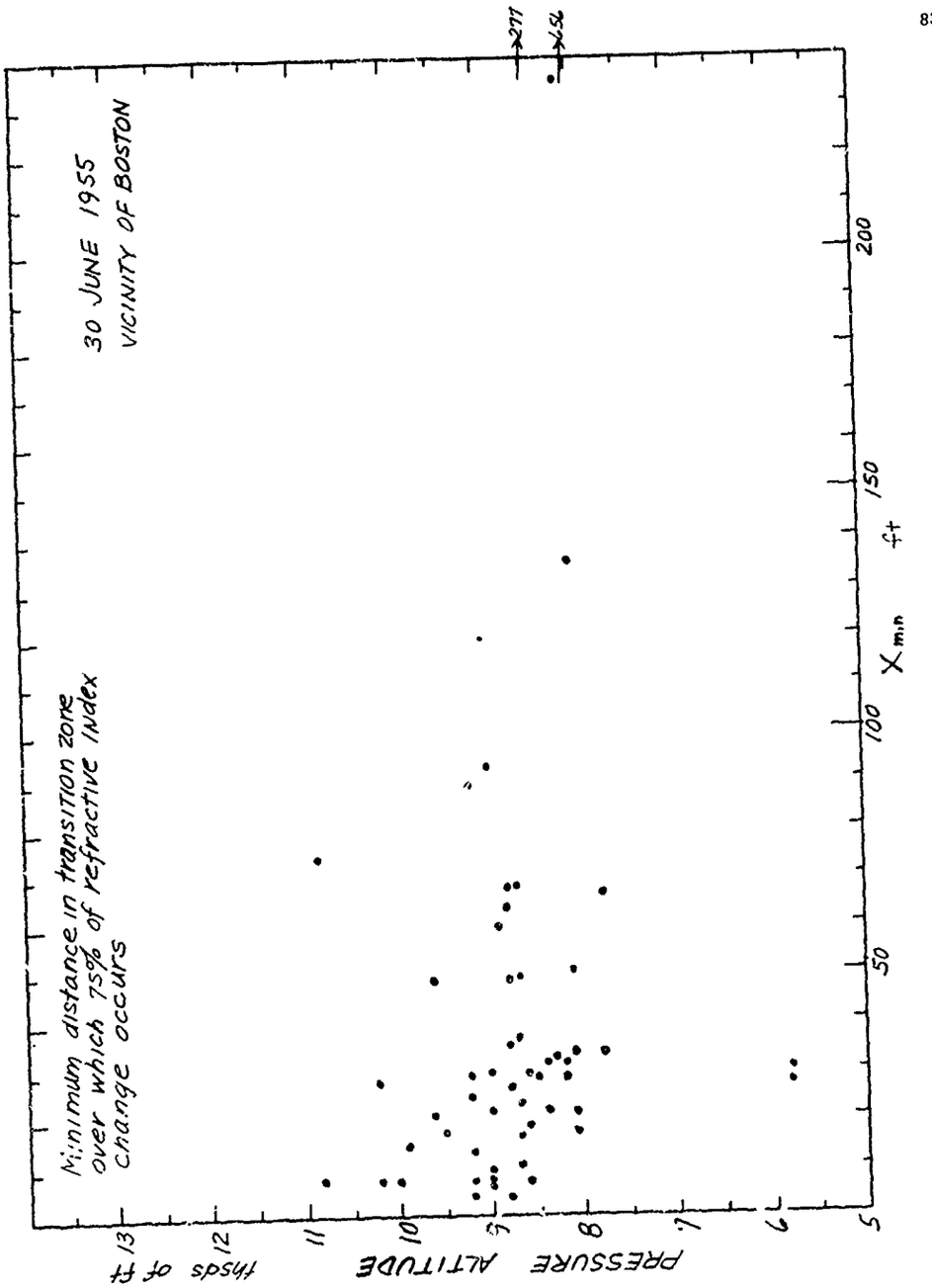
30 JUNE 1955
VICINITY OF BOSTON
Minimum distance in transition zone over which 75% of refractive index change occurs
PRESSURE ALTITUDE
thsds of ft
X_{min} ft
277
452
5
7
9
10
11
12
13
50
100
150
200

FIGURE 43

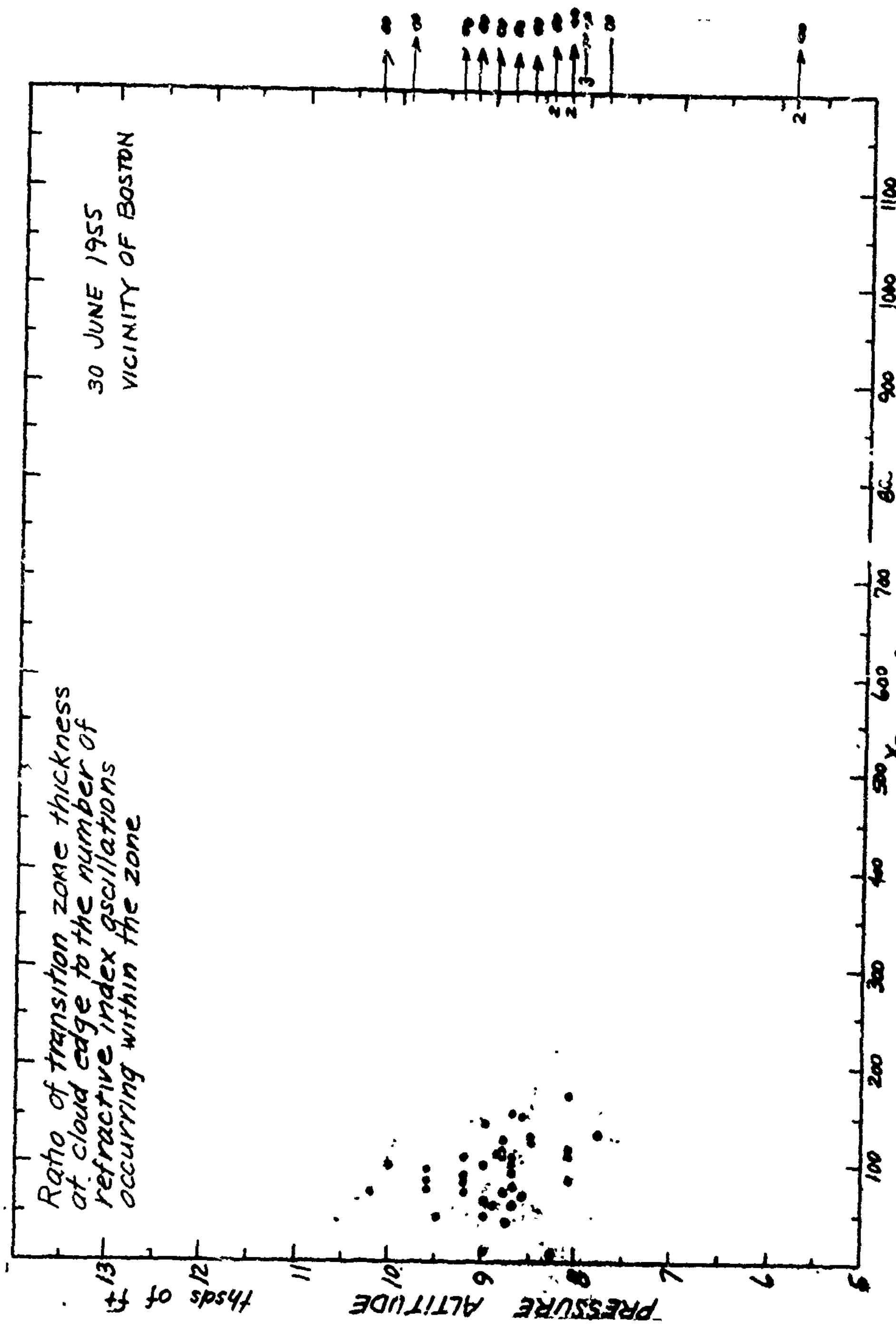
30 JUNE 1955
VICINITY OF BOSTON
Ratio of transition zone thickness at cloud edge to the number of refractive index oscillations occurring within the zone
PRESSURE ALTITUDE
thsds of ft
ft

FIGURE 44

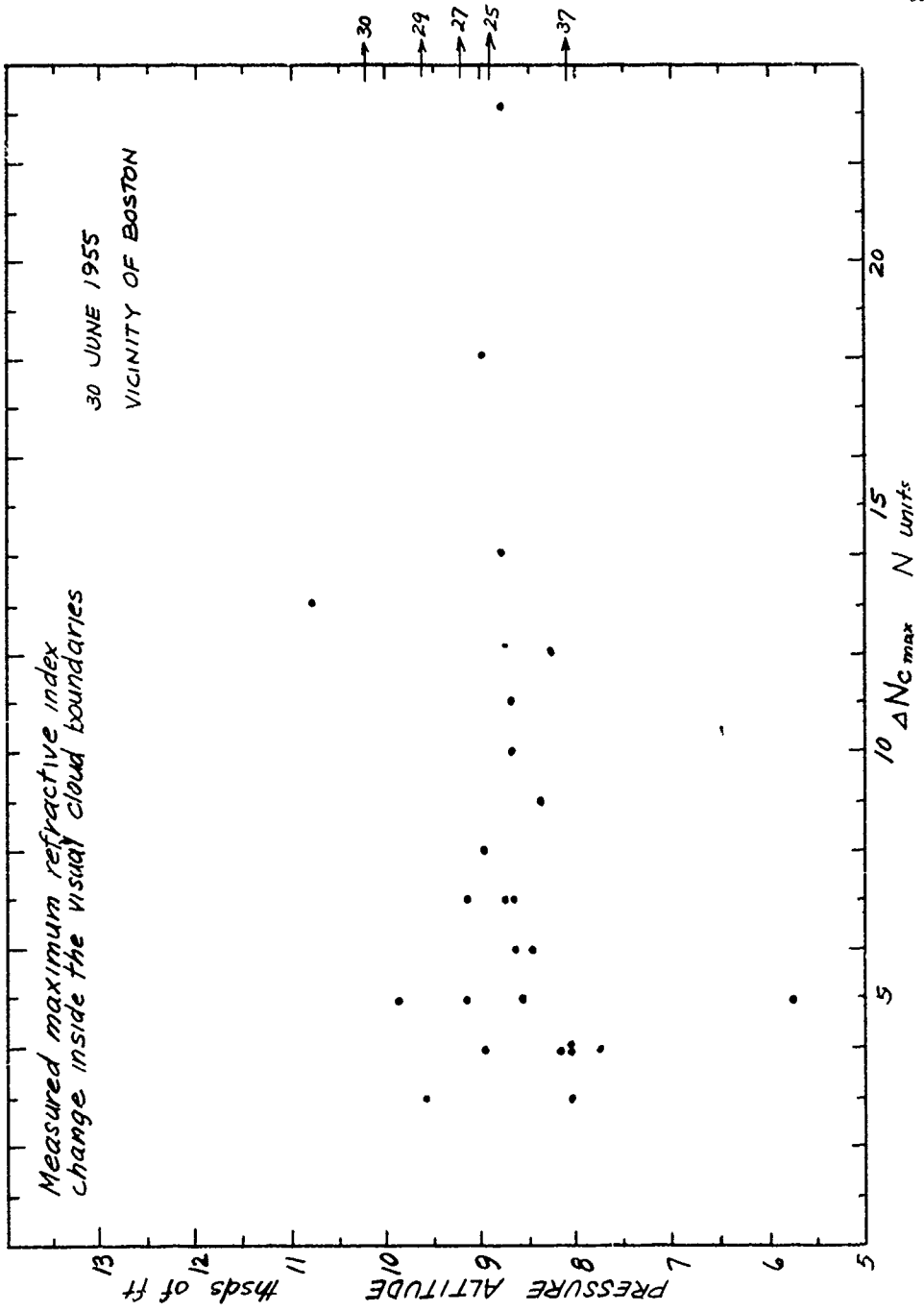
Measured maximum refractive index change inside the visual cloud boundaries
30 JUNE 1955
VICINITY OF BOSTON
30
29
27
25
37
PRESSURE ALTITUDE
thsds of ft
13
12
11
10
9
8
7
6
5
5
10
15
20
10 ΔNc max N units

FIGURE 45

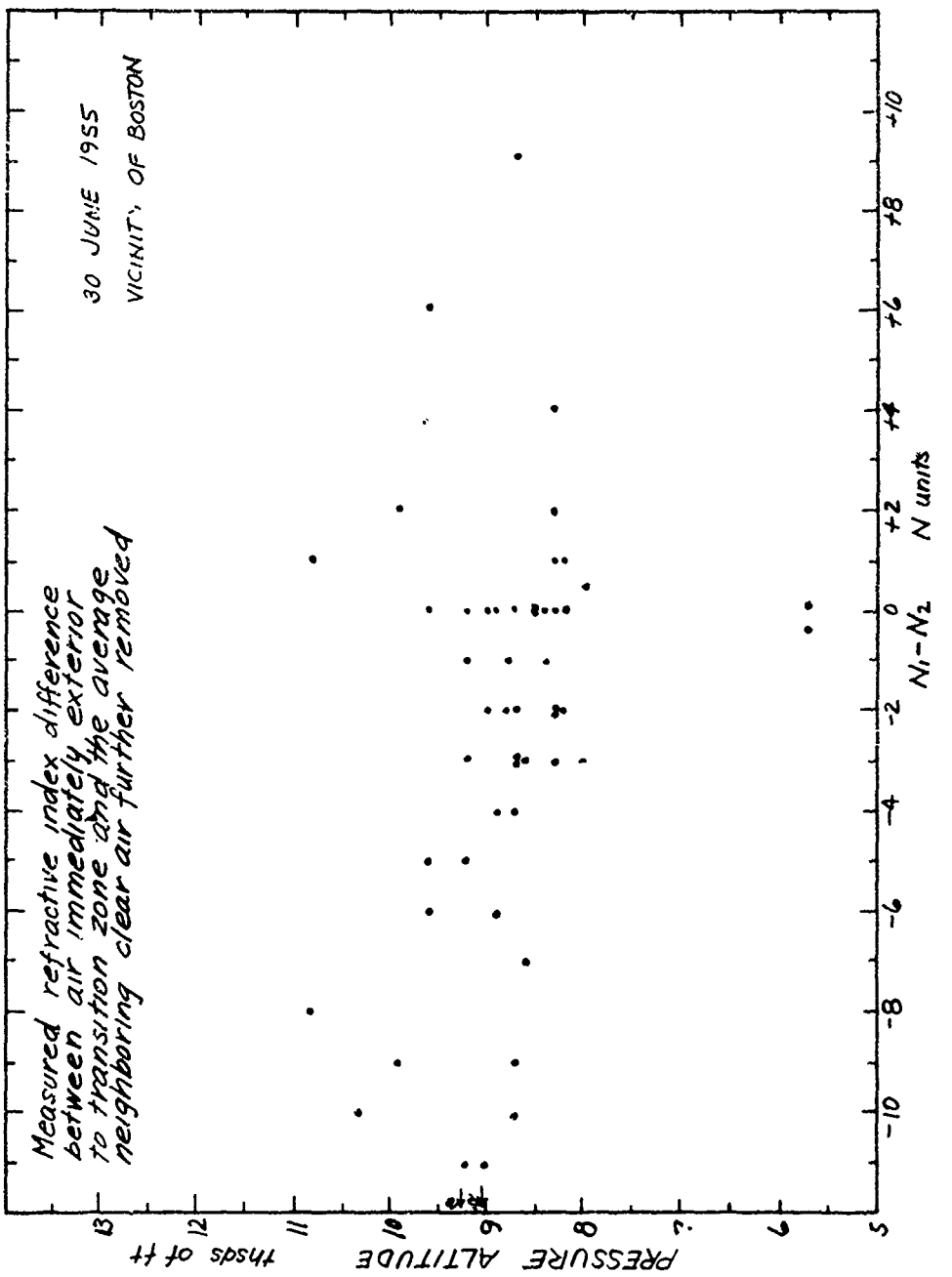
Measured refractive index difference
between air immediately exterior
to transition zone and the average
neighboring clear air further removed
30 JUNE 1955
VICINITY OF BOSTON
PRESSURE ALTITUDE
thsds of ft
13
12
11
10
9
8
7
6
5
-10
-8
-6
-4
-2
0
+2
+4
+6
+8
+10
$N_1 - N_2$ N units

FIGURE 46

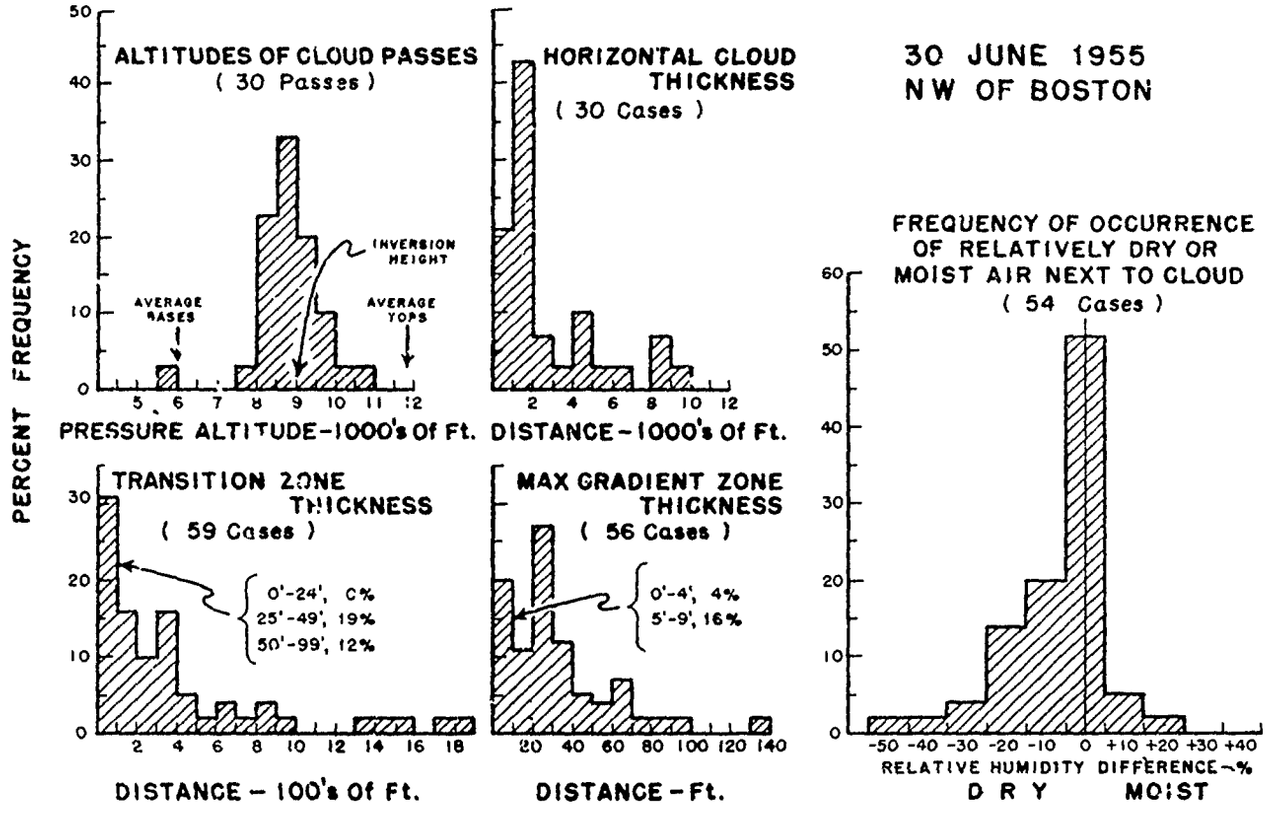
30 JUNE 1955
NW OF BOSTON
ALTITUDES OF CLOUD PASSES
(30 Passes)
AVERAGE BASES
INVERSION HEIGHT
AVERAGE TOPS
PERCENT FREQUENCY
PRESSURE ALTITUDE-1000's Of Ft.
HORIZONTAL CLOUD THICKNESS
(30 Cases)
DISTANCE-1000's Of Ft.
TRANSITION ZONE THICKNESS
(59 Cases)
0'-24', 6%
25'-49', 19%
50'-99', 12%
DISTANCE - 100's Of Ft.
MAX GRADIENT ZONE THICKNESS
(56 Cases)
0'-4', 4%
5'-9', 16%
DISTANCE - Ft.
FREQUENCY OF OCCURRENCE OF RELATIVELY DRY OR MOIST AIR NEXT TO CLOUD
(54 Cases)
RELATIVE HUMIDITY DIFFERENCE-%
D R Y
MOIST

FIGURE 47

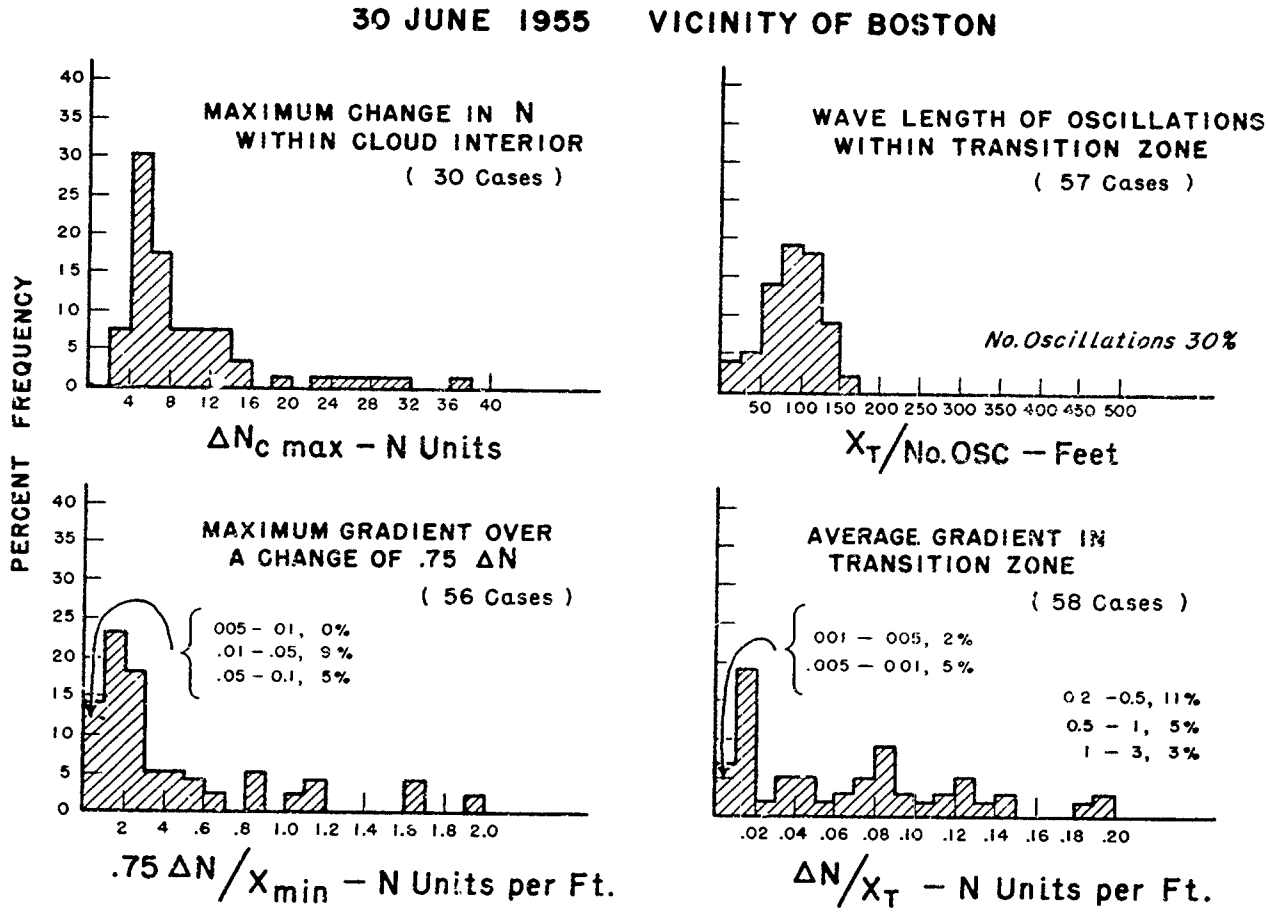
30 JUNE 1955 VICINITY OF BOSTON
PERCENT FREQUENCY
MAXIMUM CHANGE IN N WITHIN CLOUD INTERIOR
(30 Cases)
ΔNc max – N Units
WAVE LENGTH OF OSCILLATIONS WITHIN TRANSITION ZONE
(57 Cases)
No. Oscillations 30%
XT/No. OSC – Feet
MAXIMUM GRADIENT OVER A CHANGE OF .75 ΔN
(56 Cases)
005 – 01, 0%
.01 – .05, 9%
.05 – 0.1, 5%
.75 ΔN/Xmin – N Units per Ft.
AVERAGE GRADIENT IN TRANSITION ZONE
(58 Cases)
001 – 005, 2%
.005 – 001, 5%
0 2 –0.5, 11%
0.5 – 1, 5%
1 – 3, 3%
ΔN/XT – N Units per Ft.

FIGURE 48

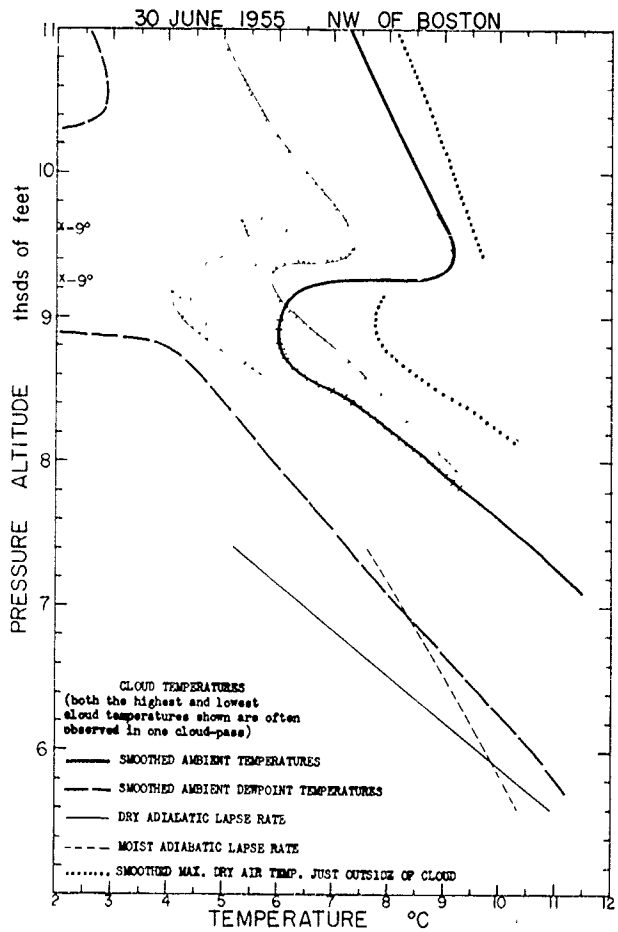
30 JUNE 1955 NW OF BOSTON
PRESSURE ALTITUDE thsds of feet
TEMPERATURE °C
CLOUD TEMPERATURES
(both the highest and lowest
cloud temperatures shown are often
observed in one cloud-pass)
SMOOTHED AMBIENT TEMPERATURES
SMOOTHED AMBIENT DEWPOINT TEMPERATURES
DRY ADIABATIC LAPSE RATE
MOIST ADIABATIC LAPSE RATE
SMOOTHED MAX. DRY AIR TEMP. JUST OUTSIDE OF CLOUD

FIGURE 49

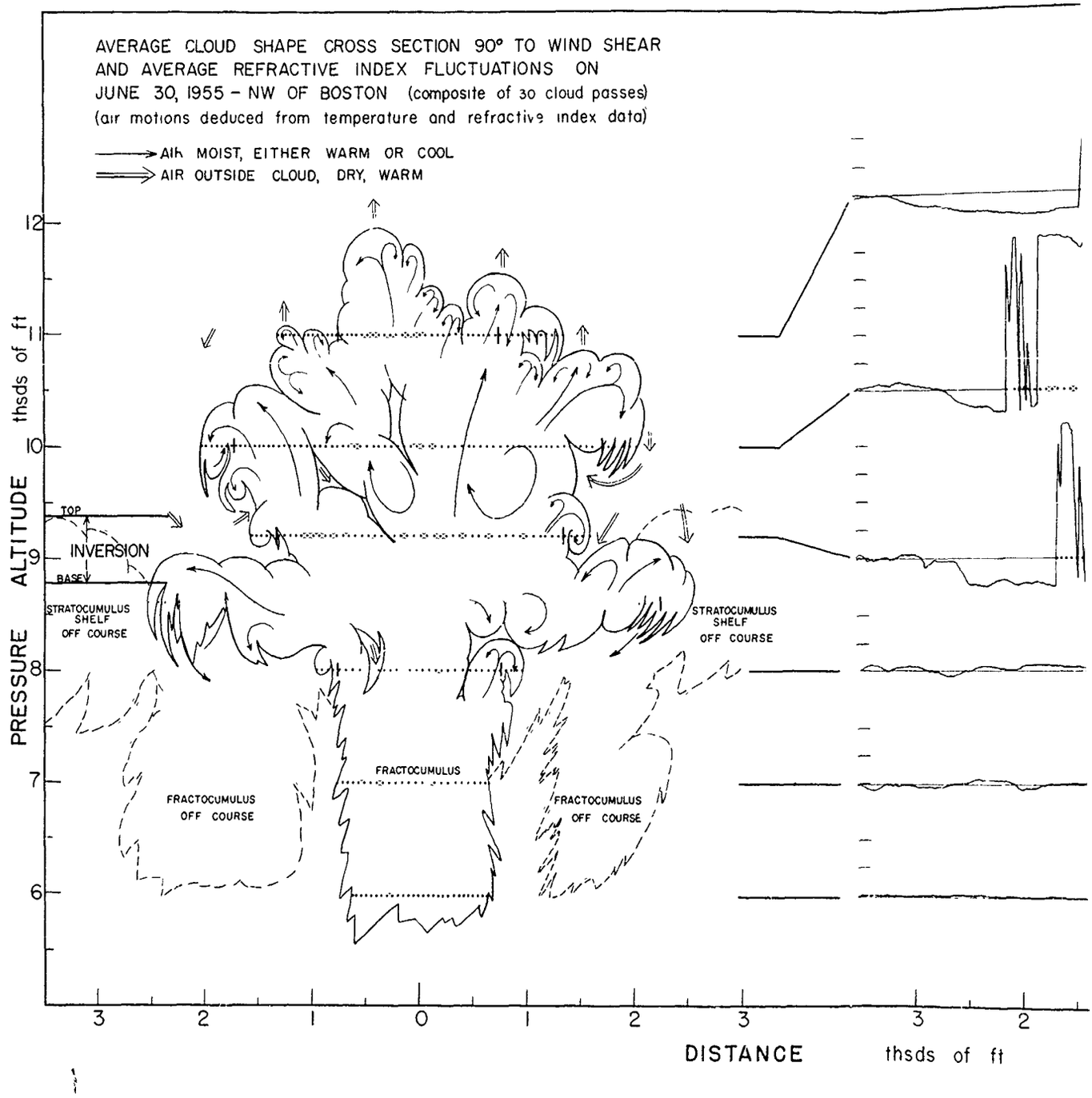

Figure 50.

The Murray Printing Company, Wakefield, Mass., 2-11-57 --- 1000

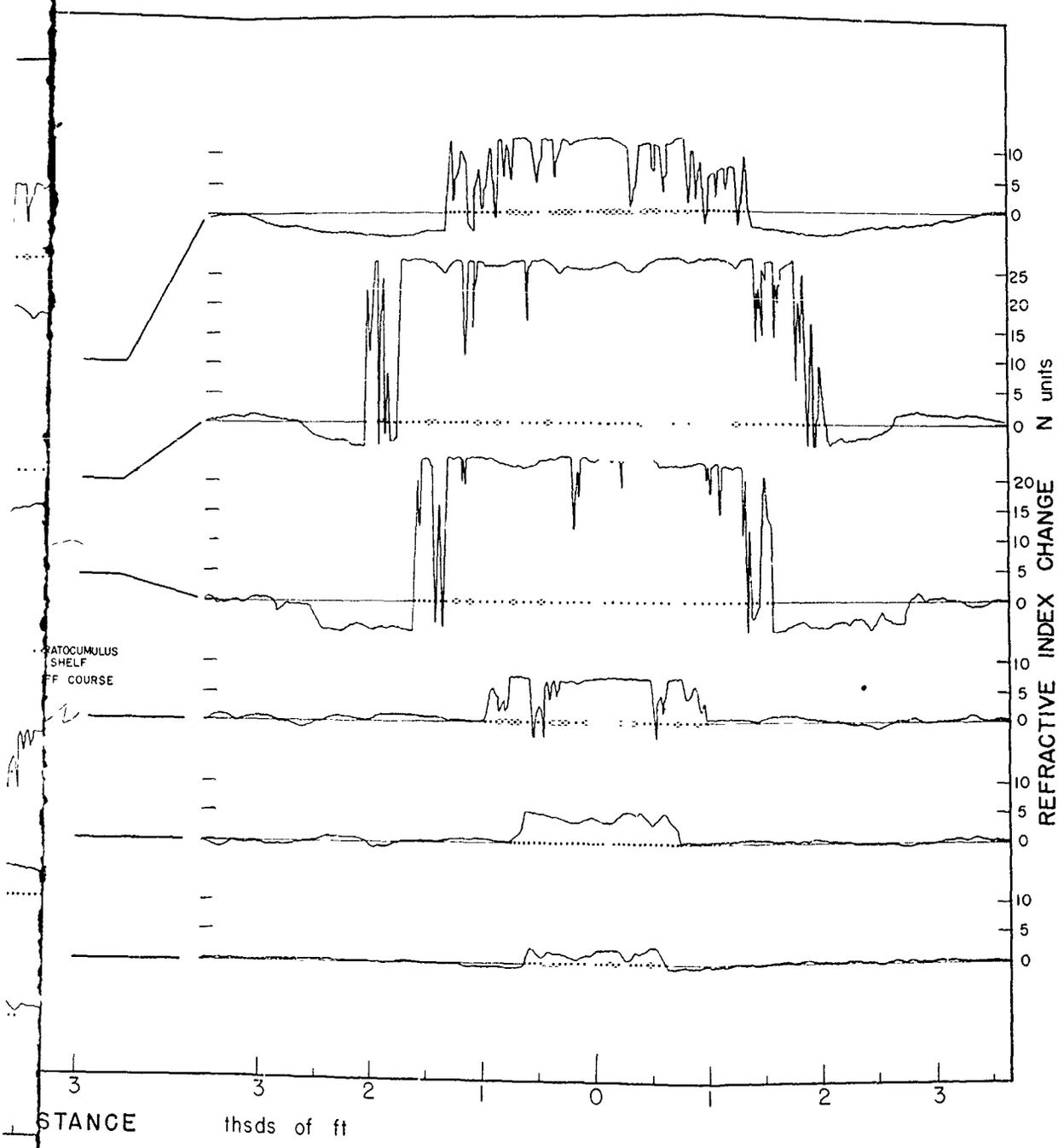
REFRACTIVE INDEX CHANGE N units
10
5
0
25
20
15
10
5
0
20
15
10
5
0
10
5
0
10
5
0
10
5
0
ATOCUMULUS
SHELF
F COURSE
3
3
2
1
0
1
2
3
STANCE
thsds of ft

Figure 50.

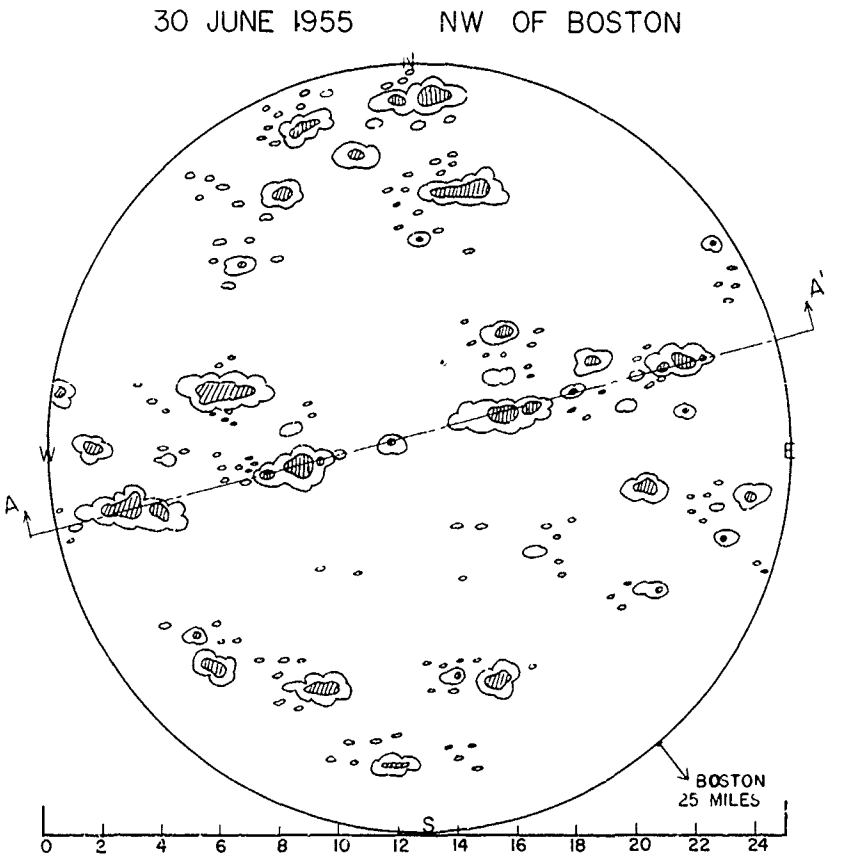

PLAN VIEW OF REPRESENTATIVE CUMULUS COVERAGE IN REGION OF FLIGHT 1400-1600 EDT
5000-9000 ft 9000-11500 ft

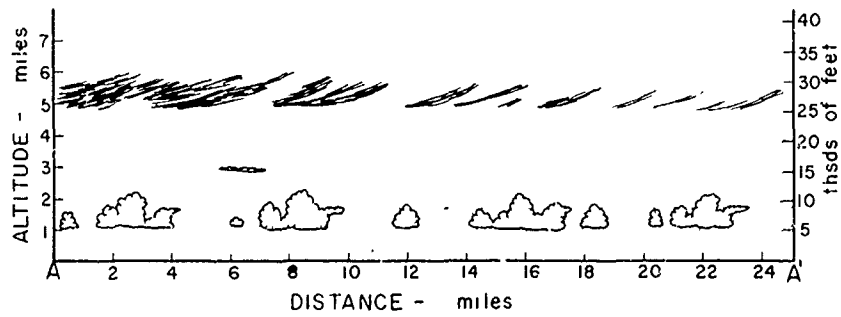

CROSS SECTION ALONG LINE OF MAXIMUM CLOUDINESS AA'

Figure 51

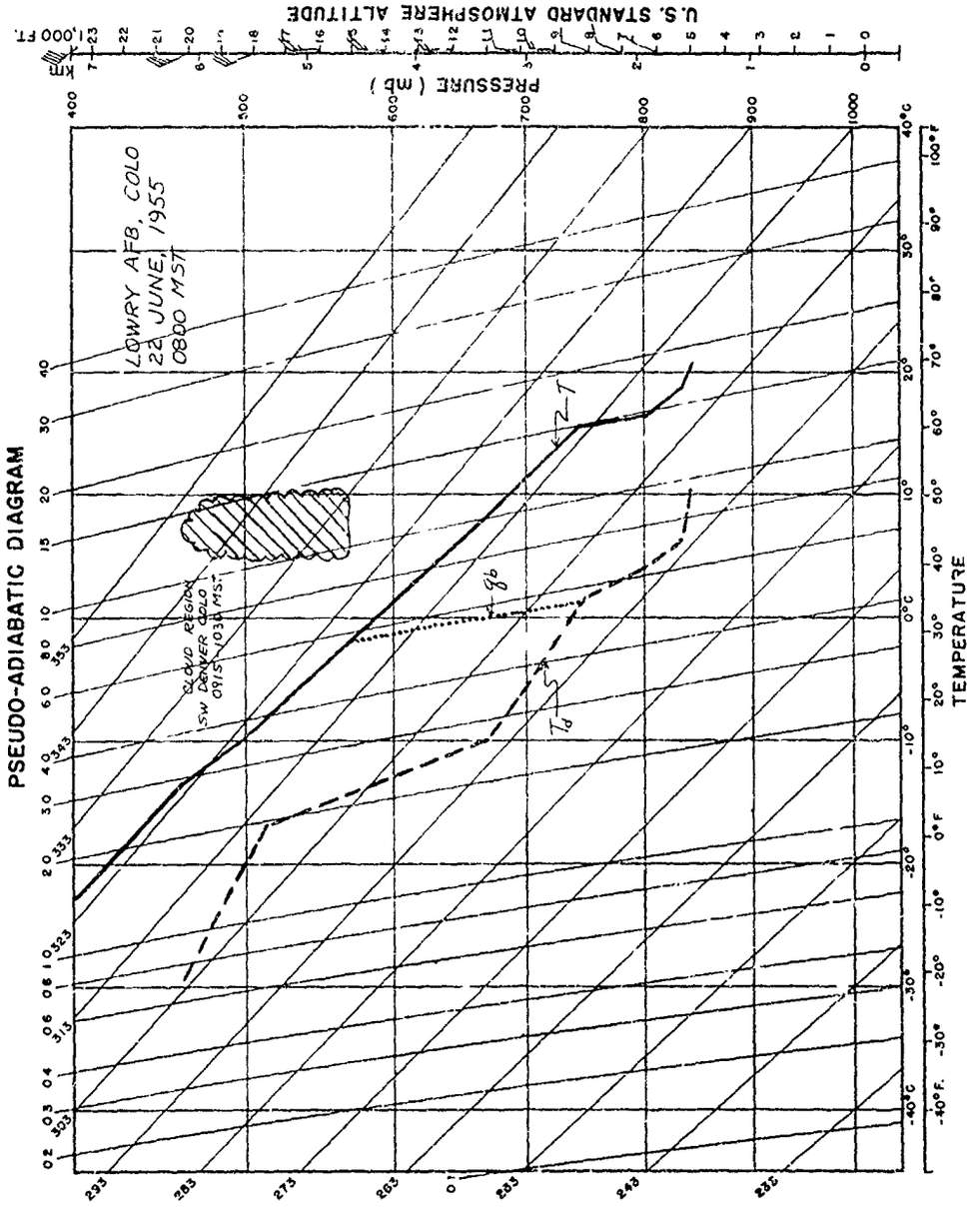
U.S. STANDARD ATMOSPHERE ALTITUDE
PRESSURE (mb)
PSEUDO-ADIABATIC DIAGRAM
TEMPERATURE
LOWRY AFB, COLO
22 JUNE, 1955
0800 MST
CLOUD REGION
15W DENVER COLO
0915-1030 MST
T-T_d

FIGURE 52

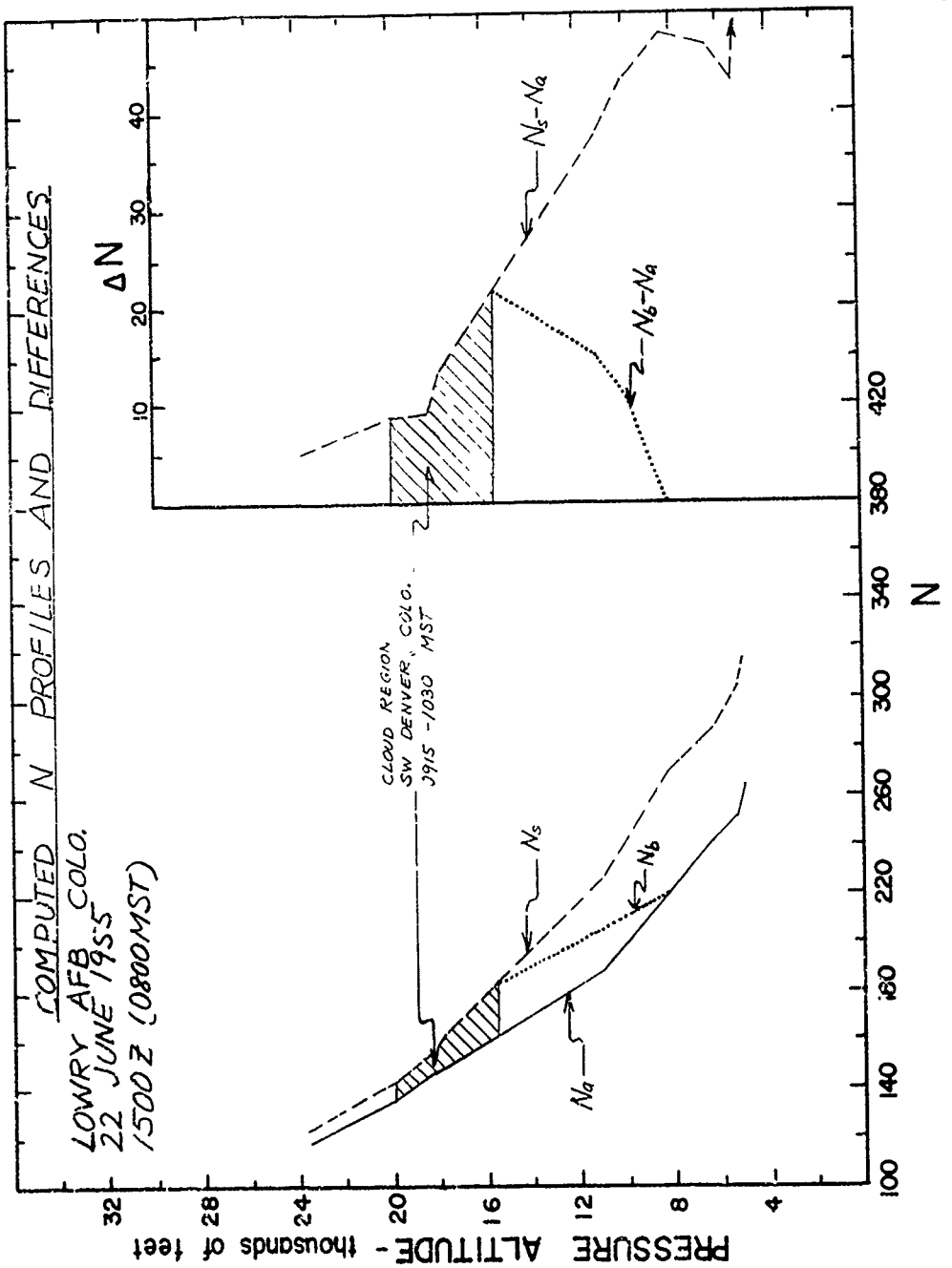
COMPUTED N PROFILES AND DIFFERENCES
LOWRY AFB COLO.
22 JUNE 1955
1500 Z (0800 MST)
CLOUD REGION
SW DENVER, COLO.
1915 - 1030 MST
Ns
Nb
Na
Ns-Na
2-Nb-Na
ΔN
PRESSURE ALTITUDE - thousands of feet
N

FIGURE 53

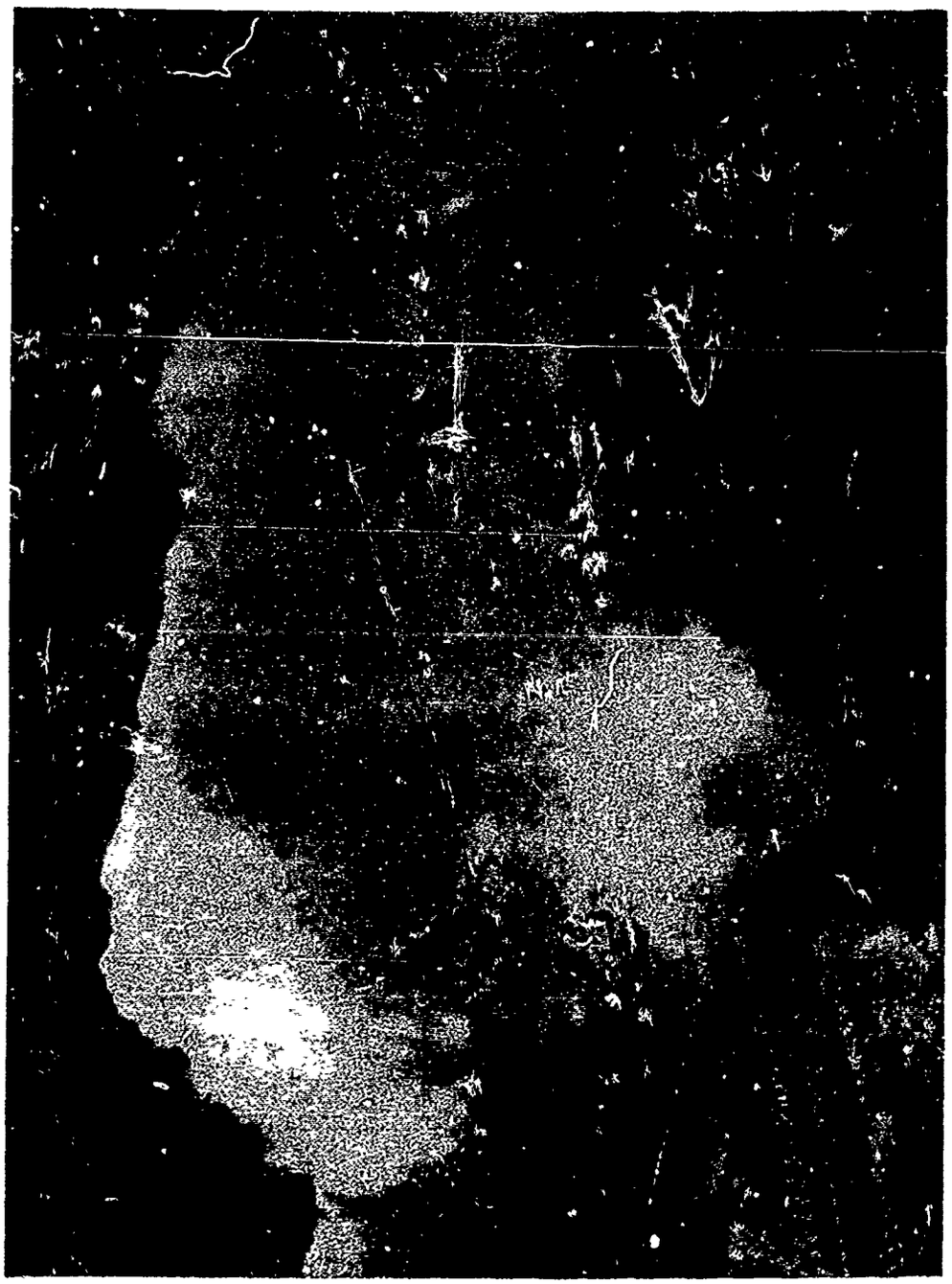

FIGURE 54

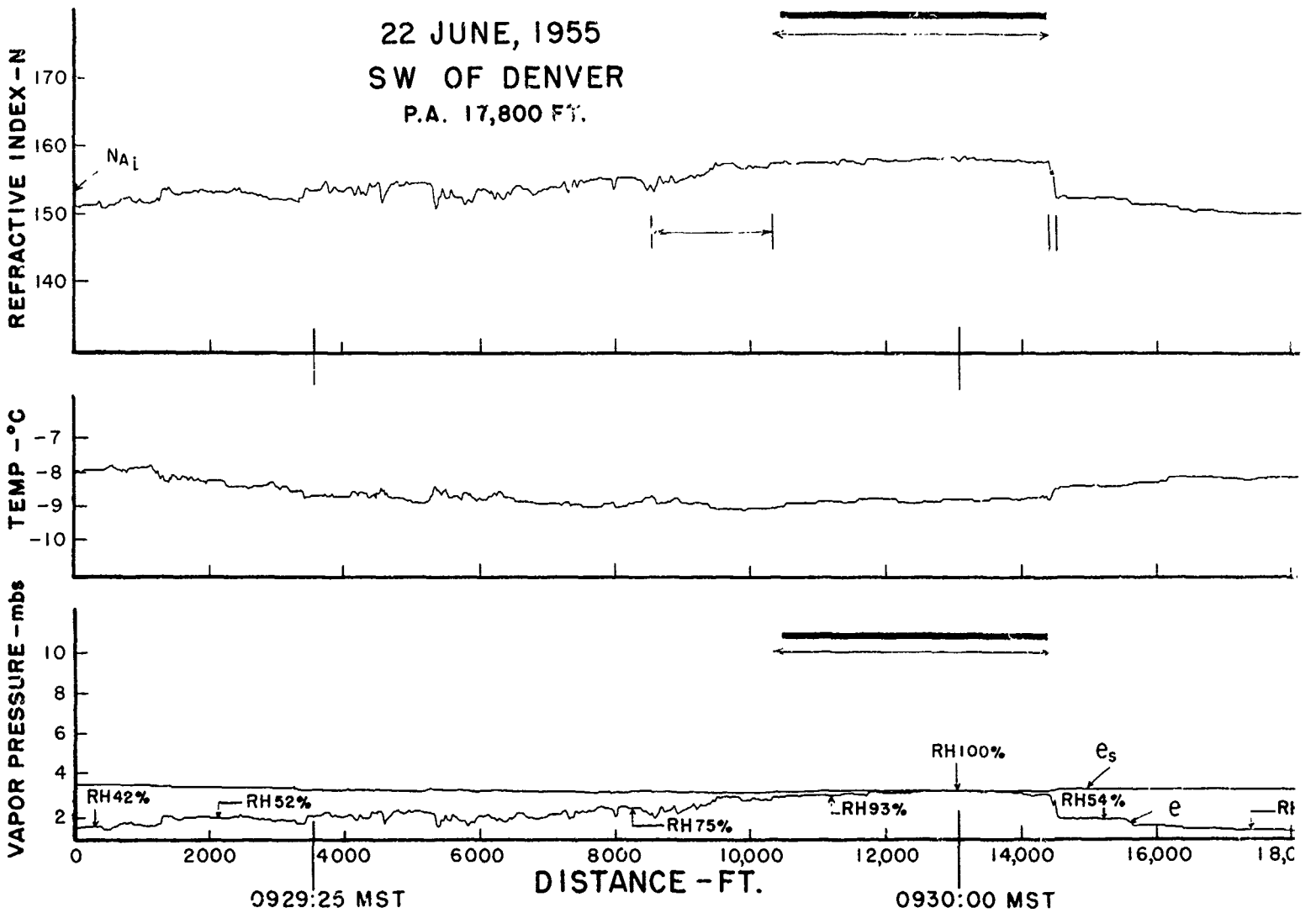

Figure 55.

The Murray Printing Company, Wakefield, Mass., 2-11-57 — 1000

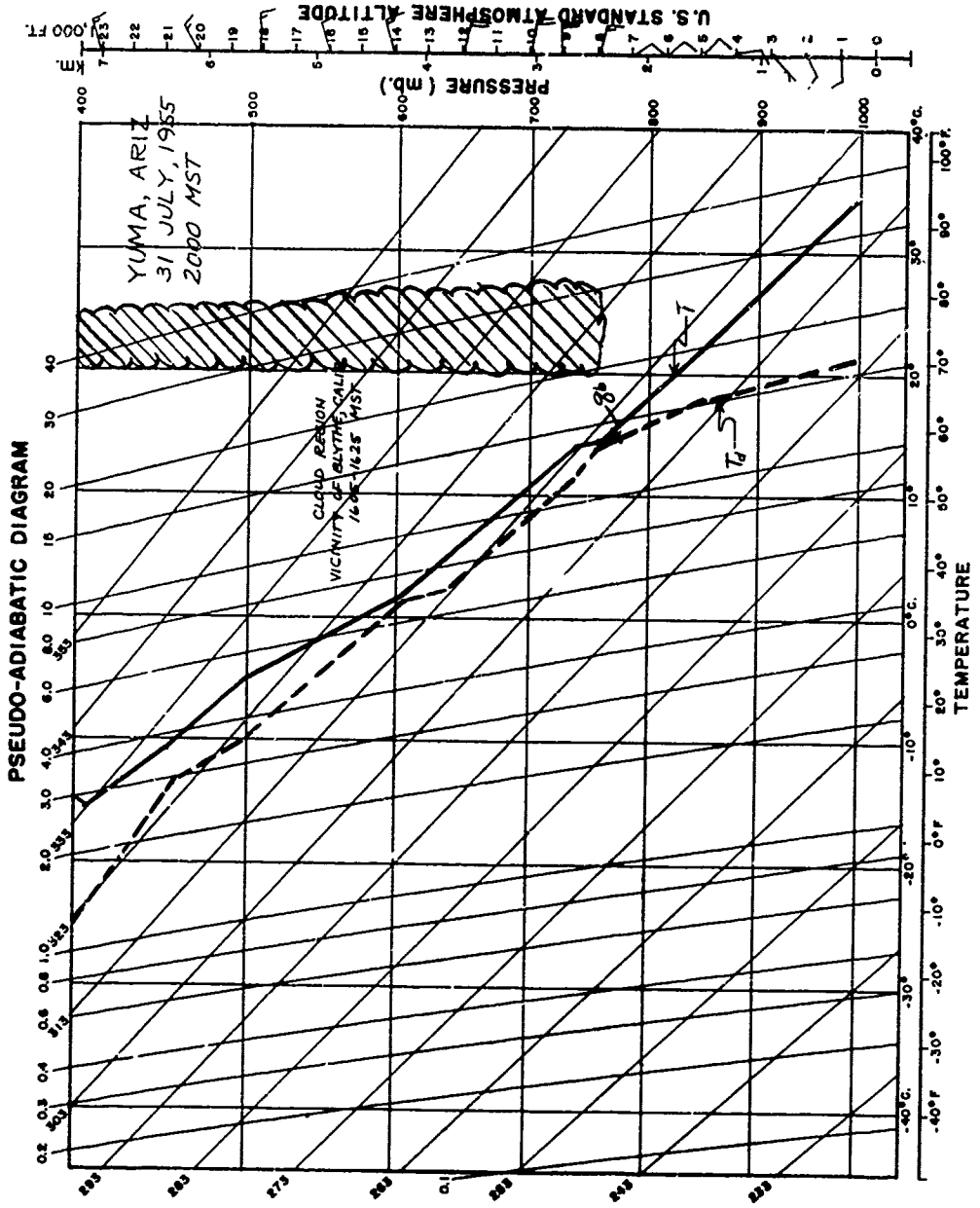
U.S. STANDARD ATMOSPHERE ALTITUDE
PRESSURE (mb.)
YUMA, ARIZ.
31 JULY, 1955
2000 MST
CLOUD REGION
VICINITY OF BLYTHE, CALIF.
1600-1625 MST
T
Td
PSEUDO-ADIABATIC DIAGRAM
TEMPERATURE

FIGURE 56

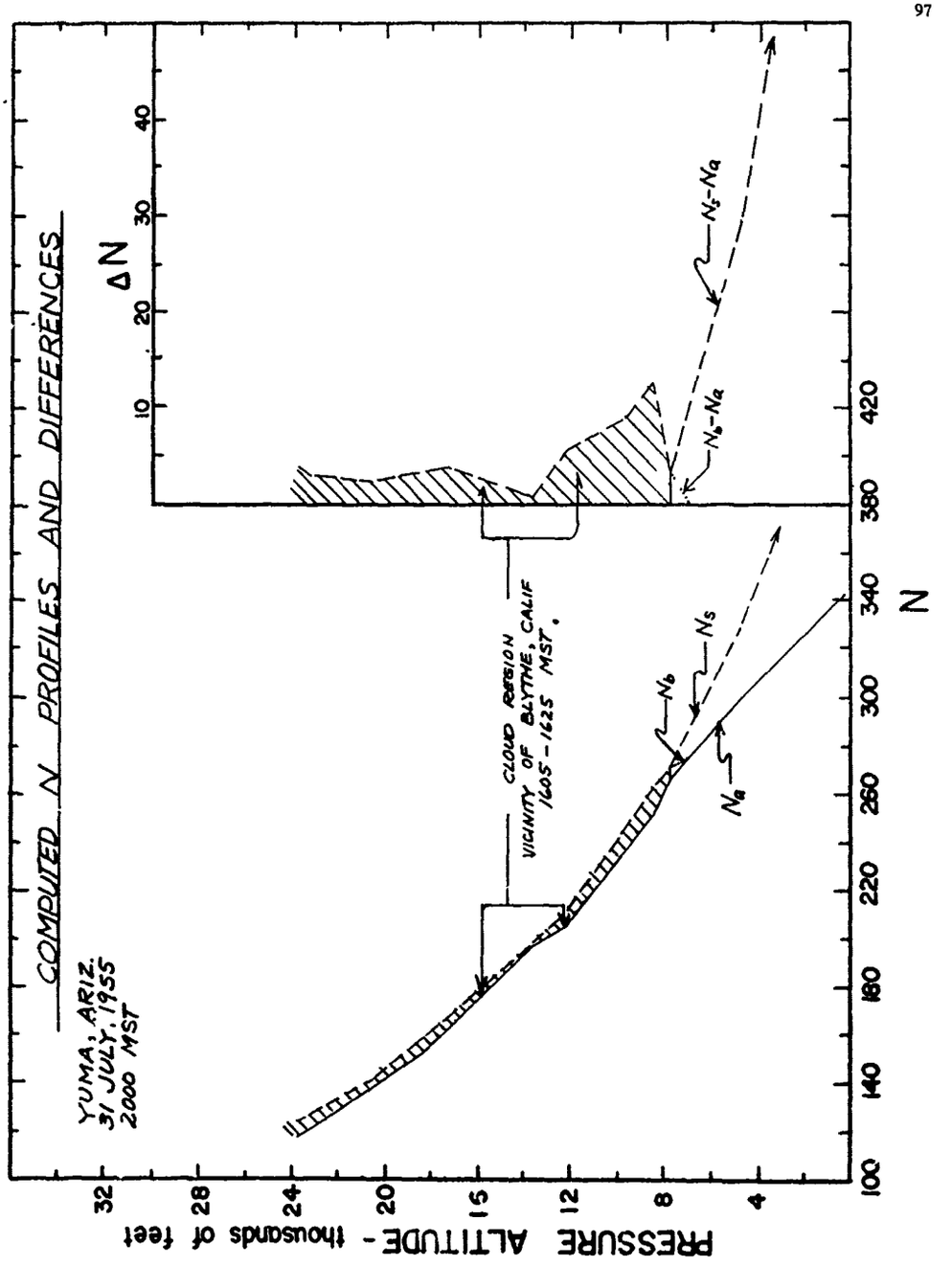
COMPUTED N PROFILES AND DIFFERENCES
YUMA, ARIZ.
31 JULY, 1955
2000 MST
CLOUD REGION
VICINITY OF BLYTHE, CALIF
1605 - 1625 MST.
Nb
Ns
Na
Ns-Na
Nb-Na
ΔN
PRESSURE ALTITUDE - thousands of feet
N

FIGURE 57

FIGURE 4

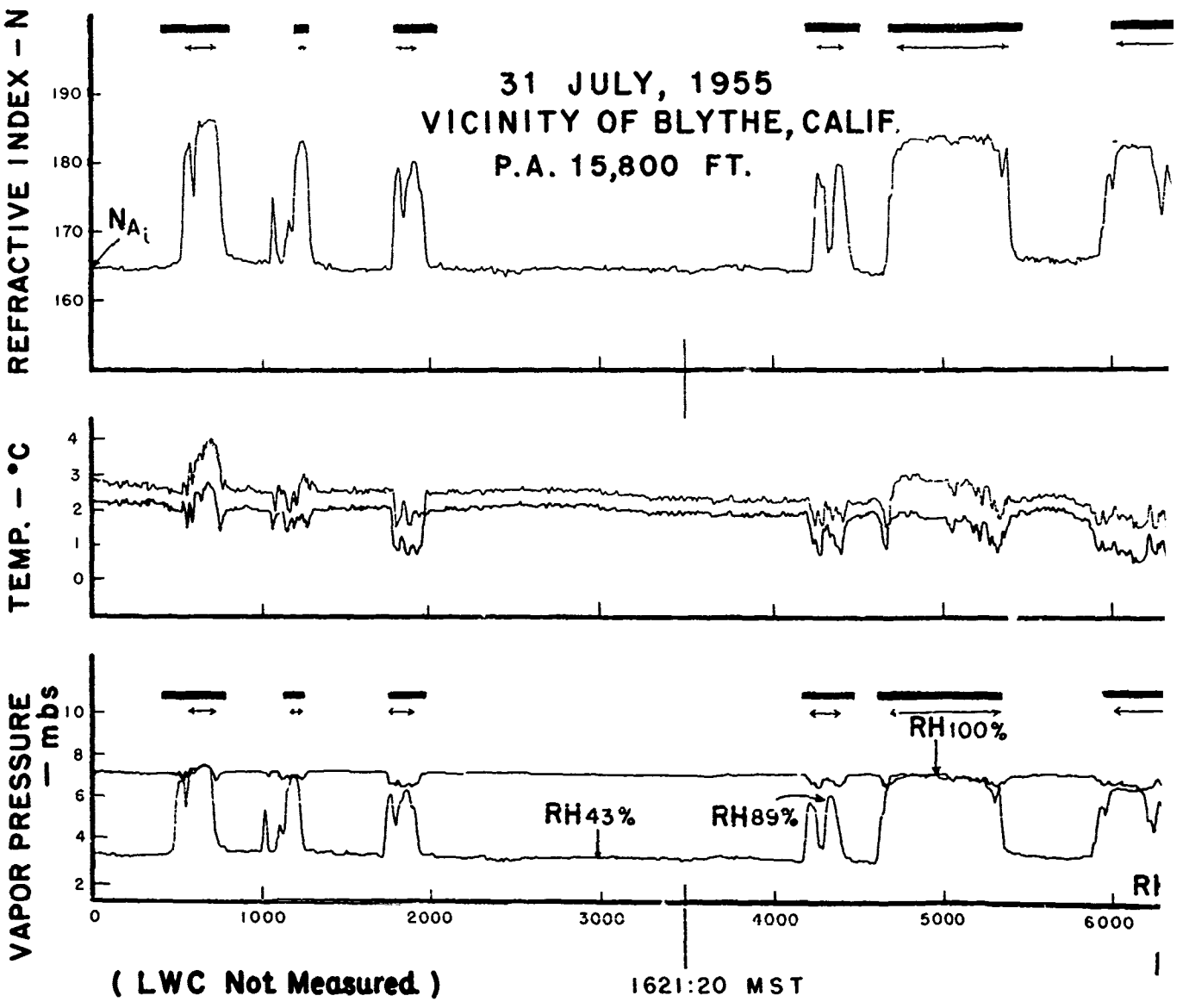

The Murray Printing Company, Wakefield, Mass., 2-11-57 --- 1000

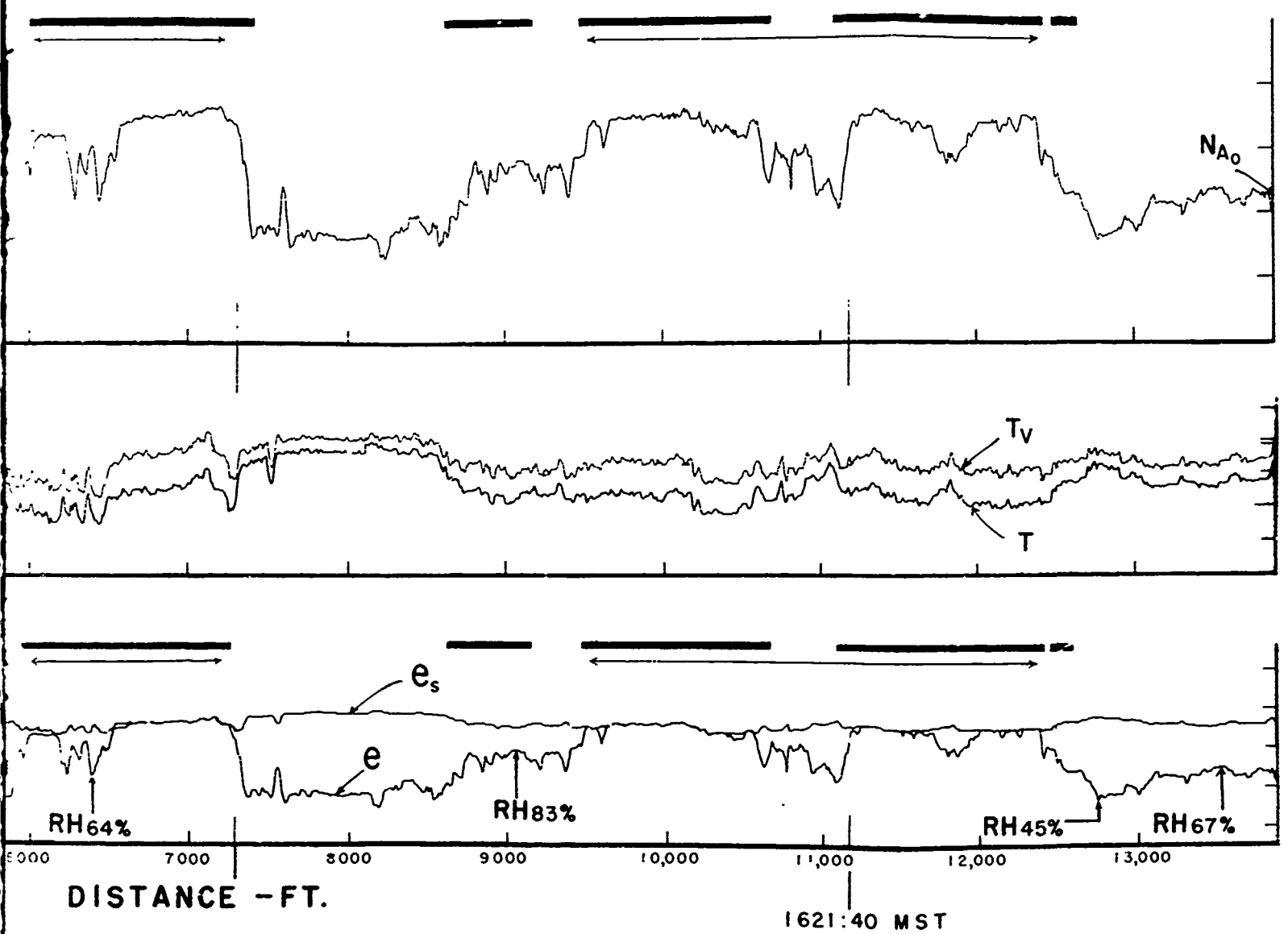
N_{A_0}
T_V
T
e_s
e
RH64%
RH83%
RH45%
RH67%
7000
8000
9000
10,000
11,000
12,000
13,000
DISTANCE - FT.
1621:40 MST

Figure 59.

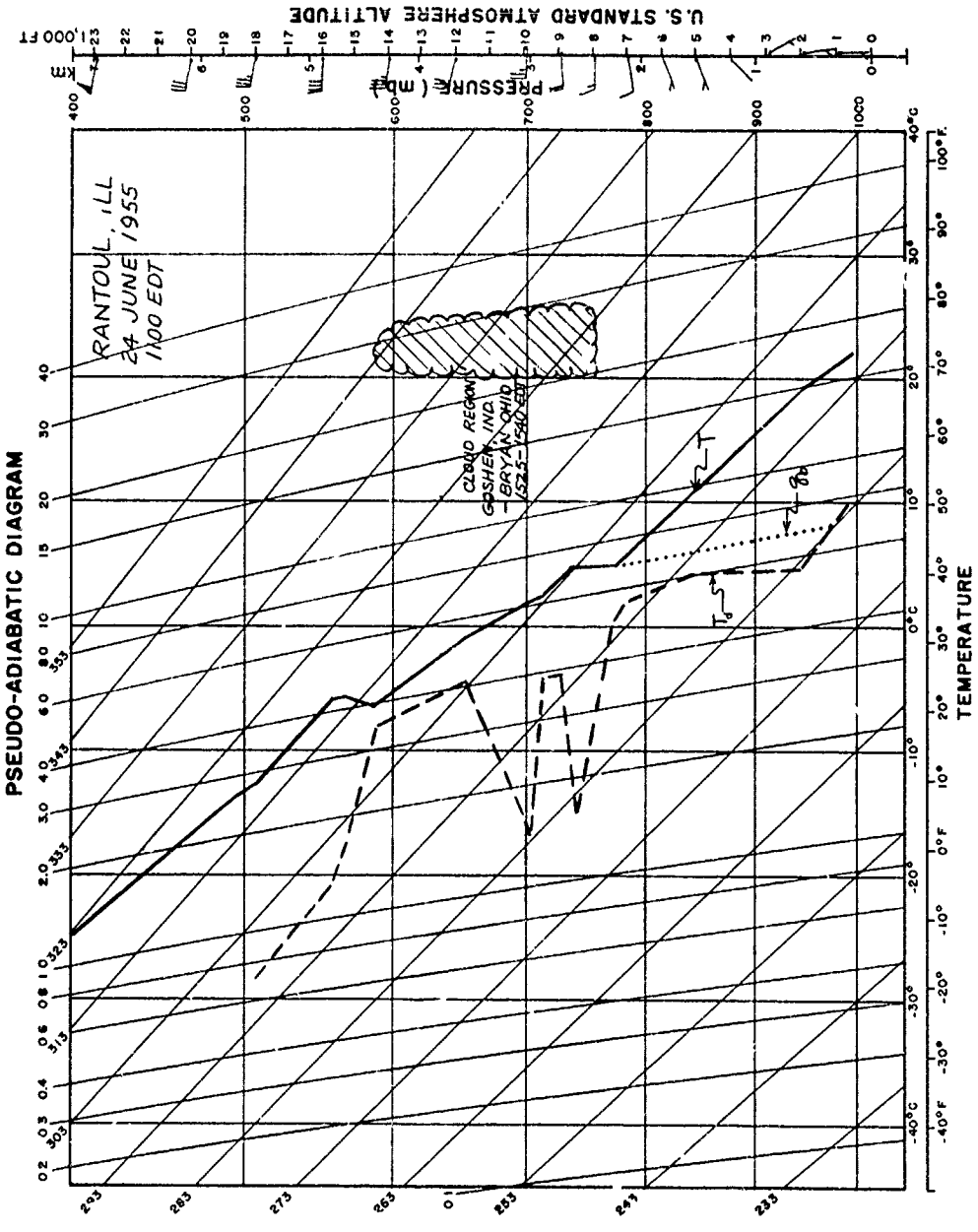
U.S. STANDARD ATMOSPHERE ALTITUDE
PRESSURE (mb)
RANTOUL, ILL
24 JUNE 1955
1100 EDT
CLOUD REGIONS
GOSHEN, IND.
BRYAN, OHIO
1525-1540 EDT
PSEUDO-ADIABATIC DIAGRAM
TEMPERATURE

FIGURE 60

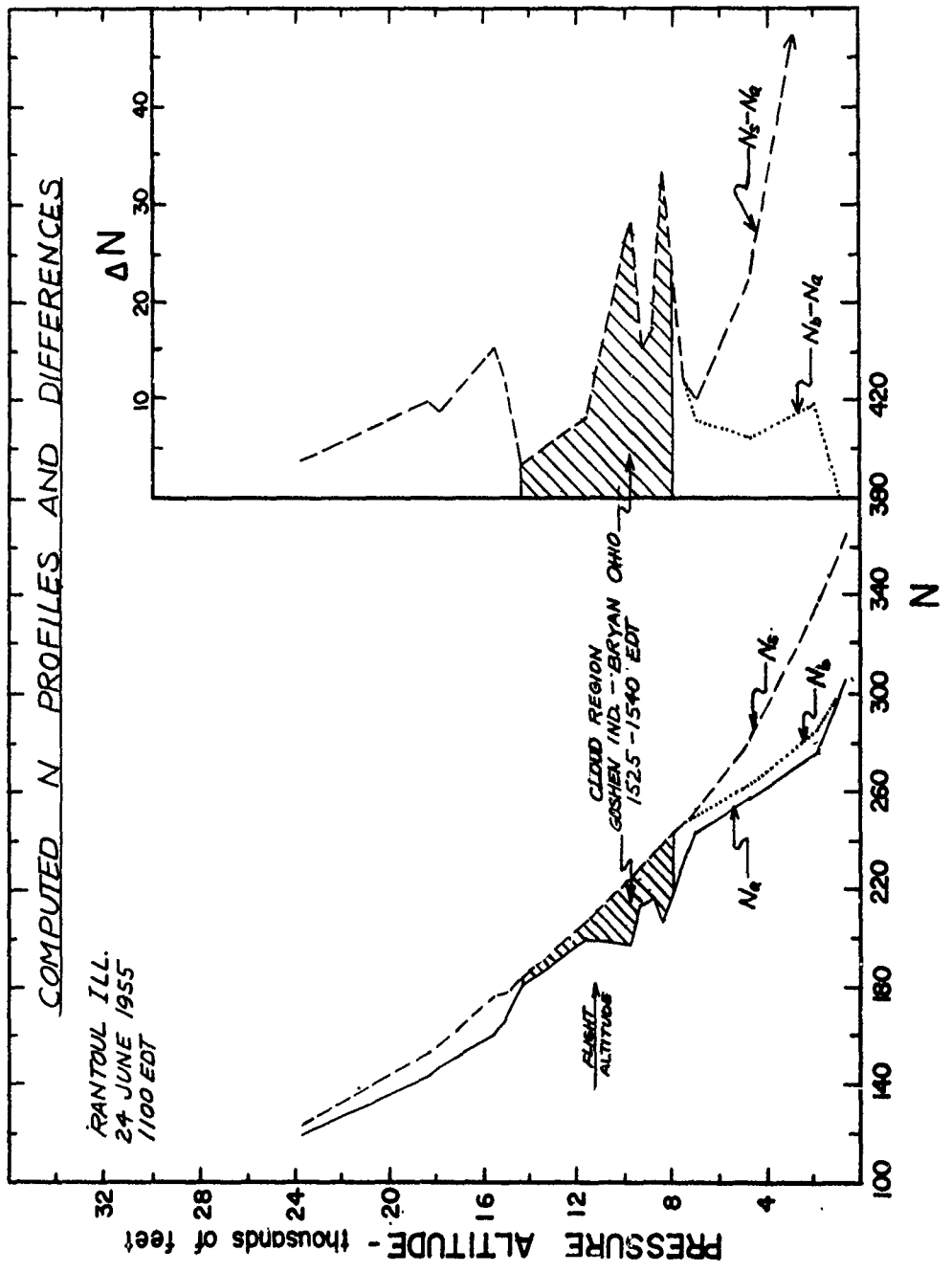
COMPUTED N PROFILES AND DIFFERENCES
RANTOUL ILL.
24 JUNE 1955
1100 EDT
CLOUD REGION
GOSHEN IND. - BRYAN OHIO
1525 - 1540 EDT
FLIGHT ALTITUDE
PRESSURE ALTITUDE - thousands of feet
N
ΔN
N5-N4
N3-N2
N4
N5
N3
32
28
24
20
16
12
8
4
100
140
180
220
260
300
340
380
420
10
20
30
40

FIGURE 61

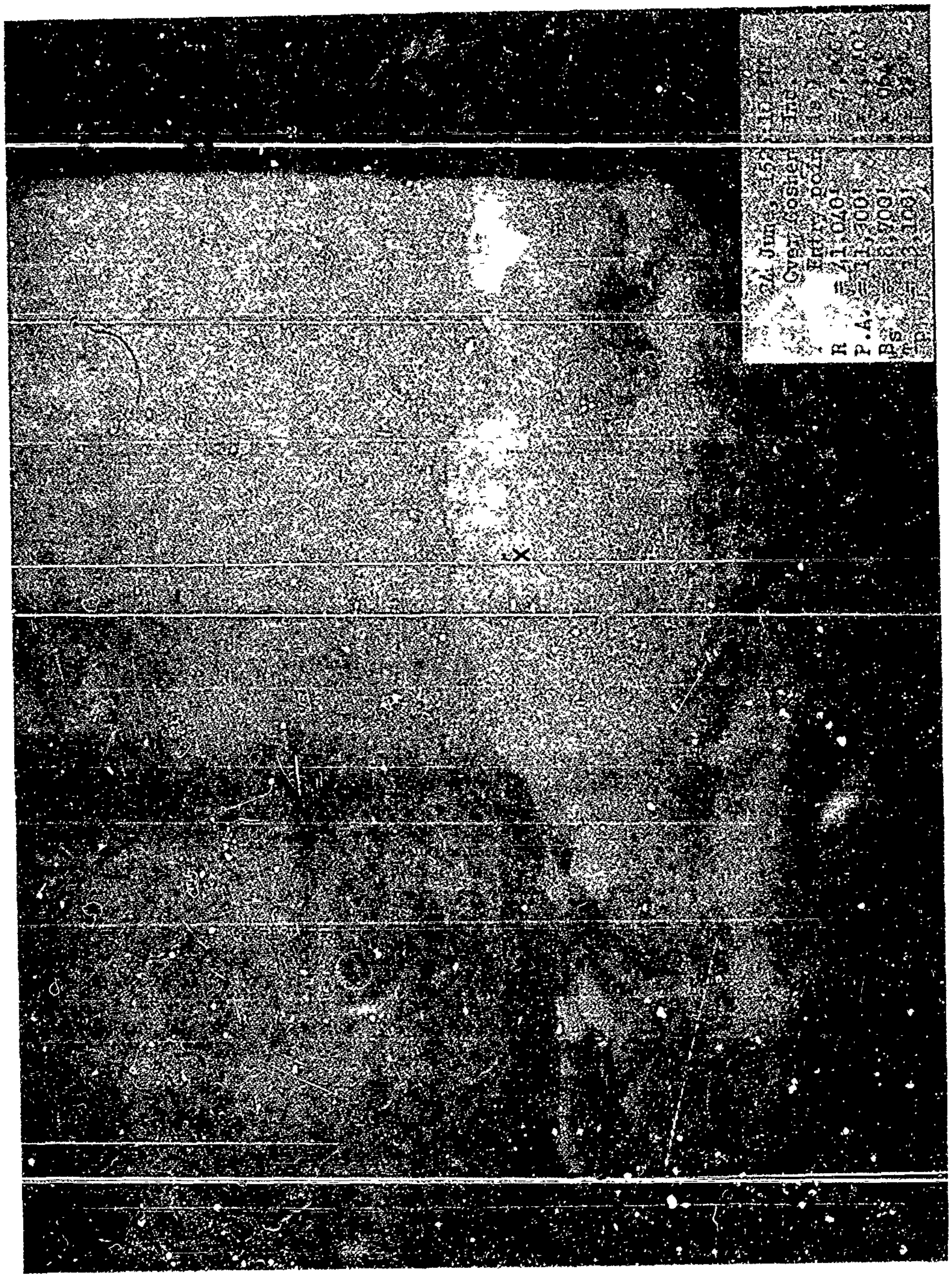

FIGURE 62

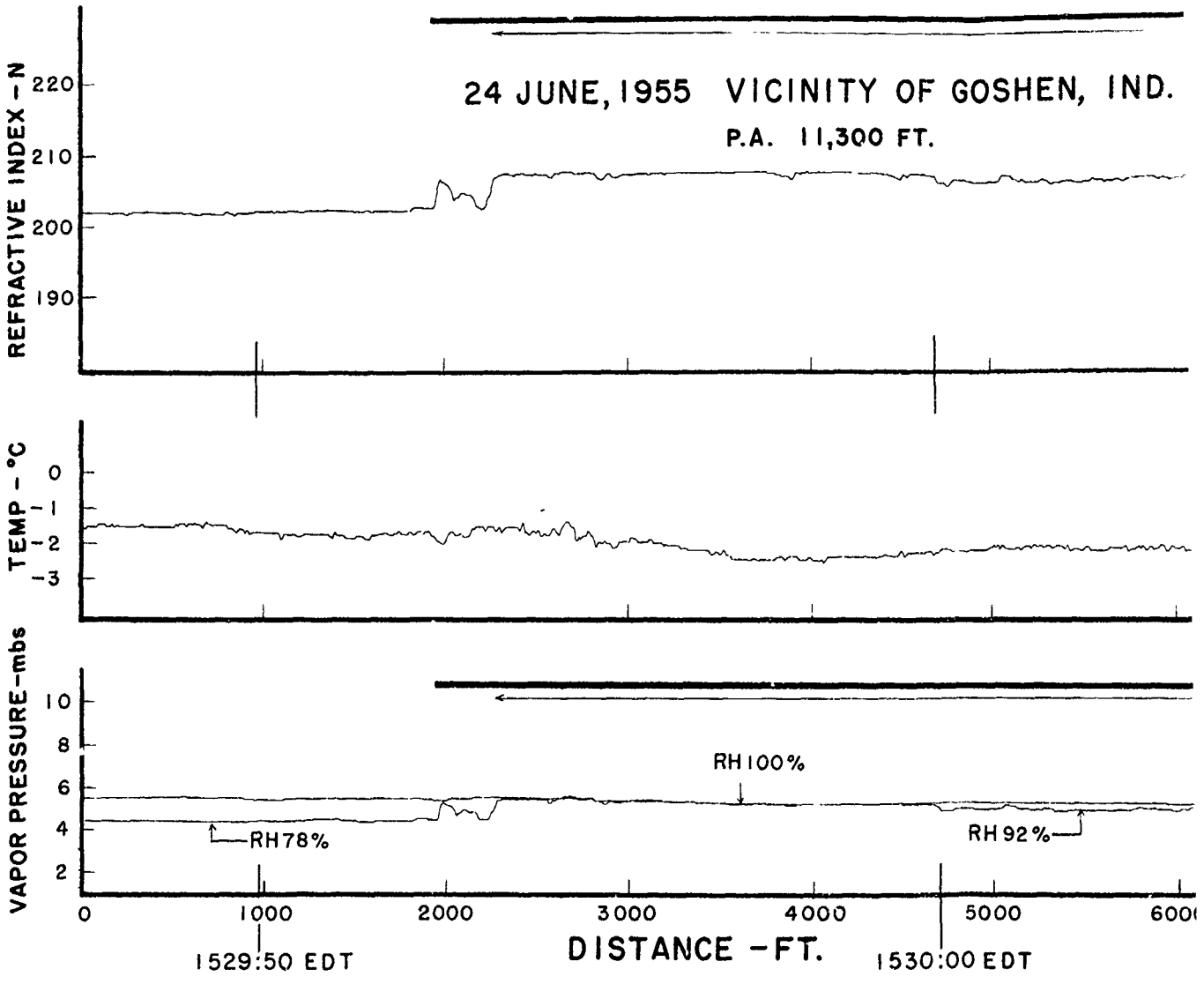

Figure 63.

The Murray Printing Company, Wakefield, Mass., 2-11-57 --- 1000

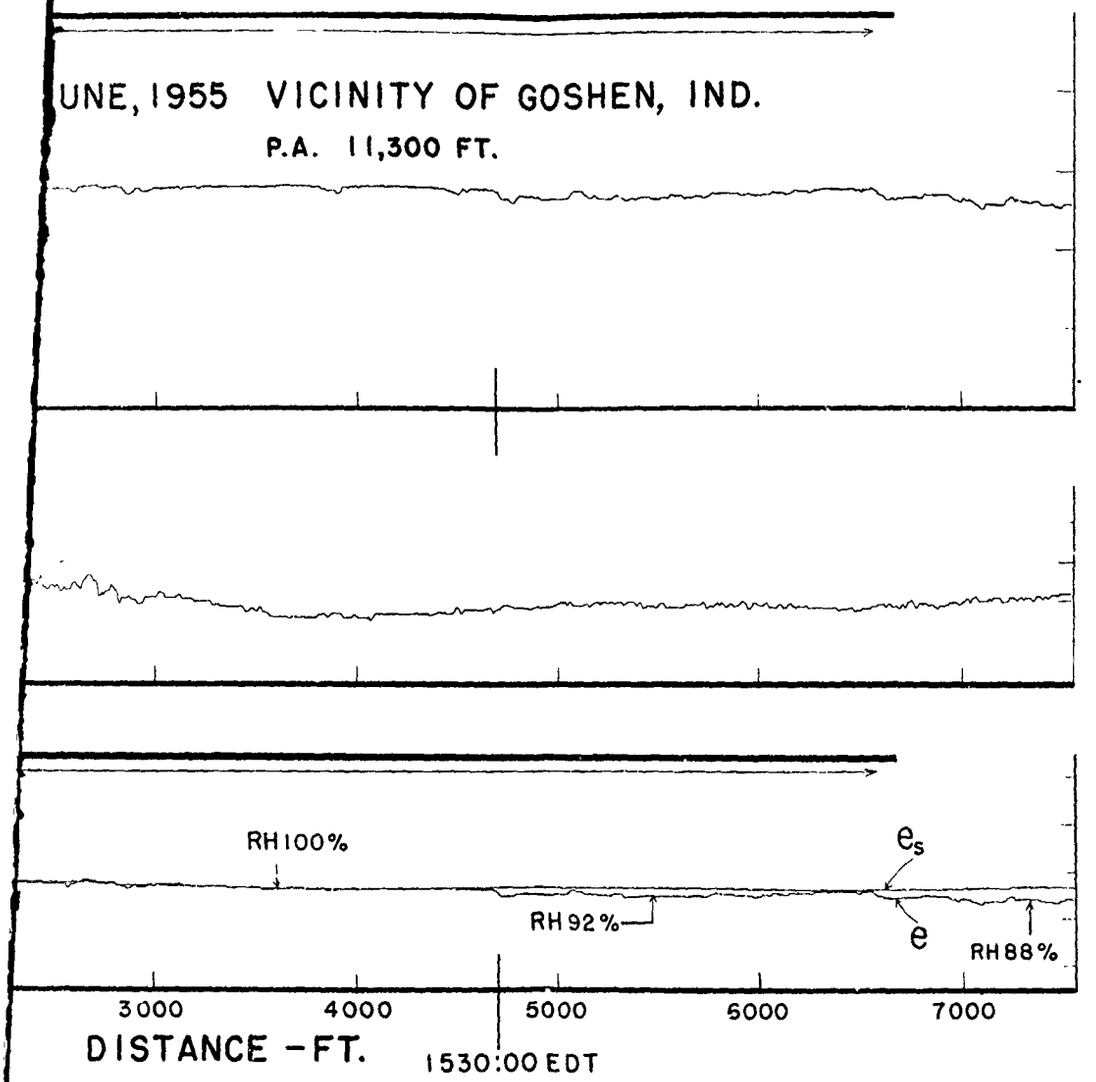
UNE, 1955 VICINITY OF GOSHEN, IND.
P.A. 11,300 FT.
RH 100%
e_s
RH 92%
e
RH 88%
3000
4000
5000
6000
7000
DISTANCE - FT.
1530:00 EDT

Figure 63.

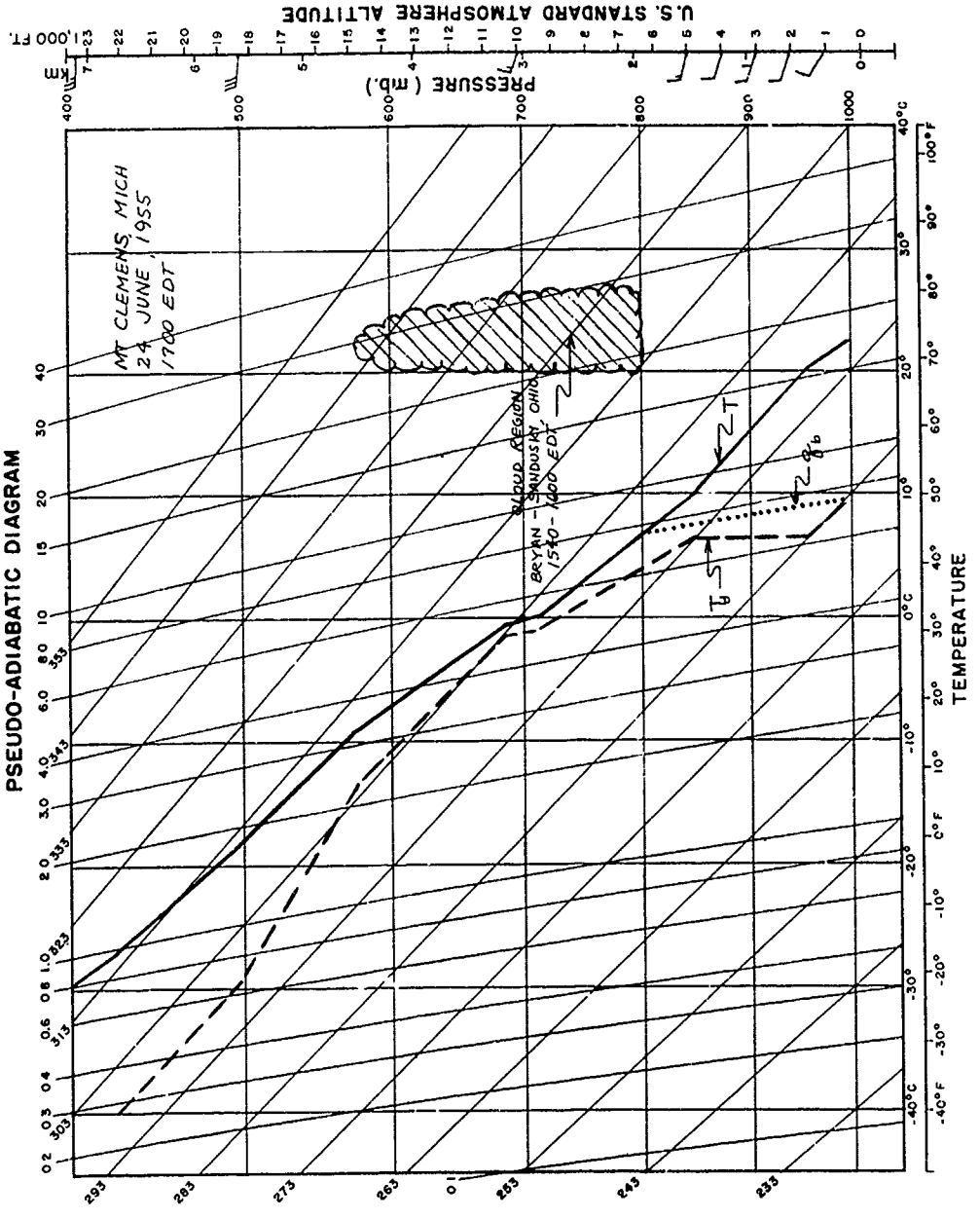
U.S. STANDARD ATMOSPHERE ALTITUDE
PRESSURE (mb.)
PSEUDO-ADIABATIC DIAGRAM
TEMPERATURE
MT CLEMENS, MICH
24 JUNE, 1955
1700 EDT
BRYAN - SANDUSKY, OHIO
1540 - 1600 EDT
CLOUD REGION

FIGURE 64

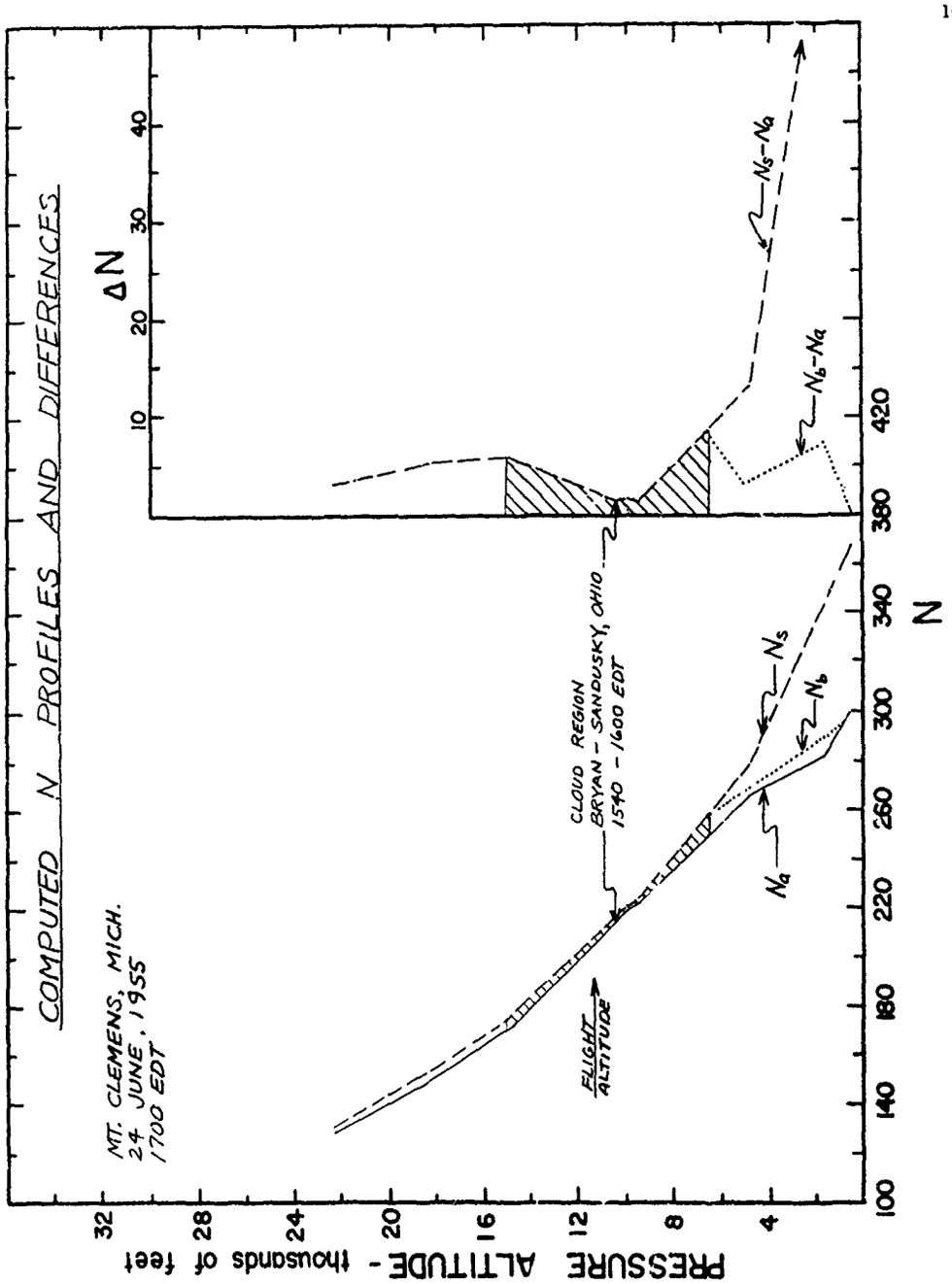
COMPUTED N PROFILES AND DIFFERENCES
MT. CLEMENS, MICH.
24 JUNE, 1955
1700 EDT
CLOUD REGION
BRYAN - SANDUSKY, OHIO
1540 - 1600 EDT
FLIGHT ALTITUDE
N_a
N_b
N_s
$N_b - N_a$
$N_s - N_a$
PRESSURE ALTITUDE - thousands of feet
N
ΔN

FIGURE 65

FIGURE 66

GEOPHYSICAL RESEARCH PAPERS

No. 1. Isotropic and Non-Isotropic Turbulence in the Atmospheric Surface Layer, Heinz Lettau, Geophysics Research Directorate, December 1949.

No. 2. Effective Radiation Temperatures of the Ozonosphere over New Mexico, Adel, Geophysics R-D, December 1949.

No. 3. Diffraction Effects in the Propagation of Compressional Waves in the Atmosphere, Norman A. Haskell, Geophysics Research Directorate, March 1950.

No. 4. Evaluation of Results of Joint Air Force-Weather Bureau Cloud Seeding Trials Conducted During Winter and Spring 1949, Charles E. Anderson, Geophysics Research Directorate, May 1950.

No. 5. Investigation of Stratosphere Winds and Temperatures From Acoustical Propagation Studies, Albert P. Crary, Geophysics Research Directorate, June 1950.

No. 6. Air-Coupled Flexural Waves in Floating Ice, F. Press, M. Ewing, A. P. Crary, S. Katz, and J. Oliver, Geophysics Research Directorate, November 1950.

No. 7. Proceedings of the Conference on Ionospheric Research (June 1949), edited by Bradford B. Underhill and Ralph J. Donaldson, Jr., Geophysics Research Directorate, December 1950.

No. 8. Proceedings of the Colloquium on Mesospheric Physics, edited by N. C. Gerson, Geophysics Research Directorate, July 1951.

No. 9. The Dispersion of Surface Waves on Multi-Layered Media, Norman A. Haskell, Geophysics Research Directorate, August 1951.

No. 10. The Measurement of Stratospheric Density Distribution with the Searchlight Technique, L. Elterman, Geophysics Research Directorate, December 1951.

No. 11. Proceedings of the Conference on Ionospheric Physics (July 1950) Part A, edited by N. C. Gerson and Ralph J. Donaldson, Jr., Geophysics Research Directorate, April 1952.

No. 12. Proceedings of the Conference on Ionospheric Physics (July 1950) Part B, edited by Ludwig Katz and N. C. Gerson, Geophysics Research Directorate, April 1952.

No. 13. Proceedings of the Colloquium on Microwave Meteorology, Aerosols and Cloud Physics, edited by Ralph J. Donaldson, Jr., Geophysics Research Directorate, May 1952.

No. 14. Atmospheric Flow Patterns and Their Representation by Spherical-Surface Harmonics, B. Haurwitz and Richard A. Craig, Geophysics Research Directorate, July 1952.

No. 15. Back-Scattering of Electromagnetic Waves From Spheres and Spherical Shells, A. L. Aden, Geophysics Research Directorate, July 1952.

No. 16. Notes on the Theory of Large-Scale Disturbances in Atmospheric Flow With Applications to Numerical Weather Prediction, Philip Duncan Thompson, Major, U. S. Air Force, Geophysics Research Directorate, July 1952.

GEOPHYSICAL RESEARCH PAPERS (Continued)

No. 17. The Observed Mean Field of Motion of the Atmosphere, Yale Mintz and Gordon Dean, Geophysics Research Directorate, August 1952.

No. 18. The Distribution of Radiational Temperature Change in the Northern Hemisphere During March, Julius London, Geophysics Research Directorate, December 1952.

No. 19. International Symposium on Atmospheric Turbulence in the Boundary Layer, Massachusetts Institute of Technology, 4-8 June 1951, edited by E. W. Hewson, Geophysics Research Directorate, December 1952.

No. 20. On the Phenomenon of the Colored Sun, Especially the "Blue" Sun of September 1950, Rudolf Penndorf, Geophysics Research Directorate, April 1953.

No. 21. Absorption Coefficients of Several Atmospheric Gases, K. Watanabe, Murray Zelikoff and Edward C. Y. Inn, Geophysics Research Directorate, June 1953.

No. 22. Asymptotic Approximation for the Elastic Normal Modes in a Stratified Solid Medium, Norman A. Haskell, Geophysics Research Directorate, August 1953.

No. 23. Forecasting Relationships Between Upper Level Flow and Surface Meteorological Processes, J. J. George, R. O. Roche, H. B. Visscher, R. J. Shafer, P. W. Funke, W. R. Biggers and R. M. Whiting, Geophysics Research Directorate, August 1953.

No. 24. Contributions to the Study of Planetary Atmospheric Circulations, edited by Robert M. White, Geophysics Research Directorate, November 1953.

No. 25. The Vertical Distribution of Mie Particles in the Troposphere, R. Penndorf, Geophysics Research Directorate, March 1954.

No. 26. Study of Atmospheric Ions in a Nonequilibrium System, C. G. Stergis, Geophysics Research Directorate, April 1954.

No. 27. Investigation of Microbarometric Oscillations in Eastern Massachusetts, E. A. Flaureud, A. H. Mears, F. A. Crowley, Jr., and A. P. Crary, Geophysics Research Directorate, May 1954.

No. 28. The Rotation-Vibration Spectra of Ammonia in the 6- and 10-Micron Regions, R. G. Breene, Jr., Capt., USAF, Geophysics Research Directorate, June 1954.

No. 29. Seasonal Trends of Temperature, Density, and Pressure in the Stratosphere Obtained With the Searchlight Probing Technique, Louis Elterman, July 1954.

No. 30. Proceedings of the Conference on Auroral Physics, edited by N. C. Gerson, Geophysics Research Directorate, July 1954.

No. 31. Fog Modification by Cold-Water Seeding, Vernon G. Plank, Geophysics Research Directorate, August 1954.

No. 32. Adsorption Studies of Heterogeneous Phase Transitions, S. J. Birstein, Geophysics Research Directorate, December 1954.

No. 33. The Latitudinal and Seasonal Variations of the Absorption of Solar Radiation by Ozone, J. Pressman, Geophysics Research Directorate, December 1954.

No. 34. Synoptic Analysis of Convection in a Rotating Cylinder, D. Fultz and J. Corn, Geophysics Research Directorate, January 1955.

No. 35. Balance Requirements of the General Circulation, V. P. Starr and R. M. White, Geophysics Research Directorate, December 1954.

No. 36. The Mean Molecular Weight of the Upper Atmosphere, Warren E. Thompson, Geophysics Research Directorate, May 1955.

No. 37. Proceedings on the Conference on Interfacial Phenomena and Nucleation.
I. Conference on Nucleation.
II. Conference on Nucleation and Surface Tension.
III. Conference on Adsorption.
Edited by H. Reiss, Geophysics Research Directorate, July 1955.

No. 38. The Stability of a Simple Baroclinic Flow With Horizontal Shear, Leon S. Pocinki, Geophysics Research Directorate, July 1955.

No. 39. The Chemistry and Vertical Distribution of the Oxides of Nitrogen in the Atmosphere, L. Miller, Geophysics Research Directorate, April 1955.

No. 40. Near Infrared Transmission Through Synthetic Atmospheres, J. N. Howard, Geophysics Research Directorate, November 1955.

No. 41. The Shift and Shape of Spectral Lines, R. G. Breene, Geophysics Research Directorate, October 1955.

No. 42. Proceedings on the Conference on Atmospheric Electricity, R. Holzer, W. Smith, Geophysics Research Directorate, December 1955.

No. 43. Methods and Results of Upper Atmospheric Research, J. Kaplan, G. Schilling, H. Kallman, Geophysics Research Directorate, November 1955.

No. 44. Luminous and Spectral Reflectance as Well as Colors of Natural Objects, R. Penndorf, Geophysics Research Directorate, February 1956.

No. 45. New Tables of Mie Scattering Functions for Spherical Particles, R. Penndorf, B. Goldberg, Geophysics Research Directorate, March 1956.

No. 46. Results of Numerical Forecasting With the Barotropic and Thermotropic Models, W. Gates, L. S. Pocinki, C. F. Jenkins, Geophysics Research Directorate, April 1956.

GEOPHYSICAL RESEARCH PAPERS (Continued)

No. 47. A Meteorological Analysis of Clear Air Turbulence (A Report on the U. S. Synoptic High-Altitude Gust Program), H. Lake, Geophysics Research Directorate, February 1956.

No. 48. A Review of Charge Transfer Processes in Gases, S. N. Ghosh, W. F. Sheridan, J. A. Dillon, Jr., and H. D. Edwards, Geophysics Research Directorate, July 1955.

No. 49. Theory of Motion of a Thin Metallic Cylinder Carrying a High Current, C. W. Dube, Geophysics Research Directorate, October 1955.

No. 50. Hurricane Edna, 1954: Analysis of Radar, Aircraft, and Synoptic Data, E. Kessler, III and D. Atlas, Geophysics Research Directorate, July 1956.